



The SPIRITS Sample of Luminous Infrared Transients: Uncovering Hidden Supernovae and Dusty Stellar Outbursts in Nearby Galaxies*

Jacob E. Jencson^{1,18}, Mansi M. Kasliwal¹, Scott M. Adams¹, Howard E. Bond^{2,3}, Kishalay De¹, Joel Johansson⁴, Viraj Karambelkar⁵, Ryan M. Lau^{1,6}, Samaporn Tanyanont¹, Stuart D. Ryder^{7,8}, Ann Marie Cody⁹, Frank J. Masci¹⁰, John Bally¹¹, Nadejda Blagorodnova¹², Sergio Castellón¹³, Christoffer Fremming¹, Robert D. Gehrz¹⁴, George Helou¹⁰, Charles D. Kilpatrick¹⁵, Peter A. Milne¹⁶, Nidia Morrell¹³, Daniel A. Perley¹⁷, M. M. Phillips¹³, Nathan Smith¹⁶, Schuyler D. van Dyk¹⁰, and Robert E. Williams^{3,15}

¹ Division of Physics, Mathematics and Astronomy, California Institute of Technology, Pasadena, CA 91125, USA; jj@astro.caltech.edu

² Department of Astronomy & Astrophysics, Pennsylvania State University, University Park, PA 16802, USA

³ Space Telescope Science Institute, 3700 San Martin Drive, Baltimore, MD 21218, USA

⁴ Department of Physics and Astronomy, Division of Astronomy and Space Physics, Uppsala University, Box 516, SE 751 20 Uppsala, Sweden

⁵ Department of Physics, Indian Institute of Technology Bombay, Mumbai 400076, India

⁶ Institute of Space & Astronautical Science, Japan Aerospace Exploration Agency, 3-1-1 Yoshinodai, Chuo-ku, Sagami-hara, Kanagawa 252-5210, Japan

⁷ Australian Astronomical Observatory, 105 Delhi Road, North Ryde, NSW 2113, Australia

⁸ Department of Physics & Astronomy, Macquarie University, NSW 2109, Australia

⁹ NASA Ames Research Center, Moffet Field, CA 94035, USA

¹⁰ Caltech/IPAC, Mailcode 100-22, Pasadena, CA 91125, USA

¹¹ Astrophysical and Planetary Sciences Department University of Colorado, UCB 389, Boulder, CO 80309, USA

¹² Department of Astrophysics/IMAPP, Radboud University, Nijmegen, The Netherlands

¹³ Las Campanas Observatory, Carnegie Observatories, Casilla 601, La Serena, Chile

¹⁴ Minnesota Institute for Astrophysics, School of Physics and Astronomy, University of Minnesota, 116 Church Street SE, Minneapolis, MN 55455, USA

¹⁵ Department of Astronomy and Astrophysics, University of California, Santa Cruz, CA 95064, USA

¹⁶ University of Arizona, Steward Observatory, 933 N. Cherry Avenue, Tucson, AZ 85721, USA

¹⁷ Astrophysics Research Institute, Liverpool John Moores University, IC2, Liverpool Science Park, 146 Brownlow Hill, Liverpool L3 5RF, UK

Received 2019 February 27; revised 2019 September 29; accepted 2019 September 30; published 2019 November 18

Abstract

We present a systematic study of the most luminous (M_{IR} [Vega magnitudes] brighter than -14) infrared (IR) transients discovered by the *SPitzer* InfraRed Intensive Transients Survey (SPIRITS) between 2014 and 2018 in nearby galaxies ($D < 35$ Mpc). The sample consists of nine events that span peak IR luminosities of $M_{[4.5],\text{peak}}$ between -14 and -18.2 , show IR colors between $0.2 < ([3.6]-[4.5]) < 3.0$, and fade on timescales between $55 \text{ days} < t_{\text{fade}} < 480 \text{ days}$. The two reddest events ($A_V > 12$) show multiple, luminous IR outbursts over several years and have directly detected, massive progenitors in archival imaging. With analyses of extensive, multiwavelength follow-up, we suggest the following possible classifications: five obscured core-collapse supernovae (CCSNe), two erupting massive stars, one luminous red nova, and one intermediate-luminosity red transient. We define a control sample of all optically discovered transients recovered in SPIRITS galaxies and satisfying the same selection criteria. The control sample consists of eight CCSNe and one Type Iax SN. We find that 7 of the 13 CCSNe in the SPIRITS sample have lower bounds on their extinction of $2 < A_V < 8$. We estimate a nominal fraction of CCSNe in nearby galaxies that are missed by optical surveys as high as $38.5^{+26.0}_{-21.9}\%$ (90% confidence). This study suggests that a significant fraction of CCSNe may be heavily obscured by dust and therefore undercounted in the census of nearby CCSNe from optical searches.

Key words: dust, extinction – infrared: general – stars: massive – supernovae: general – supernovae: individual (SPIRITS 14buu, SPIRITS 15c, SPIRITS 15ud, SPIRITS 16ix, SPIRITS 16tn, SPIRITS 17lb)

Supporting material: data behind figures, machine-readable tables

1. Introduction

While there are now several known classes of stellar transient phenomena for which the observable emission is predominantly infrared (IR), exploration of the landscape of IR-dominated transients is just beginning. Often due to the effects of astrophysical dust, a host of eruptive and explosive stellar phenomena may be best observed in the IR. In particular, otherwise optically luminous transients such as supernovae (SNe) may be significantly obscured by dust in their host galaxies and/or local environments. Dust in the immediate

circumstellar environment of a luminous transient, which may have condensed in a steady wind of the progenitor or formed during previous eruptive mass-loss events, may also efficiently reprocess shorter-wavelength emission into the IR. Some transients, particularly those associated with cool, low-velocity outflows, are themselves copious dust producers, leading to IR-dominated spectral energy distributions (SEDs).

Since 2014, we have been conducting the *SPitzer* InfraRed Intensive Transients Survey (SPIRITS; PIDs 11063, 13053, 14089; PI M. Kasliwal, Kasliwal et al. 2017) to discover transients in nearby $D \lesssim 35$ Mpc galaxies using the 3.6 and 4.5 μm imaging bands ([3.6] and [4.5]) of the Infrared Array Camera (IRAC; Fazio et al. 2004) on board the warm *Spitzer* Space Telescope (*Spitzer*; Werner et al. 2004; Gehrz et al. 2007). In this paper, we focus on a thorough investigation of all

* This paper includes data gathered with the 6.5 m Magellan Telescopes located at Las Campanas Observatory, Chile.

¹⁸ National Science Foundation Graduate Research Fellow.

luminous ($M_{[4.5]}$ [Vega magnitudes] brighter than -14) IR transients discovered by SPIRITS in the past 5 yr (Section 2.3). We compare this sample to a well-defined control sample of all optically discovered and spectroscopically classified transients hosted by SPIRITS galaxies and satisfying the same selection criteria (Section 2.4). Our sample of luminous infrared transients may represent diverse origins, including obscured core-collapse supernovae (CCSNe) and other known classes of IR-dominated transients such as stellar mergers or massive-star eruptions (MSEs).

CCSNe, the explosive deaths of stars of initial masses $\gtrsim 8 M_{\odot}$, are now found in numbers exceeding several hundreds of events per year by numerous, primarily optical, searches. Arising from recently formed, massive stars, CCSNe may be subject to significant extinction from the dusty regions of active star formation in their host galaxies. The fraction of CCSNe missed optically owing to the obscuring effects of dust is therefore an important consideration for measurements of the CCSN rate (e.g., Grossan et al. 1999; Maiolino et al. 2002). Horiuchi et al. (2011) claimed that half of all SNe were missing from observed CCSN rate estimates in comparison to the rate of massive-star formation both locally and across cosmic time from redshifts $0 < z < 1$; however, other studies have found better agreement (e.g., Cappellaro et al. 2015). Accounting for obscured or otherwise optically dim CCSNe may also resolve this discrepancy (e.g., Mannucci et al. 2007; Mattila et al. 2012). Direct searches for CCSNe at wavelengths less sensitive to extinction are thus required to accurately measure the CCSN rate. Significant work (e.g., Varenus et al. 2019; Kool et al. 2018, and references therein; see discussion in Section 7) has been dedicated to uncovering extinguished CCSNe in the densely obscured and highly star-forming regions of starburst and (ultra)luminous infrared galaxies (U/LIRGS). In contrast, our SPIRITS sample focuses on local galaxies encompassing a wide variety of galaxy morphologies, masses, and star formation rates with unbiased sampling of all environments within galaxies (Section 2.1).

Other categories of luminous IR transients include intermediate-luminosity red transients (ILRTs), luminous red novae (LRNe), and giant eruptions of luminous blue variables (LBVs).¹⁹ The prototypical objects for ILRTs are the “impostor” SN 2008S and the 2008 transient in NGC 300 (NGC 300 OT2008-1; Bond et al. 2009), suggested to be explosions of ≈ 10 – $15 M_{\odot}$ stars, possibly extreme asymptotic giant branch (AGB) stars, self-obscured by a dusty wind (Prieto et al. 2008; Bond et al. 2009; Thompson et al. 2009). Extragalactic LRNe are believed to be massive analogs of stellar mergers observed in the Galaxy, including the striking example of the ≈ 1 – $3 M_{\odot}$ contact binary merger V1309 Sco (Tylenda et al. 2011) and the B-type stellar merger V838 Mon (Bond et al. 2003; Sparks et al. 2008). While sharing many observational properties with, e.g., ILRTs, a key difference is that LRNe have surviving remnants (e.g.,

NGC 4490 OT2011-1; Smith et al. 2016). Surviving dust in the circumstellar environments of LBVs may also result in an observed IR excess during some nonterminal giant eruptions (e.g., η Carinae; Humphreys et al. 1999, UGC 2773OT; Smith et al. 2010).

It is particularly telling that known examples and even class prototypes of known IR-dominated events have almost exclusively been identified via their optical emission. It has been proposed, for example, that early dust formation in some LRNe may even entirely obscure or dramatically shorten the optical luminosity peak, while still producing a bright, long-lived infrared transient (e.g., Metzger & Pejcha 2017). Kashi & Soker (2017) have also suggested that dense, equatorial material may obscure transients driven by strong binary interactions, but that dust formation in polar outflows may still power IR emission in these events. As suggested by Bally & Zinnecker (2005), dynamical interactions of massive, compact-multiple systems in star-forming regions may also produce luminous transients, the energy released likely emerging in the IR given their densely obscured environments (see also recent events in the Galactic star-forming regions Sh2-255 and NGC 6334; Caratti o Garatti et al. 2017; Hunter et al. 2017; Brogan et al. 2018). SPIRITS overcomes the selection biases of optical discovery and is sensitive to redder events that may lack optical counterparts altogether (e.g., the recently discovered eSPecially Red Intermediate-luminosity Transient Events [SPRITEs]; Kasliwal et al. 2017).

We have undertaken extensive follow-up, including optical/IR photometry, spectroscopy, and radio imaging, to characterize the nature of each luminous IR transient presented in this work (Section 3). We describe our analysis of the full data set, including host galaxy properties, progenitor constraints, photometric evolution, spectroscopic feature identification, and extinction estimates, in Section 4. In Section 5, we combine all available observational constraints in comparison to well-studied objects and attempt to classify each luminous SPIRITS transient. In Section 6, we discuss the A_V distribution of nearby, luminous IR transients and CCSNe in particular, and in Section 7, we derive statistically robust estimates of the rate of CCSNe missed in nearby galaxies relative to the control sample of optically discovered CCSNe in SPIRITS galaxies. Finally, in Section 8, we summarize the main results and conclusions of this work.

2. Survey Design and Sample Selection

2.1. Galaxy Sample and Imaging Cadence

A full description of the SPIRITS survey design is given in Kasliwal et al. (2017). It is a targeted search of nearby galaxies using the $5 \times 5'$ field of view of the IRAC camera. SPIRITS monitored a sample of 190 nearby galaxies for 3 yr from 2014 to 2016. The sample was selected based on the following criteria: (1) the 37 galaxies within 5 Mpc including both early- and late-type galaxies, dwarf galaxies, and giant galaxies, (2) the 116 most luminous galaxies between 5 and 15 Mpc, including 83% of the B -band starlight within 15 Mpc; and (3) the 37 most luminous and massive galaxies in the Virgo Cluster at 17 Mpc.

In 2014, each galaxy was observed 3 times at ~ 1 -month and ~ 6 -month intervals. In 2015–2016, baselines of 1- and 3-week timescales were added. In 2017–2018, the galaxy sample was reduced to focus on only the 105 galaxies most likely to host new transients and SNe, including the 58 galaxies that had previously hosted at least one IR transient, and the

¹⁹ Distinguishing among classes of hydrogen-rich, intermediate-luminosity transients is difficult, as they may share many observational properties, and the nomenclature referring to these classes varies throughout the literature. We use the terms ILRT (originally suggested by Bond et al. 2009), LRN (e.g., Kulkarni et al. 2007), and “giant eruption” or LBV to refer to these classes as described in the main text. In the literature, giant eruptions may also be referred to as “SN imposters” or “ η Carinae variables” (Humphreys et al. 1999; Van Dyk et al. 2000; Pastorello et al. 2010; Smith et al. 2010; Smith 2014). ILRTs are sometimes included in this class, though their progenitors are believed to be lower mass than classical LBVs. Our choice of nomenclature is similar to that used by, e.g., Kashi & Soker (2016), who also adopted the umbrella term “intermediate-luminosity optical transient” of Berger et al. (2009) to refer to all three of these classes together.

47 remaining most luminous and star-forming galaxies ($L > 2 \times 10^{10} L_{\odot}$). Our cadence was also reduced to ~ 6 -month intervals, typically with one observation per galaxy per visibility window. Each SPIRITS observation consists of seven dithered 100 s exposures in both IRAC bands. The nominal 5σ point-source limiting magnitudes of these observations are 20.0 and 19.1 at [3.6] and [4.5], respectively, using the zero-magnitude fluxes given in the IRAC instrument handbook²⁰ of $F_{\nu,0} = 280.9$ Jy for [3.6] and $F_{\nu,0} = 179.7$ Jy for [4.5].

2.2. Image Subtraction and Transient Identification

For reference images, we make use of archival *Spitzer* frames, including Super Mosaics²¹ or S4G (*Spitzer* Survey of Stellar Structure in Galaxies; PID 61065; PI K. Sheth; Sheth et al. 2010; Muñoz-Mateos et al. 2013; Querejeta et al. 2015), or stacks of archival “bcd” images (where Super Mosaics or S4G images were not available). Further details of our image subtraction and transient identification pipelines are provided in Kasliwal et al. (2017). Transient candidates automatically identified by our pipeline in reference-subtracted images are vetted by human scanners, and sources passing human vetting are saved to our database and assigned a SPIRITS name.

Photometry is performed at the location of SPIRITS transients in the reference-subtracted images using a 4 mosaicked pixel ($2''.4$) aperture and background annulus from 4 to 12 pixels ($2''.4$ – $7''.2$). The extracted flux is multiplied by the aperture corrections of 1.215 for [3.6] and 1.233 for [4.5], as described in the IRAC instrument handbook, and converted to Vega system magnitudes using the handbook-defined zero-magnitude fluxes for each IRAC channel.

2.3. Luminous IR Transient Sample Selection

We selected events that peaked at M_{IR} brighter than -14 ($\nu L_{\nu} > 1.5 \times 10^5 L_{\odot}$ at [4.5]) in either the [3.6] channel or [4.5] channel of *Spitzer*/IRAC during SPIRITS observations.²² We further required at least two SPIRITS detections, to ensure that each event is astrophysically real and that the transients were not present in the first epoch of SPIRITS imaging, so that the age of the event is constrained by SPIRITS data. We list basic properties for these objects in Table 1. SPIRITS 14buu (first presented in Jencson et al. 2017) was identified in the first epoch of SPIRITS imaging of the galaxy IC 2163. As such, we have no constraint on the age of this object from SPIRITS data, and thus we exclude it from the primary sample. The sample then consists of nine events discovered in SPIRITS between 2014 and 2018 that, to our knowledge, were not identified and spectroscopically classified by any other survey.²³ The *Spitzer*/

IRAC [4.5] discovery images for each object, including the new science frame, reference image, and science-minus-reference subtractions, are shown in Figure 1.

2.4. Optically Discovered Control Sample

To place our sample of luminous IR transients in context, we define a control sample of optically discovered and classified transients recovered during normal operation of the SPIRITS survey, employing the same selection criteria as for the IR-selected sample. A total of 14 such transients hosted by SPIRITS galaxies and discovered at optical wavelengths have been reported since the start of the survey in 2014. We summarize basic properties of these events in Table 2.

Three events, SN 2014C (Type Ib/IIn), SN 2014J (Type Ia), and SN 2014L (Type Ic), were present in the first epoch of SPIRITS observations such that we would not have a meaningful constraint on the explosion epoch from SPIRITS data alone. Two additional events were not recovered in SPIRITS by our automated image subtraction and transient identification pipeline owing to saturation of the IRAC detector at the location of the transient. SN 2014bc (Type II) was located only $3''.4$ from the bright nucleus of NGC 4258, which is saturated in all epochs of SPIRITS imaging. SN 2016adj (Type Ib), the nearest object in the optically discovered sample at only 3.7 Mpc, is itself saturated in all epochs where the SN is present in SPIRITS imaging and was not recovered by the SPIRITS pipeline.

Thus, we define our primary comparison sample as the nine objects that were recovered by SPIRITS and have constraints on their explosion dates from SPIRITS data. By optical spectroscopic subtype this sample includes six SNe II, two SNe Ib, and one SN Iax.

Our photometry from *Spitzer*/IRAC imaging for both the IR-discovered sample of luminous IR transients and the optically discovered control sample in SPIRITS is given in Table 3 and shown in Figure 2 (see Section 4.2 for further discussion).

3. Follow-up and Supplementary Observations

3.1. Space-based Imaging

For transients that were inaccessible to ground-based observing at the time of discovery with *Spitzer*, we attempted to trigger Target of Opportunity (ToO) observations with the *Neil Gehrels Swift Observatory* UV/Optical Telescope (*Swift*/UVOT; Gehrels et al. 2004; Nousek 2004; Roming et al. 2005) to detect an optical counterpart or obtain limits on the contemporaneous optical flux. For SPIRITS 16tn we triggered a 2000 s observation on 2016 August 29.1 split between the *U*, *B*, and *V* bands, with limits reported in Adams et al. (2016a) and Jencson et al. (2018d). For SPIRITS 17lb we obtained a 1200 s integration in the *V* band on 2017 June 9.4 and derived a 5σ limiting magnitude of $V > 17.7$. For SPIRITS 17pc we obtained a 2000 s observation on 2017 November 9.1 split between *U*, *B*, and *V*. NGC 4388 was previously observed by *Swift*/UVOT 1 yr prior on 2016 November 8.8, but with shorter integrations of only ≈ 60 s in each band. We find no evidence of significant variability at the location of SPIRITS 17pc between the two epochs. We derive limits for the earlier (later) epochs of $U > 18.0$ (18.8), $B > 18.2$ (18.8), and $V > 17.2$ (18.0).

²⁰ <http://irsa.ipac.caltech.edu/data/SPITZER/docs/irac/iracinstrumenthandbook/>

²¹ Super Mosaics are available as *Spitzer* Enhanced Imaging Products through the NASA/IPAC Infrared Science Archive: <https://irsa.ipac.caltech.edu/data/SPITZER/Enhanced/SEIP/overview.html>.

²² The full sample of SPIRITS transients includes many lower-luminosity events, including IR detections of classical novae (e.g., M81 possible nova AT 2018akh; Jencson et al. 2018c), and events belonging to the diverse and mysterious class of objects called SPRITES, first described by Kasliwal et al. (2017). These events are outside the scope of this work and will be studied in future publications.

²³ An optical transient at the location of SPIRITS 15ade was first discovered on 2015 September 11.5 and reported by M. Aoki as PSN J15220552+0503160 through the Central Bureau for Astronomical Telegrams (CBAT; <http://www.cbata.harvard.edu/unconf/followups/J15220552+0503160.html>). To our knowledge, no spectroscopy for classification or host confirmation was reported before this work.

Table 1
Luminous, IR-discovered SPIRITS Transients

Name	R.A. (J2000)	Decl. (J2000)	Host (Type)	$m - M^a$ (mag)	Distance (Mpc)	$E(B - V)_{MW}^b$ (mag)	UT Discovery	Host Offset	
								(arcsec)	(kpc)
SPIRITS 14buu	06:16:27.2	-21:22:29.2	IC 2163 (SBc pec)	32.75 ± 0.4	35.5	0.077	2014 Jan 13.9 ^c	11.5	2.0
SPIRITS 14azy	09:45:40.92	-31:12:07.8	NGC 2997 (SABc)	30.43 ± 0.16	12.2	0.027	2014 Jul 26.0	48.4	2.9
SPIRITS 15c	06:16:28.49	-21:22:42.2	IC 2163 (SBc pec)	32.75 ± 0.4	35.5	0.077	2015 Feb 04.4	11.6	2.0
SPIRITS 15ud	12:22:55.29	+15:49:22.0	M100 (SABbc)	30.72 ± 0.06	13.9	0.023	2015 Sep 06.7	7.5	0.5
SPIRITS 15ade	15:22:05.55	+05:03:15.9	NGC 5921 (SBbc)	31.9 ± 0.2	24.0	0.036	2015 Nov 11.9	146.3	17.0
SPIRITS 16ix	12:29:03.16	+13:11:30.7	NGC 4461 (SB0 ⁺)	31.48 ± 0.25	19.8	0.02	2016 Mar 30.9	29.2	2.8
SPIRITS 16tn	11:11:20.40	+55:40:17.3	NGC 3556 (SBcd)	29.7 ± 0.4	8.7	0.015	2016 Aug 15.0	89.9	3.8
SPIRITS 17lb	06:16:27.78	-21:22:51.7	IC 2163 (SBc pec)	32.75 ± 0.4	35.5	0.077	2017 May 28.7	18.8	3.2
SPIRITS 17pc	12:25:44.43	+12:39:44.5	NGC 4388 (SAb)	31.3 ± 0.4	18.2	0.029	2017 Oct 12.8	33.9	3.0
SPIRITS 17qm	03:33:38.85	-36:08:09.4	NGC 1365 (SBb)	31.31 ± 0.06	18.3	0.018	2017 Nov 05.2	34.1	3.0

Notes.

^a References for distance moduli: NGC 2997 (Hess et al. 2009), IC 2163 (Theureau et al. 2007), M100 and NGC 4461 (Tully et al. 2013), NGC 5921 (Rodríguez et al. 2014), NGC 3556 and NGC 4388 (Sorce et al. 2014), NGC 1365 (Riess et al. 2016).

^b Galactic extinction estimates taken from NED using the Schlafly & Finkbeiner (2011) recalibration of the Schlegel et al. (1998) IR-based dust map assuming a Fitzpatrick (1999) extinction law with $R_V = 3.1$.

^c Transient present in first 2014 SPIRITS epoch and therefore excluded from the primary sample.

We also executed *Hubble Space Telescope* (HST) ToO observations of SPIRITS 16tn using the Wide Field Camera 3 (WFC3) in the UVIS channel with the F814W filter and the IR channel with the F110W and F160W filters as part of our program to follow up SPIRITS transients (GO-14258; PI: H. Bond) on 2016 September 25 as described in Jencson et al. (2018d).

3.2. Ground-based Imaging

SPIRITS galaxies were regularly monitored from the ground in the optical and near-IR with several telescopes. For the SPIRITS transient host galaxies discussed here, sequences of optical $g'r'i'$ -band images of IC 2163, M100, NGC 4461, NGC 3556, and NGC 4388 were obtained with the CCD camera on the fully automated Palomar 60-inch telescope (P60; Cenko et al. 2006) throughout 2014–2018 and reduced by a fully automated pipeline. Where available, we used Sloan Digital Sky Survey (SDSS) images as templates for image subtraction to remove host galaxy background emission and obtain deeper limits on optical emission from the transients.

Similarly for SPIRITS galaxies located in the southern hemisphere, namely, NGC 2997, IC 2163, and NGC 1365, sequences of optical gri -band images were obtained with the CCD camera on the 1 m Swope Telescope at Las Campanas Observatory (LCO) throughout 2014–2015. Near-IR YJH -band images were also obtained throughout 2014–2015 with the RetroCam IR camera (Morgan et al. 2005) on the 2.5 m du Pont Telescope at LCO. Photometry was performed at the locations of the transients by fitting the point-spread function (PSF) of the images, measured using stars in the field, simultaneously with the background emission, modeled using low-order polynomials.

We also obtained and performed PSF photometry on the images of NGC 5921 reported at CBAT for PSN J15220552+0503160 (SPIRITS 15ade), including unfiltered CCD images obtained by M. Aoki, G. Masi, and T. Noguchi, along with post-discovery images of this galaxy in the R band from the Hiroshima One-shot Wide-field Polarimeter (HOWpol; Kawabata et al. 2008) on the Kanata 1.5 m telescope at Higashi-Hiroshima Observatory and in the r band with the Dark Energy Camera (DECam) on the Blanco 4 m telescope at Cerro Tololo Inter-American Observatory (CTIO).

Post-discovery, ground-based follow-up imaging in the optical and near-IR was also obtained for several SPIRITS transients. Near-IR JHK_s -band images were obtained with the Multi-object Spectrometer for Infra-red Exploration (MOS-FIRE; McLean et al. 2010, 2012) on the 10 m Keck I Telescope of the W. M. Keck Observatory on the summit of Maunakea, the Wide Field Infrared Camera (WIRC; Wilson et al. 2003) on the 200-inch telescope at Palomar Observatory (P200), and the FourStar IR camera (Persson et al. 2013) on the Magellan Baade Telescope at LCO. Flat-fielding, background subtraction, astrometric alignment, and final stacking of images in each filter were performed using a custom pipeline. Additional near-IR imaging for SPIRITS 17lb was obtained with the FLAMINGOS-2 imaging spectrograph on the 8.1 m Gemini S Telescope (PID GS-2017B-Q-15; PI J. Jencson) and reduced using the Gemini IRAF package following procedures online in the FLAMINGOS-2 Data Reduction Cookbook.²⁴ Optical imaging was obtained for SPIRITS 17pc using the DEep Imaging Multi-Object Spectrograph (DEIMOS; Faber et al. 2003) on the 10 m Keck II Telescope and reduced using standard tasks in IRAF.

Additional near-IR imaging was obtained with the Wide Field Camera (WFCAM; Casali et al. 2007) on the United Kingdom Infrared Telescope (UKIRT) at Maunakea Observatories. Simultaneous optical/near-IR $rizYJH$ were obtained with the Reionization and Transients InfraRed camera (RATIR; Butler et al. 2012) on the 1.5 m Johnson Telescope at the Mexican Observatorio Astronómico Nacional on the Sierra San Pedro Martir in Baja California, Mexico (Watson et al. 2012).

For our follow-up imaging, we performed simple aperture photometry at the location of the transients with the aperture size defined by the seeing in each image. Our photometry (including PSF photometry above) was calibrated using $\gtrsim 10$ isolated stars in SDSS for the optical images and in the Two Micron All Sky Survey (2MASS) for the near-IR images. Where necessary, we adopt the conversions of Jordi et al. (2006) to convert from the Sloan $ugriz$ system to $UBVRI$

²⁴ Data reduction procedures for FLAMINGOS-2 are found at <https://gemini-iraf-flamingos-2-cookbook.readthedocs.io/en/latest/>.

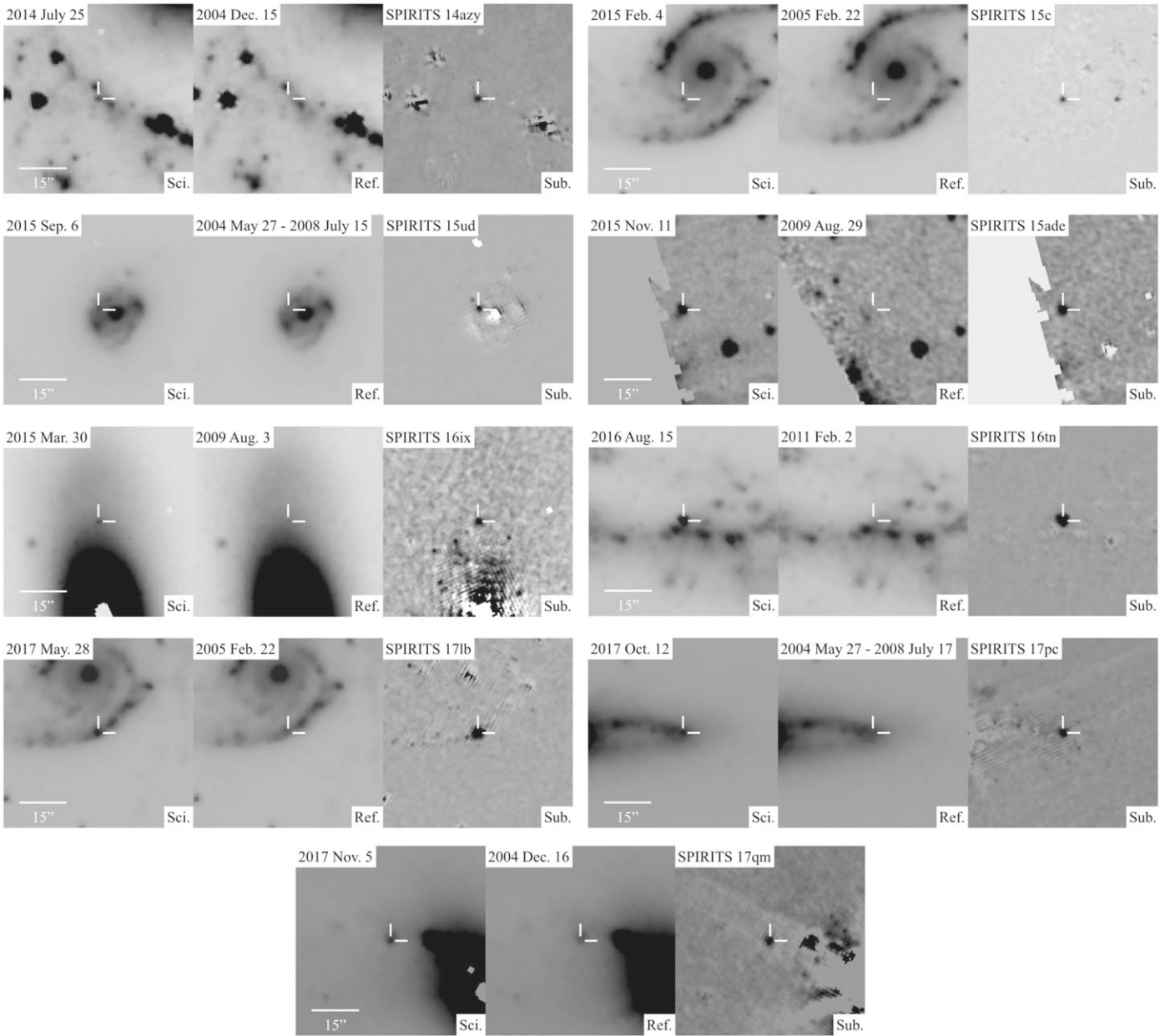


Figure 1. *Spitzer*/IRAC [4.5] discovery images for each luminous SPIRITS-discovered transient in our sample. In each panel, from left to right, we show the new science frame, reference frame, and science-minus-reference subtraction image. The dates of each image and labels for each object are shown along the top of each panel, and the locations of the transients are indicated by white crosshairs. Each image is $1' \times 1'$, oriented with N up and E left.

magnitudes. For *Y*-band images, we adopt the conversion from 2MASS used for the UKIRT/WFCAM from Hodgkin et al. (2009). Unfiltered CCD images of NGC 5921 were calibrated to the SDSS *r* band. Our supplementary photometry is included in Table 4 and shown for each object in Figure 12.

3.3. Spectroscopy

We obtained near-IR spectroscopy of the luminous IR SPIRITS transients at several epochs using the Folded-port InfraRed Echellette spectrograph (FIRE; Simcoe et al. 2008, 2013) on the Magellan Baade Telescope at LCO, MOSFIRE on the Keck I Telescope, the Near-Infrared Echellette Spectrometer²⁵ (NIREs) on the Keck II Telescope,

the Gemini Near-Infrared Spectrograph (GNIRS; Elias et al. 2006) on the 8.1 m Gemini N Telescope (PIDs GN-2016B-FT-25, GN-2017B-Q-14; PI J. Jencson), and the FLAMINGOS-2 spectrograph (Eikenberry et al. 2006) on the 8.1 m Gemini S Telescope (PID GS-2017B-Q-15; PI J. Jencson). Optical spectroscopy was obtained for SPIRITS 16tn, SPIRITS 17pc, and SPIRITS 17qm with the Low Resolution Imaging Spectrometer (LRIS; Goodrich & Cohen 2003) on the Keck I telescope. Our spectroscopic observations, including the integration times used, are summarized in Table 5.

The FIRE and MOSFIRE spectra of SPIRITS 15c and the GNIRS and LRIS spectra of SPIRITS 16tn, as well as details of the data reduction procedures, were previously published in Jencson et al. (2017, 2018d).

For the LRIS observations of SPIRITS 17pc and SPIRITS 17qm, we used the D560 dichroic to split the light

²⁵ <https://www2.keck.hawaii.edu/inst/nires/>

Table 2
Optically Discovered and Classified Transients in SPIRITS

Name	SPIRITS Name ^a	R.A. (J2000)	Decl. (J2000)	Host (Type)	$m - M^b$ (mag)	D (Mpc)	$E(B - V)_{MW}^c$ (mag)	A_V^d (mag)	UT Discovery ^e	Host Offset		Type ^f
										(arcsec)	(kpc)	
SN 2014C	SPIRITS 14aom	22:37:05.60	+34:24:31.9	NGC 7331 (SAb)	30.71 ± 0.08	13.9	0.08	0.22	2014 Jan 05.1 ^g	31.0	2.1	Ib/II _n
SN 2014J	SPIRITS 14pw	09:55:42.14	+69:40:26.0	M82 (I0)	27.74 ± 0.08	3.5	0.14	0.98	2014 Jan 21.8 ^g	58.6	1.0	Ia
SN 2014L	SPIRITS 14we	12:18:48.68	+14:24:43.5	NGC 4254 (SAc)	30.7 ± 0.2	13.8	0.11	...	2014 Jan 26 ^g	20.8	1.4	Ic
SN 2014bc	...	12:18:57.71	+47:18:11.3	NGC 4258 (SABbc)	29.32 ± 0.05	7.3	0.01	...	2014 May 19.3	3.7	0.1	II
SN 2014bi	SPIRITS 15bx	12:06:02.99	+47:29:33.5	NGC 4096 (SABc)	30.4 ± 0.4	12.1	0.02	4.3	2014 May 31.3	54.4	3.2	IIP
SN 2014df	SPIRITS 14bsc	03:44:23.99	-44:40:08.1	NGC 1448 (SAcd)	31.31 ± 0.05	18.3	0.01	~0	2014 Jun 03.2	121.1	10.7	Ib
ASASSN-14 ha	SPIRITS 15yp	04:20:01.41	-54:56:17.0	NGC 1566 (Sab pec?)	31.1 ± 0.4	16.8	0.01	~0	2014 Sep 10.3	8.6	0.7	II
SN 2014dt	SPIRITS 15sd	12:21:57.57	+04:28:18.5	M61 (SABbc)	31.43 ± 0.07	19.3	0.02	~0	2014 Oct 29.8	40.5	3.8	Iax
SN 2016C	SPIRITS 16ot	13:38:05.30	-17:51:15.3	NGC 5247 (SABc)	31.7 ± 0.4	21.9	0.07	~0.2	2016 Jan 03.8	111.9	11.9	IIP
SN 2016adj	...	13:25:24.11	-43:00:57.5	Cen A (S0 pec)	27.82 ± 0.06	3.7	0.10	0.23	2016 Feb 08.6	40.1	0.7	Ib
SN 2016bau	SPIRITS 16is	11:20:59.02	+53:10:25.6	NGC 3631 (SAc)	31.2 ± 0.4	17.4	0.01	~3.3	2016 Mar 14.0	37.8	3.2	Ib
SN 2016bkv	SPIRITS 17eb	10:18:19.31	+41:25:39.3	NGC 3184 (SABcd)	30.79 ± 0.05	14.4	0.01	0.0	2016 Mar 21.7	30.3	2.1	IIP
SN 2016cok	SPIRITS 17ft	11:20:19.10	+12:58:56.0	M66 (SABb)	29.78 ± 0.07	9.0	0.03	0.16	2016 May 28.5	69.1	3.0	IIP
SN 2017eaw	SPIRITS 18k	20:34:44.24	+60:11:35.9	NGC 6946 (SABcd)	28.73 ± 0.05	5.6	0.30	$\lesssim 0.13$	2017 May 14.2	154.1	4.2	IIP

Notes.

^a SN 2014bc was located near the saturated nucleus of NGC 4258 in the *Spitzer*/IRAC images and not detected in SPIRITS. SN 2016adj itself was saturated in the *Spitzer*/IRAC images of Centaurus A and not recovered by the SPIRITS pipeline.

^b References for distance moduli: NGC 7331, M82, NGC 4254, NGC 4258, Centaurus A, M66 (Tully et al. 2013), NGC 4096, (Sorce et al. 2014), NGC 1448 (Riess et al. 2016), NGC 1566 (Nasonova et al. 2011), M61 and NGC 6946 (Rodríguez et al. 2014), NGC 5247 (Tully 1988), NGC 3631 (Theureau et al. 2007), NGC 3184 (Ferrarese et al. 2000).

^c Galactic extinction estimates taken from NED using the Schlafly & Finkbeiner (2011) recalibration of the Schlegel et al. (1998) IR-based dust map assuming a Fitzpatrick (1999) extinction law with $R_V = 3.1$.

^d References for host extinction estimates: SN 2014C (Milisavljevic et al. 2015), SN 2014J (with $R_V = 1.4$; Amanullah et al. 2014), SN 2014bi (J. Johansson et al. 2019, in preparation), SN 2014dt (Foley et al. 2015), SN 2016adj (with $R_V = 2.57$; Banerjee et al. 2018), SN 2016bkv (Hossein-zadeh et al. 2018), SN 2016cok (Kochanek et al. 2017), SN 2017eaw (Kilpatrick & Foley 2018).

^e References for SN discovery: SN 2014C (Kim et al. 2014), SN 2014J (Fossey et al. 2014), SN 2014L (Zhang et al. 2014), SN 2014bc (Smartt et al. 2014), SN 2014bi (Kumar et al. 2014), SN 2014df (Monard et al. 2014), ASASSN-14 ha (Kiyota et al. 2014), SN 2014dt (Nakano et al. 2014), SN 2016C (Aoki 2016), SN 2016ajd (Marples et al. 2016), SN 2016bau (Arbour 2016), SN 2016bkv (Itagaki 2016), SN 2016cok (Bock et al. 2016), and SN 2017eaw (Wiggins 2017).

^f References for SN classification: SN 2014C (Kim et al. 2014; Milisavljevic et al. 2015), SN 2014J (Cao et al. 2014), SN 2014L (Li et al. 2014), SN 2014bc (Cortini et al. 2014); SN 2014bi (Kumar et al. 2014), SN 2014df (Monard et al. 2014), ASASSN-14 ha (Arcavi et al. 2014), SN 2014dt (Ochner et al. 2014), SN 2016C (Sahu et al. 2016), SN 2016adj (Stritzinger et al. 2016), SN 2016bau (Granata et al. 2016), SN 2016bkv (Hossein-zadeh et al. 2016), SN 2016cok (Zhang et al. 2016), and SN 2017eaw (Cheng et al. 2017).

^g SN present in first 2014 SPIRITS epoch and therefore excluded from the control sample.

Table 3
Spitzer/IRAC Photometry of Luminous, IR Transients in SPIRITS^a

Name	MJD	Phase ^b (days)	$f_{\nu,[3.6]}$ (μ Jy)	$f_{\nu,[4.5]}$ (μ Jy)	[3.6] (Vega mag.)	[4.5] (Vega mag.)	$M_{[3.6]}$	$M_{[4.5]}$
SPIRITS 14azy	56,715.5	−56.5	13.5 ± 1.4	8.1 ± 1.5	18.29 ± 0.11	18.37 ± 0.20	−12.1	−12.1
	56,740.5	−31.5	<23.8	7.4 ± 1.3	>17.7	18.46 ± 0.19	>−12.8	−12.0
	56,864.0	92.0	66.1 ± 1.8	70.3 ± 1.4	16.57 ± 0.03	16.02 ± 0.02	−13.9	−14.4
	57,245.1	473.1	19.9 ± 1.7	16.3 ± 1.4	17.88 ± 0.09	17.60 ± 0.09	−12.6	−12.8
	57,251.0	479.0	18.3 ± 1.6	15.9 ± 1.4	17.96 ± 0.09	17.63 ± 0.10	−12.5	−12.8
	57,271.8	499.8	12.1 ± 1.6	19.7 ± 1.5	18.41 ± 0.14	17.40 ± 0.08	−12.0	−13.0
	57,464.6	692.6	10.3 ± 1.5	11.8 ± 1.8	18.59 ± 0.16	17.96 ± 0.17	−11.8	−12.5
	57,472.0	700.0	<8.2	9.0 ± 1.4	>18.8	18.25 ± 0.17	>−11.6	−12.2
	57,486.0	714.0	<10.7	9.8 ± 1.3	>18.5	18.16 ± 0.14	>−11.9	−12.3
	57,826.1	1054.1	<7.3	<7.9	>19.0	>18.4	>−11.5	>−12.0
	57,974.2	1202.2	<8.2	<6.6	>18.8	>18.6	>−11.6	>−11.9
SN 2014bi ^c (SPIRITS 15bx)	56,737.5	−70.8	<8.9	<9.8	>18.8	>18.2	>−11.6	>−12.2
	56,847.1	38.8	585.3 ± 10.8	453.7 ± 8.4	14.20 ± 0.02	13.99 ± 0.02	−16.2	−16.4
	57,072.5	264.2	11.7 ± 2.1	108.1 ± 2.0	18.45 ± 0.20	15.55 ± 0.02	−11.9	−14.8
	57,076.8	268.5	15.2 ± 2.4	99.1 ± 2.0	18.17 ± 0.17	15.65 ± 0.02	−12.2	−14.8
	57,080.5	272.2	14.1 ± 2.1	99.6 ± 1.8	18.25 ± 0.16	15.64 ± 0.02	−12.2	−14.8
	57,102.2	293.9	15.8 ± 1.9	83.6 ± 1.8	18.12 ± 0.13	15.83 ± 0.02	−12.3	−14.6
	57,253.6	445.3	21.0 ± 1.6	44.4 ± 1.9	17.81 ± 0.08	16.52 ± 0.05	−12.6	−13.9
	57,464.4	656.1	<8.4	17.2 ± 1.7	>18.8	17.55 ± 0.11	>−11.6	−12.9
	57,470.9	662.6	<8.8	18.7 ± 1.5	>18.8	17.46 ± 0.09	>−11.6	−12.9
	57,484.4	676.1	<8.8	18.5 ± 1.4	>18.8	17.47 ± 0.08	>−11.6	−12.9
	57,842.9	1034.6	<8.8	<11.0	>18.8	>18.0	>−11.6	>−12.4
	57,963.7	1155.4	<7.5	<9.1	>18.9	>18.2	>−11.5	>−12.2

Notes.

^a We show measurements for SPIRITS 14azy and SN 2014bi to illustrate the form and content of this table. A full version including all nine objects in each of IR-discovered and optical control samples is published in machine-readable format.

^b Time since t_0 as reported in Table 8 for the IR-discovered sample, and time since discovery as reported in Table 2 for the optical control sample.

^c Measurements through MJD = 57,253.6 were previously reported in Tinianont et al. (2016).

(This table is available in its entirety in machine-readable form.)

between the red and blue sides, and we used a 1'' long slit with the 400/8500 grating on the red side and the 400/3400 grism on the blue side providing the resolution and wavelength coverage given in Table 5. Spectroscopic reductions for LRIS were performed using the analysis pipeline LPIPE²⁶ (Perley 2019). For SPIRITS 17pc, a weak trace is visible at the position of the transient on the red-side camera. For SPIRITS 17qm, there is no obvious continuum trace; however, we detect several emission lines associated with the transient on the red side. No emission was detected on the blue side for either object. The 1D spectra were extracted at these positions along the slit and flux-calibrated using observations of the standard stars G191-B2B and BD +75°325. Our optical spectra of SPIRITS 16tn, SPIRITS 17pc, and SPIRITS 17qm are shown in Figure 3.

For observations with the near-IR spectrographs the target was nodded along the slit between exposures to allow for accurate subtraction of the sky background. Observations of an A0V telluric standard star near the target location were also taken immediately before or after each science target observation for flux calibration and correction of the strong near-IR telluric absorption features. For MOSFIRE, we used a 0''.7 slit with the standard grating/filter setups for each of the *YJHK* spectral regions, providing the wavelength coverage and resolution listed for each observation in Table 5. For GNIRS, we used the cross-dispersed (XD), multiorder mode providing

coverage of the full near-IR spectral region at once, with a 0''.45 slit, 32 line mm^{−1} grating, and the short blue camera with its XD prism, providing an average spectral resolution of $R = 1200$. For FLAMINGOS-2, we use the long-slit mode and the low-resolution *HK* grism with a 3 pixel, 0''.54 slit providing wavelength coverage from 13,500 to 24,000 Å and an average spectral resolution of $R = 600$. NIRES employs a 0''.55 slit and provides wavelength coverage from 9500 to 24,600 Å across five spectral orders at a mean resolution of $R = 2700$.

Reductions for MOSFIRE, including flat-fielding, the wavelength solution, background subtraction, and frame stacking for each object on a given night, were performed with the MOSFIRE Data Reduction Pipeline.²⁷ 1D extractions, where the continuum trace of the target and/or emission lines were visible in the reduced 2D spectra, were performed using standard tasks in IRAF.²⁸ For GNIRS and FLAMINGOS-2 reductions, including detector pattern noise cleaning and radiation event removal (GNIRS only), flat-fielding, background subtraction, spatial distortion corrections (GNIRS only), wavelength calibration, and 1D extractions, we used standard tasks in the Gemini IRAF package following procedures outlined on the Gemini webpage.²⁹ NIRES data

²⁷ <https://keck-datareductionpipelines.github.io/MosfireDRP/>

²⁸ IRAF is distributed by the National Optical Astronomy Observatory, which is operated by the Association of Universities for Research in Astronomy (AURA) under a cooperative agreement with the National Science Foundation.

²⁹ Procedures for reducing GNIRS XD spectra are found at <http://www.gemini.edu/sciops/instruments/gnirs/data-format-and-reduction/reducing-xd-spectra>.

²⁶ Software available at <http://www.astro.caltech.edu/~dperley/programs/lpipe.html>.

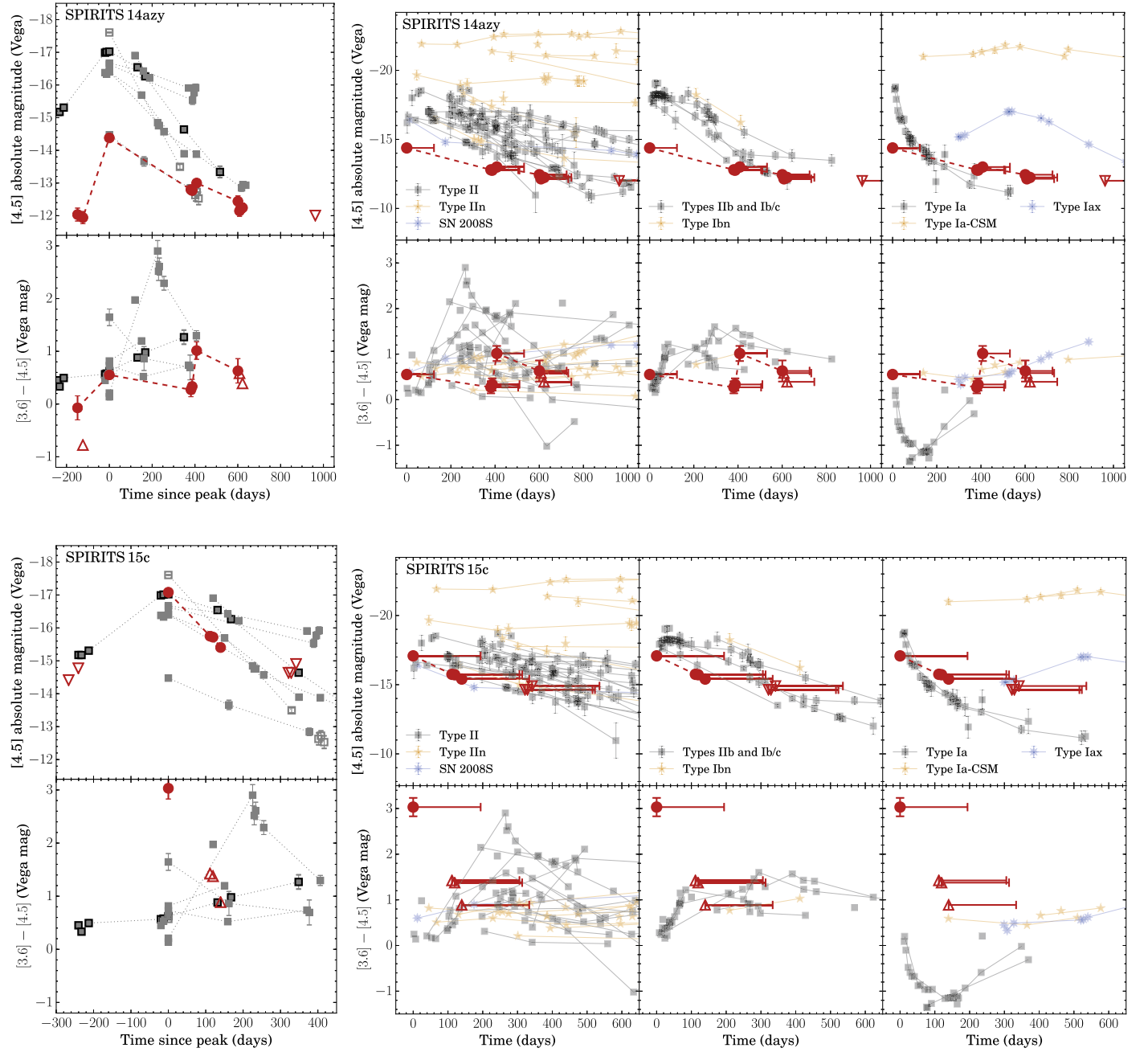


Figure 2. For each luminous IR SPIRITS transient, we show the [4.5] light curve (top row) and [3.6]–[4.5] color curve (bottom row) as the large red circles. In the left panel for each object, the phase is measured in days since the observed IR peak, and we compare to the control sample of optically discovered SNe recovered in SPIRITS as described in Section 2.4, including SNe II (light-gray squares), stripped-envelope SNe Ib (open squares), and the Type Iax SN 2014dt (black outlined squares). In the right panel for each object, we compare to the full sample of SNe detected by *Spitzer* compiled by Szalai et al. (2019), including previous compilations by Szalai & Vinkó (2013), Tinianont et al. (2016), and Johansson et al. (2017), and references therein. Additionally, we include the SNe observed by SPIRITS since 2014 and presented in this work. From left to right, we compare to SNe II (IIn), stripped-envelope SNe IIb and Ib/c (Ibn), and SNe Ia (Ia-CSM) as light-gray squares (orange stars). The blue, eight-pointed stars indicate the prototypical for its class SN 2008S and the unusual, dusty Type Iax SN 2014dt. The phase for comparison SNe is measured as days since discovery, and for obscured SN candidates we represent our uncertainty in the phase of the primary outburst by the horizontal error bars. Upper (lower) limits from nondetections are indicated by open, downward-pointing (upward-pointing) triangles.

were reduced, including flat-fielding, wavelength calibration, background subtraction, and 1D spectral extractions steps, using a version of the IDL-based data reduction package *Spextool* developed by Cushing et al. (2004), updated by M. Cushing specifically for NIRES. Corrections for the strong near-IR telluric absorption features and flux calibrations for spectra from all instruments were performed with the A0V standard-star observations using the method developed by Vacca et al. (2003) implemented with the IDL tools *XTELLCOR*

or *XTELLCOR_GENERAL* developed by Cushing et al. (2004) as part of *Spextool*.

We did not detect any line emission or a discernible continuum trace from the transients in the MOSFIRE spectrum of SPIRITS 15ud, the MOSFIRE 2016 April 16.6 *Y*-band and 2016 May 30.5 *H*-band spectra of SPIRITS 15ade, the MOSFIRE spectrum of SPIRITS 16ix, or the 2017 November 20.6 MOSFIRE spectrum of SPIRITS 17lb. The full sequence of near-IR spectra for which we detected emission from the

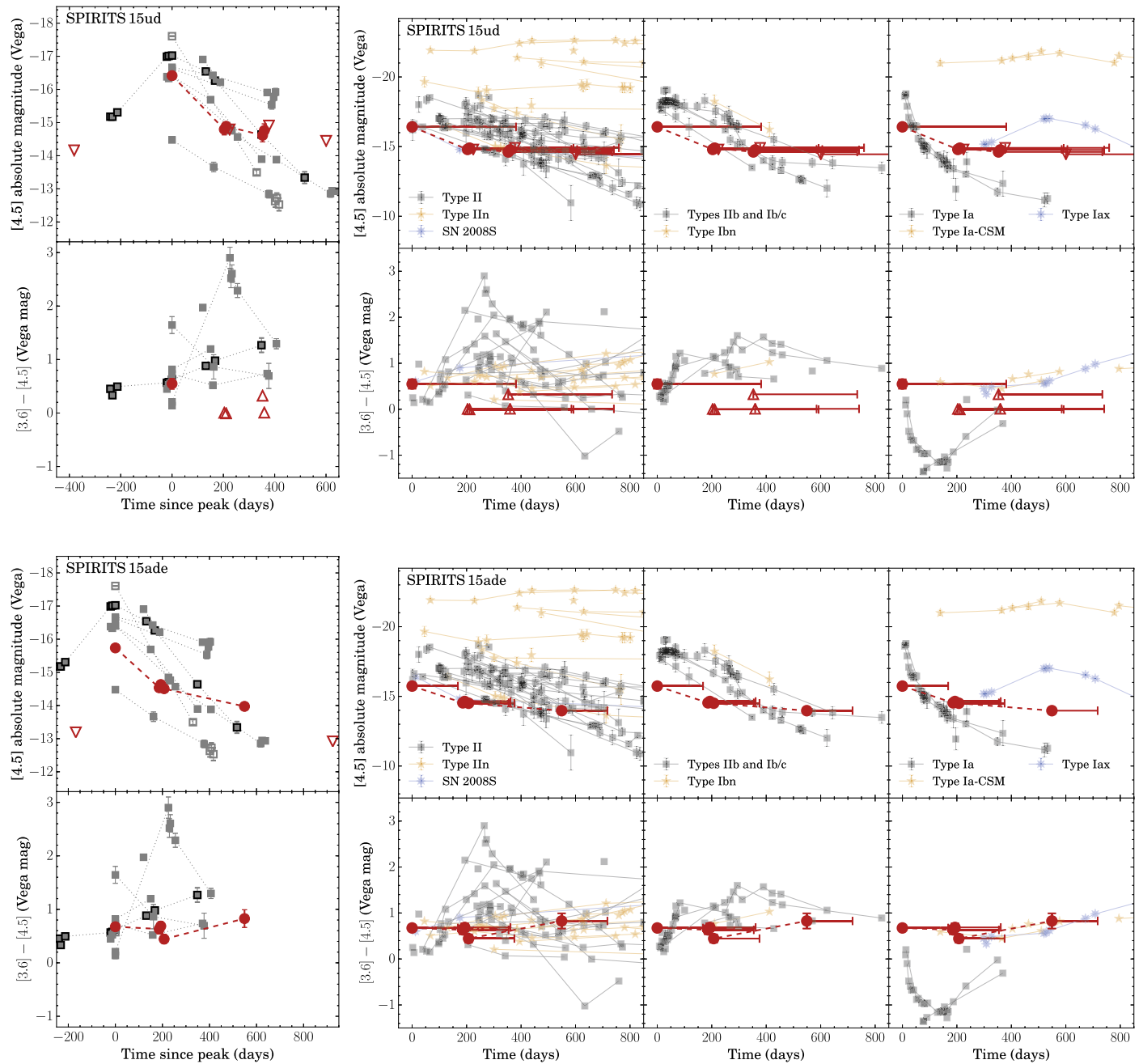


Figure 2. (Continued.)

transient, either a continuum trace or specific emission lines, is shown in Figure 4.

3.4. Radio Observations

We obtained radio continuum imaging observations of each of our luminous IR transients, primarily using the Karl G. Jansky Very Large Array (VLA) between 2017 June and 2018 April in the C, B, and A configurations with 3.4, 11.1, and 36.4 km maximum baselines, respectively (PIDs 16B-388, 17A-365, 17B-331, 18A-418; PI J. Jencson). The bulk of our observations were carried out in 1 hr blocks in C band (6 GHz central frequency) using the full, wide-band capabilities of the upgraded VLA with 3-bit samplers offering 4 GHz bandwidth. For some objects and epochs, we split the block between

multiple bands including the S (3 GHz central frequency, 2 GHz bandwidth with 8 bit samplers), X (10 GHz central frequency, 4 GHz bandwidth), and Ku bands (15.5 GHz central frequency, 4 GHz bandwidth). Each observing block included observations of the VLA standard calibrators 3C 286 or 3C 138 for calibration of the flux density scale and instrument bandpass. For complex gain calibrations, we took observations of a nearby calibrator source, cycling between the calibrator and science target at sufficient intervals for the given array configuration and observing frequency based on recommendations in the VLA observing guide.³⁰

³⁰ VLA calibration information available here: <https://science.nrao.edu/facilities/vla/docs/manuals/obsguide/calibration>.

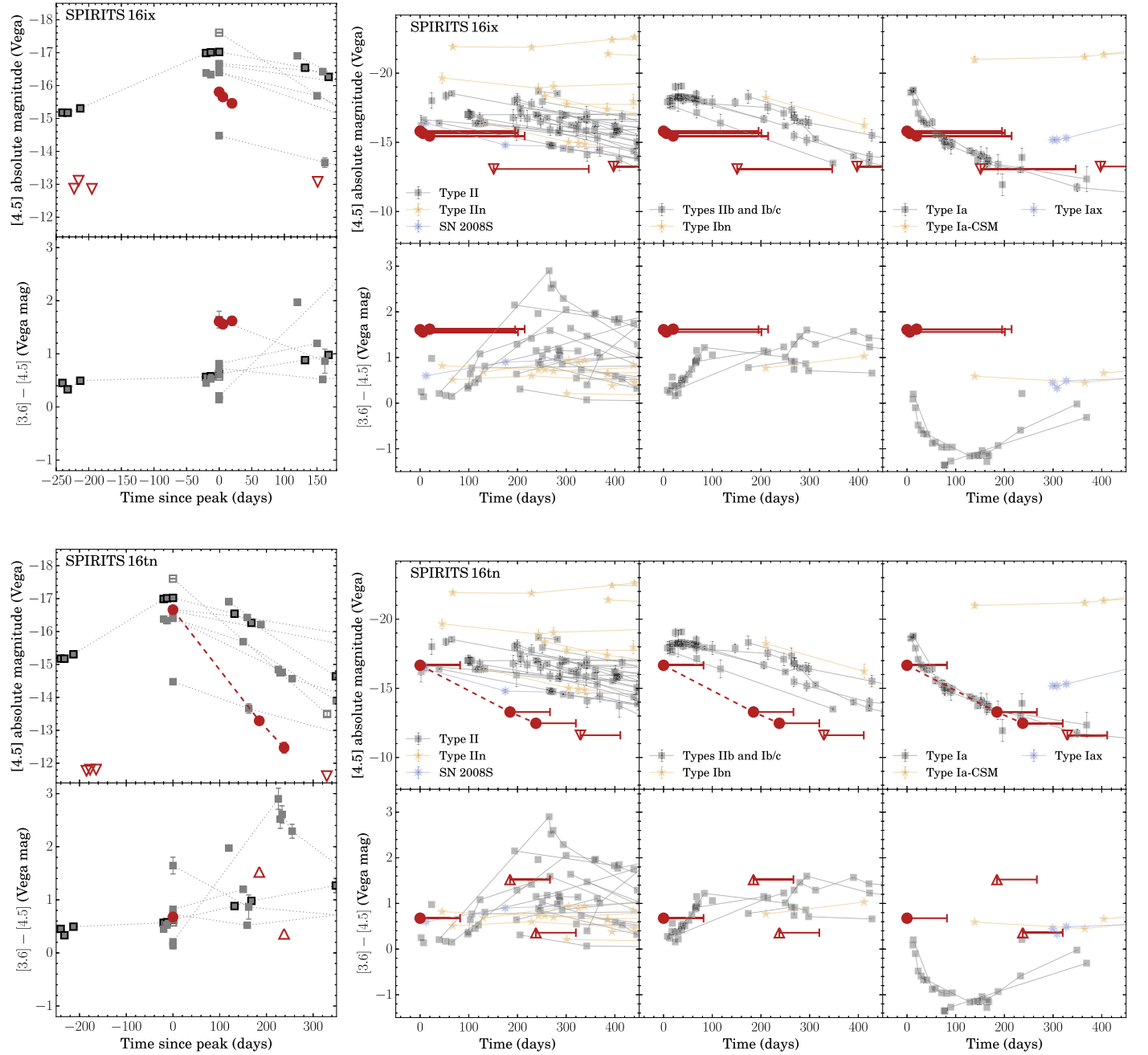


Figure 2. (Continued.)

We also analyzed the 2016 February 19 observations of IC 2163 targeting the unrelated event SN 2010jp, but fortuitously covering the sites of SPIRITS 14buu, SPIRITS 15c, and SPIRITS 17lb (PID 16A-101; PI C. Kilpatrick). These observations used the 8-bit sampler setup providing 2×1 GHz bandwidth tuned to the ranges 4.5–5.5 GHz and 6.9–7.9 GHz in C band and 8.0–9.0 GHz and 10.5–11.5 GHz in X band.

The data for each observation were run through the VLA CASA calibration pipeline,³¹ suitable for automated flagging and calibration of Stokes I continuum data sets. The calibrated data were carefully inspected, and additional flagging and recalibration were performed as necessary. We imaged our data

using the standard CLEAN task in CASA. First-pass images of SPIRITS 17pc in NGC 4388 were limited in sensitivity owing to artifacts from residual phase errors of the bright nucleus of the host, a known Seyfert 2 active galactic nucleus. We performed self-calibration of the visibility phases on the nucleus, which significantly improved the final images, reaching near the theoretical thermal noise sensitivity for our observations.

We inspected the location of the transients in each image for the presence of a coincident point source and report our flux measurements with 1σ errors, estimated as the rms noise in a relatively clean region of the image, in Table 6. In several cases, the location of the transients suffered significant contamination from extended emission from the host galaxy or nearby star-forming regions, particularly in the lower-

³¹ <https://science.nrao.edu/facilities/vla/data-processing/pipeline/scripted-pipeline>

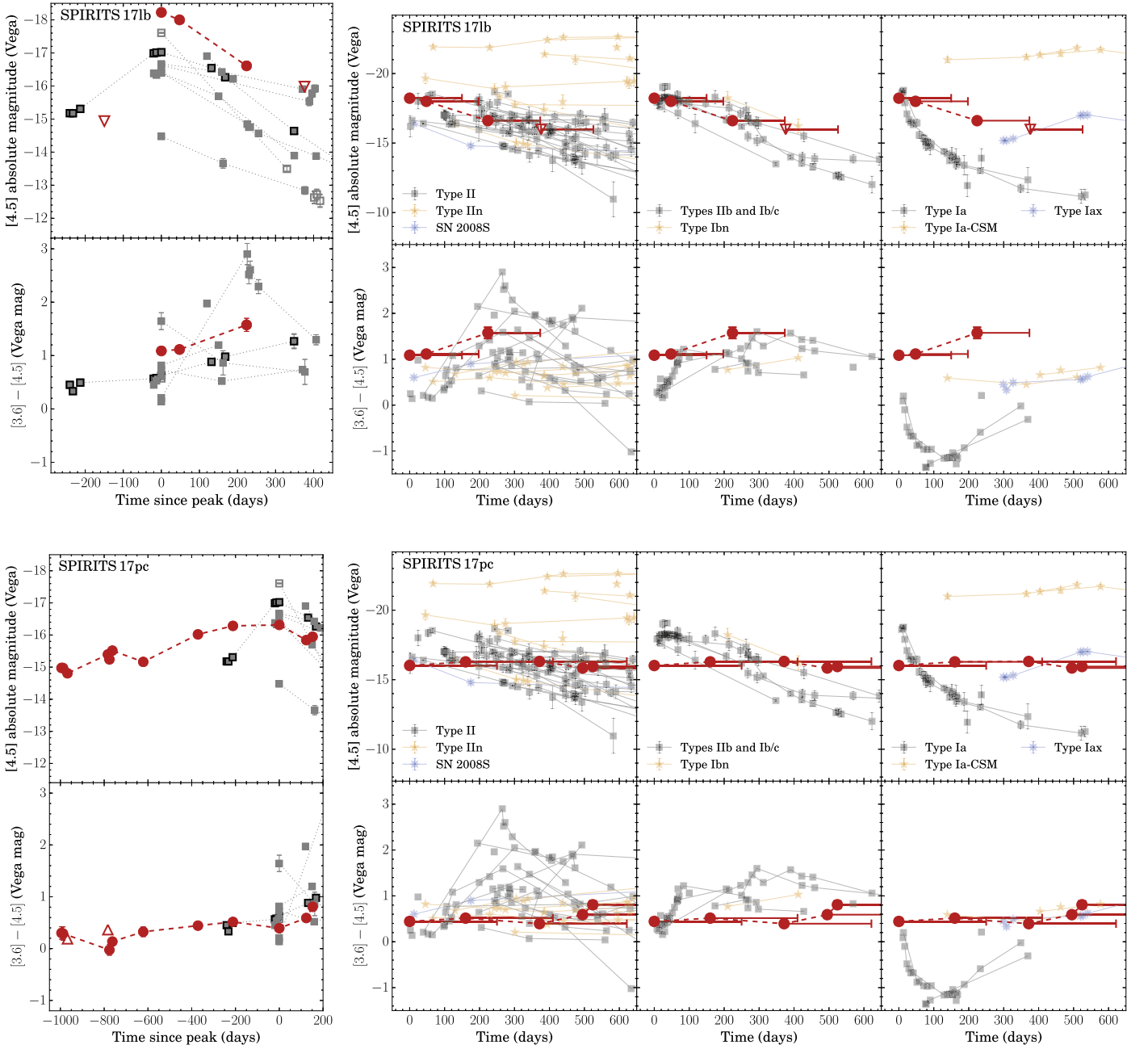


Figure 2. (Continued.)

resolution *C*-configuration observations. For nondetections or when possible emission from the transient cannot be distinguished from background contamination, we report upper limits on the transient flux as either 5σ ($5 \times$ image rms), or the level of the contaminating flux at the location plus $2 \times$ image rms, whichever is larger.

Specifically for the 2016 February 19.1 *C*-band measurement of SPIRITS 15c, a source is clearly detected at the position and has faded significantly in the subsequent image on 2017 June 10.8 (taken in the same configuration with similar resolution), confirming its association with the transient. We note, however, that possible residual emission from the transient in the later epoch is blended with a nearby, somewhat extended contaminating source. We adopt the flux at the transient location as an estimate of the maximum contamination for our previous

measurement and adopt this as a lower bound on the flux in Table 6. In the subsequent epochs in the larger B and A configurations, the contaminating emission appears resolved out, and the radio counterpart to SPIRITS 15c is clearly detected as a relatively isolated, fading point source.

Radio observations of SPIRITS 16tn were also obtained with the Arcminute Microkelvin Image Large Array (AMI-LA), which were previously reported in Jencson et al. (2018d). Additional observations of IC 2163 containing SPIRITS 14buu, SPIRITS 15c, and SPIRITS 17lb were obtained with the Australia Telescope Compact Array (ATCA) over 6 hr on 2017 September 4 at 9.0 and 5.5 GHz simultaneously. The ATCA primary flux calibrator, PKS B1934–638, was used to set the absolute flux scale, as well as define the bandpass calibration in each 2 GHz band. Frequent observations of the nearby source PKS 0606–223

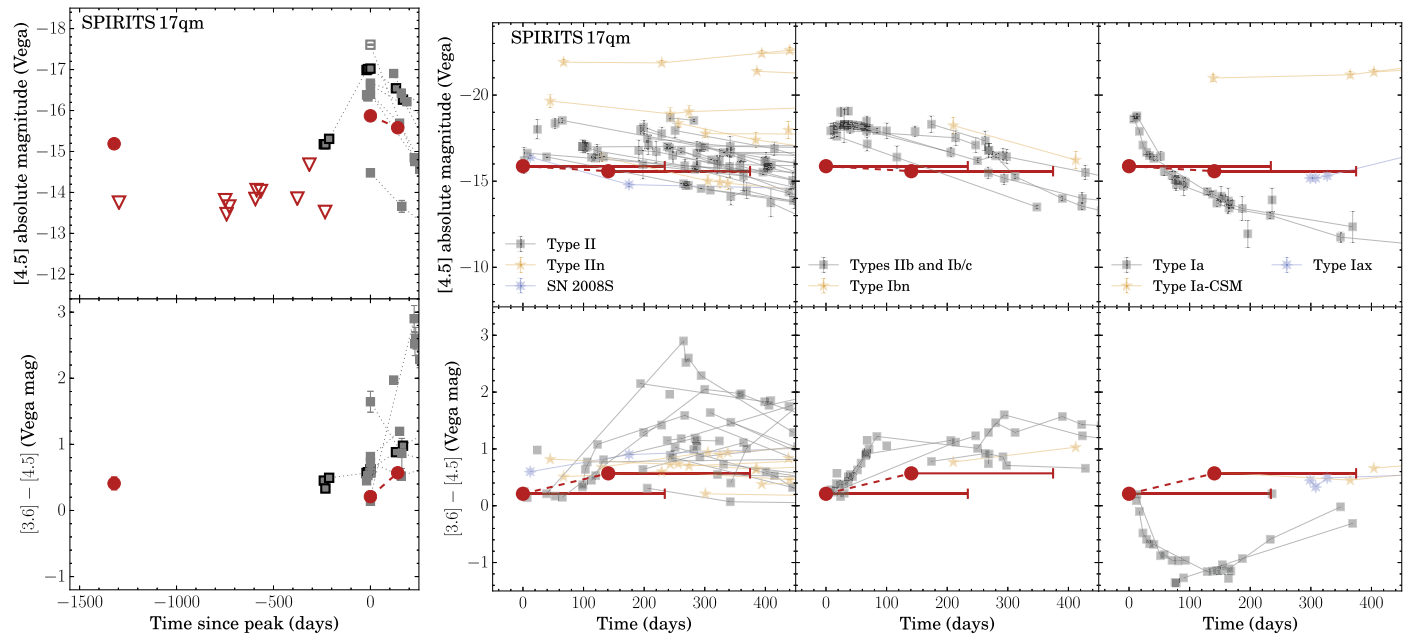


Figure 2. (Continued.)

allowed us to monitor and correct for variations in gain and phase throughout each run. The data were processed using the Miriad package (Sault et al. 1995) and using procedures outlined in Section 4.3 of the ATCA User Guide.³² After editing and calibrating the data, images at each frequency were made using robust weighting (robust = 0.5) and then cleaned down to $3\times$ the rms noise level. No point sources exactly matching the locations of these three SNe were evident at either frequency within the clumpy disk structure. Fitting a Gaussian point source to the nearest peak of emission in each case yielded the upper limits on flux densities shown in Table 6.

3.5. Limits from Wide-field Optical Surveys

We obtained limits on the optical emission from SPIRITS transients that were fortuitously covered by the intermediate Palomar Transient Factory (iPTF) survey during their outbursts in the g , R , and/or i filters. The iPTF operated from 2013 January 1 to 2017 March 2 using a wide-field camera with a 7.26 deg^2 field of view on the 48-inch Samuel Oschin Schmidt Telescope at Palomar Observatory (P48). During its operation, iPTF images were processed through a real-time image subtraction pipeline (Cao et al. 2016) to search for transients and variables. We ran forced PSF photometry at the locations of our SPIRITS transients on iPTF reference-subtracted images using the PTF IPAC/iPTF Discovery Engine (PTFIDE) tool (Masci et al. 2017). To obtain deeper constraints, we stacked limits from individual observations within 10-day windows. Constraints on the optical emission from our sample transients from the iPTF are included in Figure 12.

4. Analysis

4.1. Host Environments and Archival Imaging

The host galaxy morphological types (obtained from NED) of our sample of IR-selected transients are given in Table 1. With the exception of SPIRITS 16ix in the lenticular SB0⁺

galaxy NGC 4461, these events were found in late-type, star-forming galaxies. Similarly, the entire control sample of optically discovered SNe was also found in star-forming galaxies (Table 2). In Figure 5, we indicate the locations of the IR-selected transients in the Digitized Sky Survey 2 (DSS2) images of their host galaxies, showing a clear trend of positional associations with the active star-forming regions of the hosts' spiral arms. This indicates a likely physical association of the bulk of the sample to ongoing star formation and young, massive stars. Of particular note, SPIRITS 15ade was discovered in the outskirts of NGC 5921 at a projected distance from the galaxy center of $146''.3$ (17.0 kpc), while SPIRITS 15ud was found very near the nucleus of M100 at a projected distance of only $7''.5$ (0.5 kpc).

We examined the location of each source in the IR-selected sample in the archival *Spitzer*/IRAC [3.6] and [4.5] reference images for the presence of possible IR progenitor stars. The regions near the objects in our sample were typically crowded by several sources or dominated by the bright, spatially variable background emission from the host galaxy. To identify possible progenitors, we constructed source catalogs and performed PSF photometry for each *Spitzer*/IRAC reference image using the DAOPHOT/ALLSTAR package (Stetson 1987), where a model of the PSF was constructed using isolated stars in the image. The PSF-fitting and photometry procedure, including corrections for the finite radius of the PSF (using the method of Khan 2017), is described in Karambelkar et al. (2019).

With the exception of SPIRITS 17qm, there are no sources in our catalogs consistent with the transient positions in *Spitzer*/IRAC reference images. We estimate upper limits on the progenitor flux as 5 times the standard deviation in a 25×25 pixel box at the transient position. The limits at [3.6] and [4.5] on the progenitor flux of each object in our sample are given in Table 7.

For SPIRITS 17qm, we identified a source in the [3.6] and [4.5] reference image PSF catalogs of NGC 1365, separated from the location of the transient by only $0''.12$ and $0''.24$,

³² http://www.narrabri.atnf.csiro.au/observing/users_guide/html/atug.html

Table 4
Supplementary Photometry^a

Name	MJD	Phase ^b (days)	Tel./Inst.	Band	Apparent Mag.	Absolute Mag. ^c
SPIRITS 14azy	56,772.0	0.0	Swope/CCD	<i>g</i>	21.94 ± 0.47	−8.8
	56,772.0	0.0	Swope/CCD	<i>r</i>	20.49 ± 0.18	−10.2
	56,772.0	0.0	Swope/CCD	<i>i</i>	19.81 ± 0.18	−10.8
	56,804.0	32.0	Swope/CCD	<i>g</i>	20.04 ± 0.10	−10.7
	56,804.0	32.0	Swope/CCD	<i>r</i>	19.02 ± 0.06	−11.7
	56,804.0	32.0	Swope/CCD	<i>i</i>	18.73 ± 0.06	−11.9
	56,828.0	56.0	Swope/CCD	<i>g</i>	20.79 ± 0.27	−10.0
	56,828.0	56.0	Swope/CCD	<i>r</i>	19.63 ± 0.10	−11.0
	56,828.0	56.0	Swope/CCD	<i>i</i>	19.20 ± 0.10	−11.4
	56,829.0	57.0	Swope/CCD	<i>g</i>	21.09 ± 0.19	−9.7
	56,829.0	57.0	Swope/CCD	<i>r</i>	19.69 ± 0.07	−11.0
	56,829.0	57.0	Swope/CCD	<i>i</i>	19.17 ± 0.07	−11.4
	56,996.8	224.8	du Pont/RetroCam	<i>H</i>	19.83 ± 0.05	−10.6
	57,053.7	281.7	du Pont/RetroCam	<i>H</i>	20.32 ± 0.19	−10.2
	57,066.7	294.7	du Pont/RetroCam	<i>H</i>	20.11 ± 0.19	−10.4
	57,069.7	297.7	Baade/FourStar	<i>J</i>	21.11 ± 0.27	−9.4
	57,069.7	297.7	Baade/FourStar	<i>K_s</i>	18.58 ± 0.27	−11.9
	57,089.7	317.7	du Pont/RetroCam	<i>H</i>	20.42 ± 0.22	−10.1
	57,115.6	343.6	du Pont/RetroCam	<i>H</i>	20.41 ± 0.11	−10.1

Notes.

^a We show measurements for SPIRITS 14azy to illustrate the form and content of this table. A full version including all of our supplementary photometry is published in machine-readable format.

^b Time since t_0 as reported in Table 8 for the IR-discovered sample.

^c Absolute magnitudes corrected for Galactic extinction to the host from NED.

(This table is available in its entirety in machine-readable form.)

respectively, less than one IRAC mosaicked pixel. However, we note that this source is heavily blended with several other sources in our catalogs, and its centroid is slightly offset from the optical progenitor star identified in archival *HST* imaging below. While the coincident IR PSF catalog sources likely contain flux from the progenitor, we consider the PSF magnitudes given in Table 7 as upper limits given the possibility of significant contamination from nearby sources.

We also examined the available archival *HST* imaging for each source in our sample. To determine the precise locations of our transients in the archival *HST* frames, we registered the archival images with a detection image of the transient, usually a *Spitzer*/IRAC image where the transient is strongly detected. We used higher-resolution images of the active transients where they were available and where registration with *Spitzer* frames was insufficient to determine a precise location of the transient. To perform the registrations, we used centroid measurements of several (at least 10) relatively isolated, bright stars detected in both frames. We then determined the geometric transformations from the archival *HST* frame to the frame containing the transient using the Space Telescope Science Data Analysis System (STSDAS)³³ GEOMAP task. By applying the GEOTRAN task to the archival frames and blinking these transformed images against the transient detection images, we verified the quality of the registrations. We then examined the precise location of each transient in the available archival frames to search for the presence of a possible progenitor star.

For SPIRITS 15c and SPIRITS 16tn, we discussed the limits we obtained on their progenitors from this procedure in

Jencson et al. (2017, 2018d). We obtained precise registrations of the *HST*/WFPC2 F555W and F814W images taken 1998 November 11.7 with program GO-6483 (PI: D. Elmegreen) using a Baade/IMACS WB6226-7171 image of SPIRITS 15c from 2015 January 20.0. We derived 5σ limiting magnitudes on the progenitor of $V > 25.1$ and $I > 24.0$, corresponding to limits on the absolute magnitude of the progenitor of $M_V > -7.9$ and $M_I > -8.9$, correcting for Galactic extinction to IC 2163 only. We constrained the flux from the progenitor of SPIRITS 16tn to $V \gtrsim 24.5$ in an archival WFPC2/WFC F606W frame from 1994 July 4.8 (PID SNAP-5446; PI: G. Illingworth), corresponding to limits on the absolute magnitude of $M_V > -5.2$ (correcting for Galactic extinction only; $L < 2.9 \times 10^4 L_\odot$ for a red supergiant [RSG] progenitor of spectral type M0); however, the limit is not constraining for an SN II progenitor if one assumes heavy extinction of $A_V \sim 8$ as was inferred for SPIRITS 16tn in Jencson et al. (2018d) based on the optical/near-IR SED of the transient.

The location of SPIRITS 14azy was imaged with WFC3/UVIS in the F336W filter on 2010 October 28.8 with program SNAP-12229 (PI L. Smith), nearly 4 yr before the discovery of the transient, which we registered with the *Spitzer*/IRAC [4.5] discovery image of the transient. The rms uncertainty in the registration is 0.9 WFC3 pixels (0''036) in both the x - and y -directions. As shown in Figure 6, the location is within an apparent dust lane, completely devoid of stars consistent with the transient position. The limiting magnitude in the image is $U \gtrsim 25.5$, which we adopt as a limit on the progenitor flux, corresponding to a limit on the absolute magnitude of the progenitor star of $M_U \gtrsim -5.4$ (Galactic extinction correction only).

³³ STSDAS is a product of STScI, which is operated by AURA for NASA.

Table 5
Spectroscopic Observations

Name	UT Date	MJD	Phase (days)	Tel./Instr.	Range (Å)	Resolution ($\lambda/\delta\lambda$)	Integration
SPIRITS 15c	2015 Mar 14.1	57,095.1	204.7	Baade/FIRE	8000–24000	300–500	4×120 s
	2015 Mar 31.2	57,112.2	221.8	Keck I/MOSFIRE	9700–11100	3400	8×180 s
	2015 Mar 31.3	57,112.3	221.9	Keck I/MOSFIRE	11400–13100	3300	6×120 s
	2015 Mar 31.3	57,112.3	221.9	Keck I/MOSFIRE	14500–17500	3700	10×120 s
	2015 Mar 31.3	57,112.3	221.9	Keck I/MOSFIRE	19500–23500	3600	6×180 s
SPIRITS 15ud	2015 Sep 19.3	57,284.6	394.2	Keck I/MOSFIRE	9700–11100	3400	10×180 s
	2016 Jan 23.6	57,410.6	138.9	Keck I/MOSFIRE	19500–23500	3600	12×180 s
SPIRITS 15ade	2016 Jan 23.6	57,410.6	134.1	Keck I/MOSFIRE	19500–23500	3600	30×180 s
	2016 Apr 16.6	57,494.6	218.1	Keck I/MOSFIRE	9700–11100	3400	2×180 s
	2016 Apr 16.6	57,494.6	218.1	Keck I/MOSFIRE	11400–13100	3300	10×120 s
	2016 May 30.5	57,538.5	262.0	Keck I/MOSFIRE	14500–17500	3700	6×120 s
SPIRITS 16ix	2016 Apr 16.5	57,494.5	16.6	Keck I/MOSFIRE	19500–23500	3600	10×180 s
SPIRITS 16tn	2016 Nov 2.6	57,694.6	79.5	Keck I/LRIS	3500–6000	600	1800 s
	2016 Nov 2.6	57,694.6	79.5	Keck I/LRIS	5500–10300	1000	2×860 s
	2016 Dec 29.5	57,751.5	136.4	Gemini N/GNIRS	8500–25000	1200	14×300 s
	2017 Jan 9.6	57,762.6	147.5	Gemini N/GNIRS	8500–25000	1200	10×300 s
SPIRITS 17lb	2017 Sep 28.6	58,024.6	122.9	Keck I/MOSFIRE	19500–23500	3600	24×180 s
	2017 Nov 1.3	58,058.3	156.6	Gemini S/FLAMINGOS-2	13500–24000	600	24×150 s
	2017 Nov 20.6	58,077.6	175.9	Keck I/MOSFIRE	11400–13100	3300	6×120 s
	2017 Nov 20.6	58,077.6	175.9	Keck I/MOSFIRE	19500–23500	3600	8×180 s
SPIRITS 17pc	2017 Nov 11.6	58,071.6	192.8	Keck I/LRIS	3500–6000	600	1200 s
	2017 Nov 11.6	58,071.6	192.8	Keck I/LRIS	5500–10300	1000	2×560 s
	2017 Nov 20.6	58,077.6	198.8	Keck I/MOSFIRE	9700–11100	3400	6×180 s
	2017 Nov 20.7	58,077.7	198.9	Keck I/MOSFIRE	19500–23500	3600	4×180 s
	2017 Dec 7.6	58,094.6	215.8	Gemini N/GNIRS	8500–25000	1200	4×180 s
	2017 Dec 8.6	58,095.6	216.8	Gemini N/GNIRS	8500–25000	1200	8×180 s
	2017 Dec 11.6	58,098.6	219.8	Gemini N/GNIRS	8500–25000	1200	12×180 s
	2018 Jan 8.5	58,126.5	247.7	Keck I/MOSFIRE	9700–11100	3400	6×180 s
	2018 Jan 8.6	58,126.6	247.8	Keck I/MOSFIRE	11400–13100	3300	6×120 s
	2018 Jan 8.6	58,126.6	247.8	Keck I/MOSFIRE	14500–17500	3700	6×120 s
	2018 Jan 8.6	58,126.6	247.8	Keck I/MOSFIRE	19500–23500	3600	6×180 s
	2018 May 4.4	58,242.4	363.6	Keck II/NIRES	9500–24600	2700	6×300 s
SPIRITS 17qm	2017 Nov 11.5	58,071.5	9.3	Keck I/LRIS	3500–6000	600	2×1200 s
	2017 Nov 11.5	58,071.5	9.3	Keck I/LRIS	5500–10300	1000	4×560 s
	2017 Nov 20.5	58,077.5	15.3	Keck I/MOSFIRE	9700–11100	3400	14×180 s
	2018 Jan 8.2	58,126.2	64.0	Keck I/MOSFIRE	9700–11100	3400	8×180 s
	2018 Jan 8.3	58,126.3	64.1	Keck I/MOSFIRE	11400–13100	3300	12×120 s
	2018 Jan 8.3	58,126.3	64.1	Keck I/MOSFIRE	14500–17500	3700	12×120 s
	2018 Jan 8.3	58,126.3	64.1	Keck I/MOSFIRE	19500–23500	3600	10×180 s

SPIRITS 15ud is located near the nucleus of M100 and was covered in several bands at several epochs with *HST*/WFPC2 and WFC3. We selected the WFC3/UVIS F775W image from 2001 November 12.1 (PID GO-11646; PI A. Crotts) for registration with the *Spitzer*/IRAC [4.5] discovery image, for which we obtained an rms uncertainty on the position of the transient of 0.84 WFC3 pixels ($0''.034$). The transient is located in a prominent, nearly opaque dust lane (see Figure 6), and we detect no source consistent with the transient position to a limiting depth of $I \gtrsim 24.5$ ($M_I \gtrsim -6.3$; Galactic extinction only). We also examined this position in the ACS/HRC F814W frame from 2005 May 31.0 (PID GO-9776; PI D. Richstone), deriving a limit on the flux from the progenitor of $I \gtrsim 24.4$ ($M_I \gtrsim -6.4$).

SPIRITS 17lb is located near the edge of the southern spiral arm of IC 2163, with possible extinction by the foreground spiral arm of the companion galaxy NGC 2207. This location was covered in WFC3/UVIS F625W and F814W images taken on 2012 December 4.5 (PID SNAP-13029; PI A. Filippenko).

We selected the F814W image for registration with the *Spitzer*/IRAC [4.5] discovery image, for which we obtained an rms uncertainty of 0.94 WFC3 pixels ($0''.038$). The transient location is coincident with a patch of unresolved, diffuse starlight, characterized by variable extinction in the vicinity. The limits on the progenitor flux from these images are $I \gtrsim 26.2$ and $R \gtrsim 26.8$, corresponding to limits in absolute magnitude of $M_I \gtrsim -8.9$ and $M_R \gtrsim -9.4$.

We reported on the analysis of the WFC3/UVIS and IR frames covering the site of SPIRITS 17pc and SPIRITS 17qm in Jencson et al. (2018a, 2018b), respectively. The site of SPIRITS 17pc was covered in WFC3/UVIS and IR F336W, F438W, F814W, F110W, and F160W images taken on 2011 June 8 (PID GO-12185; PI J. Greene). We registered the F110W frame with a high-resolution, *J*-band image taken with the Keck II/NIRC2 adaptive optics image of the active transient from 2017 December 8.6, obtaining a registration rms uncertainty of 0.15 WFC3 pixels ($0''.02$). There are several blended sources near the location of SPIRITS 17pc in the

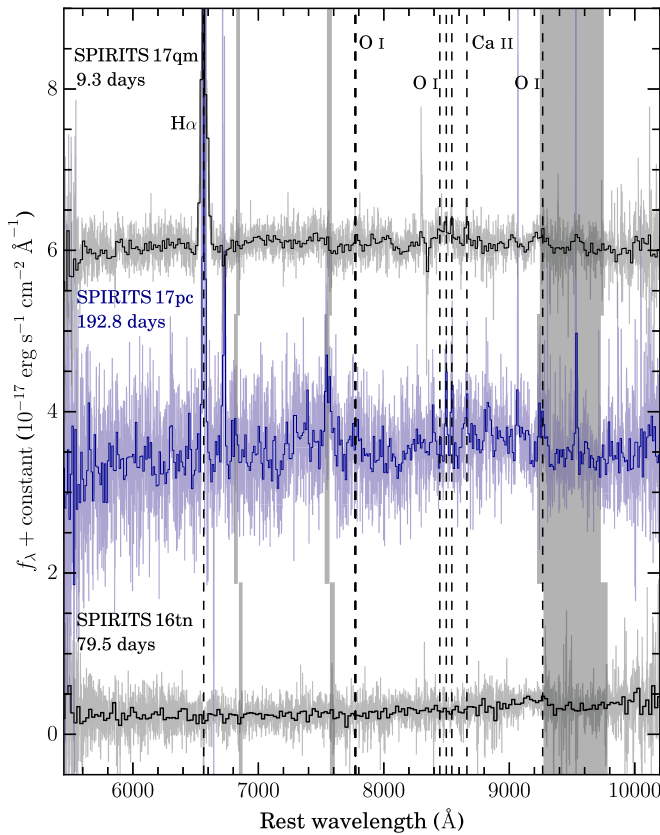


Figure 3. Optical spectroscopy from Keck I/LRIS of SPIRITS 16tn, SPIRITS 17pc, and SPIRITS 17qm in alternating colors and offset in flux by an arbitrary constant so that spectra for each object may be easily distinguished. Spectra are labeled for each object along with their respective phases along the left side of the figure. Data are shown in light gray or light blue, with binned data for each object overplotted in black or dark blue, respectively. Regions contaminated by telluric absorption are indicated by the light-gray vertical bands. Atomic emission features detected in the spectra, including broad $\approx 1000 \text{ km s}^{-1}$ $\text{H}\alpha$ and lines of O I in SPIRITS 17qm and the Ca II IR triplet in SPIRITS 17qm and SPIRITS 17pc, are indicated by the dashed black vertical lines and labeled near the top of the figure.

(The data used to create this figure are available.)

WFC3 frames. We analyzed the sources near the location using PSF-fitting photometry with DOLPHOT (Dolphin 2000, 2016). We identify a source consistent with the precise transient position and rated as a “good star” by DOLPHOT in the F814W, F110W, and F160W images. There is coincident emission in the F336W and F438W frames, but it is not point-like and is blended with nearby objects. Our PSF photometry from DOLPHOT on the candidate progenitor gives $F336W > 26.06$ mag, $F438W > 26.18$ mag, $F814W = 24.21 \pm 0.05$ mag, $F110W = 21.76 \pm 0.04$ mag, and $F160W = 20.60 \pm 0.02$ mag. At the distance to NGC 4388, the photometry can be well fit by a single blackbody component of $T = 1900 \pm 100$ K and $L = 2.1^{+0.4}_{-0.3} \times 10^5 L_{\odot}$.

There are two epochs of WFC2 F606W images taken on 2001 March 8.3 and 2001 June 9.1 (PID SNAP-8597; PI M. Regan) covering the site of SPIRITS 17qm. We registered the first WFC2 image with the *Spitzer*/IRAC [3.6] discovery image and obtained an rms uncertainty of 3.0 WFC2 pixels ($0''.3$). As shown in Figure 6, there is a single, isolated point source consistent with the location of SPIRITS 17qm in both

WFC2 frames. We obtained magnitudes from the Hubble Legacy Archive source catalogs of $V = 22.45$ (2001 March 8) and $V = 20.77$ (2001 June 9), indicating that the source is highly variable and brightened by ≈ 1.7 mag during the 3 months between the two epochs. The absolute magnitudes then are $V \approx -9.3$ and -11.0 for each epoch, respectively, indicating that the star is highly luminous. While the localization of SPIRITS 17qm in the WFC2 frames is coarse, the marked variability of the coincident star strongly suggests a physical association.

There is no archival *HST* imaging available for the sites of SPIRITS 15ade in NGC 5921 or SPIRITS 16ix in NGC 4461.

4.2. Spitzer Light Curves

The [4.5] light curves and [3.6]–[4.5] color curves of the IR-selected obscured SN candidate sample are shown in Figure 2. In the left panel for each object, we compare to those of the optically discovered control sample. We define zero phase in a uniform way for each object across both samples as the time of peak brightness in the *Spitzer*/IRAC bands. For SN 2017eaw, we adopt 2017 September 13.6 as the observed time of peak brightness; however, the SN was saturated in the images taken on this date, and we do not have a reliable flux measurement of the peak.

The [4.5] light curves of the IR-selected sample appear broadly similar to those of the control sample, usually showing a luminous initial peak and subsequent fade over a timescale of ≈ 200 –600 days. SPIRITS 17pc and SPIRITS 17qm represent notable exceptions, as both sources underwent previous luminous IR outbursts, up to nearly 1500 days before the observed peak in the case of SPIRITS 17qm. While both sources have begun to decline in IR brightness since their discovery, we will continue to monitor their IR with *Spitzer* throughout Cycle 14 ending in 2020 January.

The [3.6]–[4.5] color curves are also qualitatively similar between the two samples. Most objects are found with red colors between $0 \lesssim [3.6] - [4.5] \lesssim 1$ throughout their evolution, with a few events achieving even redder colors up to ≈ 3 mag. The reddest object we observe is SPIRITS 15c with $[3.6] - [4.5] = 3.0 \pm 0.2$ at the time of the observed IR peak, rivaled by SN 2014bi with $[3.6] - [4.5] = 2.9 \pm 0.2$ at 225.5 days post-peak.

We can make a more quantitative comparison between the IR-selected and optically selected control samples based on properties derived from the [3.6] and [4.5] light curves. In Figure 7, we show histograms for both samples of their peak absolute magnitudes at [4.5], $M_{[4.5],\text{peak}}$, their [3.6]–[4.5] colors at peak, and the characteristic fade timescales of their [4.5] light curve, $t_{\text{fade},[4.5]}$, defined as the time in days for the light curve to decline by 1 mag from a linear (in magnitudes) fit to the post-peak light curve. These properties for IR-selected events are also summarized in Table 8.

Both samples span a range in peak [4.5] luminosity, $M_{[4.5],\text{peak}}$, between -14 and -18.5 . The distributions in $M_{[4.5],\text{peak}}$ appear similar, with both peaking between ≈ -16.3 and -17.4 . We note that there is a larger fraction of low-luminosity events in the IR-selected sample, i.e., three of nine objects ($\approx 33\%$) have $M_{[4.5],\text{peak}}$ fainter than -16 , while there is only one such object of eight ($\approx 13\%$) in the control sample. In [3.6]–[4.5] color at peak, the two samples again show similar distributions that peak in the range $0.0 \lesssim [3.6] - [4.5] \lesssim 0.9$ with one-sided tails extending to redder colors. Finally, in the

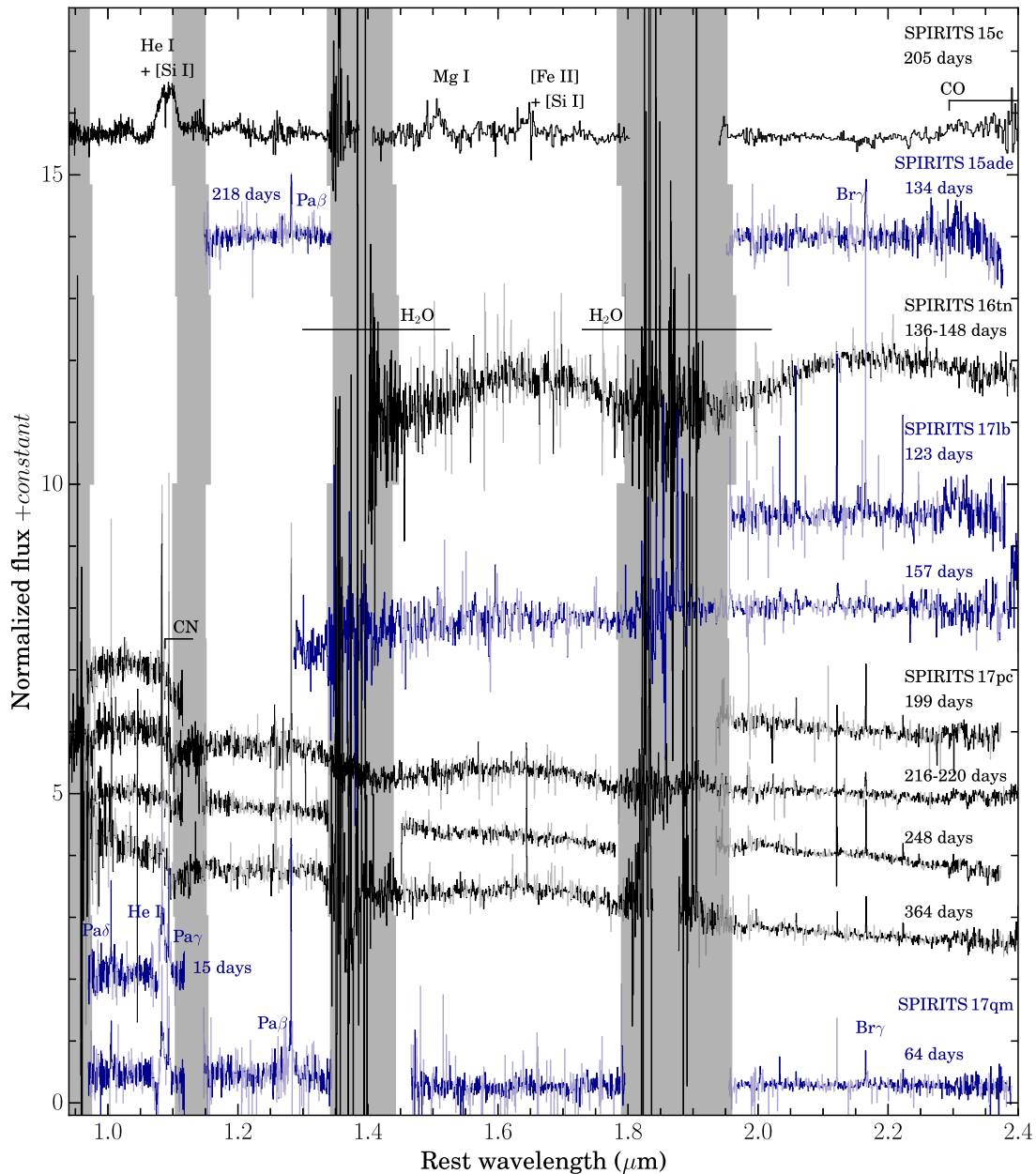


Figure 4. Full sequence of near-IR spectra obtained for the SPIRITS luminous IR transient sample. Spectra correspond to the objects and phases (measured from t_0 as in Table 8) listed along the right side of the figure, shown in alternating colors so that spectra for separate objects may be easily distinguished. The spectra for each object are shifted to the rest side of their respective host galaxies, and regions of low S/N due to coincidence with OH airglow emission lines are shown in lighter colors. The spectra have been scaled in flux and shifted by arbitrary constants for clarity. The major features identified in each spectrum and discussed in the text are labeled, including the SN Ib/Iib emission features in the spectrum of SPIRITS 15c, the $\sim 200 \text{ km s}^{-1}$ width emission lines of H I in the spectra of SPIRITS 15ade, the possible broad H₂O absorption features in the spectrum of SPIRITS 16tn, the broader $\sim 2000 \text{ km s}^{-1}$ features of H I and He I in the spectrum of SPIRITS 17qm, and the CO $\delta v = 2$ vibrational transition band heads detected in the spectra of SPIRITS 15c, SPIRITS 17lb, and SPIRITS 17pc.

(The data used to create this figure are available.)

distributions of $t_{\text{fade},[4.5]}$, we once again note the broad similarity between the two samples. The distributions extend between ≈ 50 and 500 days, with peaks between ≈ 130 and 250 days. Notably, though, the two most rapidly fading events in either sample are SPIRITS 16ix and SPIRITS 16tn, both from the IR-discovered sample, with $t_{\text{fade},[4.5]} = 55$ days for both, while the next-fastest events are SPIRITS 15c and SN 2016bau (Type Ib) with $t_{\text{fade},[4.5]} \approx 80$ days.

We performed Kolmogorov–Smirnov tests between the two samples in each of the light-curve-derived parameters discussed

above. For the distributions in $M_{[4.5],\text{peak}}$, $[3.6] - [4.5]$ color at peak, and $t_{\text{fade},[4.5]}$, the tests return p -values of 0.31, 0.91, and 0.97, respectively. Thus, we are unable to reject the null hypotheses that the IR-selected and optically discovered samples are drawn from the same parent distribution in all three parameters. The overall similarity of the two samples in their IR properties supports the suggestion that the IR-selected objects presented in this work may represent a population of SNe that were systematically missed by optical transient searches.

Table 6
Radio Observations

Name	UT Date	MJD	Phase (days)	Inst.	Max. Baseline (km)	Frequency (GHz)	Flux (mJy)	Luminosity ($\text{erg s}^{-1} \text{Hz}^{-1}$)
SPIRITS 14buu	2016 Feb 19.1	57,437.1	786.8	VLA	3.4	10.0	<0.04	$<6.0 \times 10^{25}$
	2016 Feb 19.1	57,437.1	786.8	VLA	3.4	6.0	<0.13	$<2.0 \times 10^{26}$
	2017 Jun 10.8	57,914.8	1264.5	VLA	3.4	6.0	<0.12	$<1.8 \times 10^{26}$
	2017 Sep 4	58,000	1349.7	ATCA	4.5	9.0	<22	$<3.3 \times 10^{28}$
	2017 Sep 4	58,000	1349.7	ATCA	4.5	5.5	<25	$<3.8 \times 10^{28}$
	2018 Jan 6.2	58,124.2	1473.9	VLA	11.1	6.0	<0.039	$<5.9 \times 10^{25}$
	2018 May 9.0	58,247.0	1596.7	VLA	36.4	6.0	<0.035	$<5.3 \times 10^{25}$
	2018 May 9.0	58,247.0	1596.7	VLA	36.4	6.0	<0.055	$<8.3 \times 10^{25}$
SPIRITS 14azy	2017 Jun 12.9	57,916.9	1144.9	VLA	3.4	6.0	<0.075	$<1.3 \times 10^{25}$
SPIRITS 15c	2016 Feb 19.1	57,437.1	546.7	VLA	3.4	10.0	0.12 ± 0.01	1.8×10^{26}
	2016 Feb 19.1	57,437.1	546.7	VLA	3.4	6.0	$0.23^{+0.01}_{-0.09}$	3.5×10^{26}
	2017 Jun 10.8	57,914.8	1024.4	VLA	3.4	6.0	<0.11	$<1.7 \times 10^{26}$
	2017 Sep 4	58,000	1110	ATCA	4.5	9.0	<1.7	$<2.6 \times 10^{27}$
	2017 Sep 4	58,000	1110	ATCA	4.5	5.5	<7.6	$<1.1 \times 10^{28}$
	2018 Jan 6.2	58,124.2	1233.8	VLA	11.1	6.0	0.055 ± 0.007	8.3×10^{25}
	2018 May 9.0	58,247.0	1356.6	VLA	36.4	6.0	0.051 ± 0.008	7.7×10^{25}
	2018 May 9.0	58,247.0	1356.6	VLA	36.4	3.0	0.082 ± 0.014	1.2×10^{26}
SPIRITS 15ud	2017 Jun 14.1	57,918.1	646.4	VLA	3.4	6.0	<1.1	$<2.5 \times 10^{26}$
SPIRITS 15ade	2017 Jun 16.0	57,920.0	643.5	VLA	3.4	6.0	<0.045	$<3.1 \times 10^{25}$
SPIRITS 16ix	2017 Jun 16.0	57,920.0	442.1	VLA	3.4	6.0	<0.025	$<1.2 \times 10^{25}$
SPIRITS 16tn	2016 Sep 3	57,634	19	AMI-LA	0.11	15.0	<0.3	$<2.8 \times 10^{25}$
	2016 Sep 4.0	57,635.0	20.0	VLA	11.1	10.0	<0.047	$<4.4 \times 10^{24}$
	2016 Sep 4.0	57,635.0	20.0	VLA	11.1	6.0	<0.075	$<7.0 \times 10^{24}$
	2016 Sep 4.0	57,635.0	20.0	VLA	11.1	3.0	<0.10	$<9.3 \times 10^{24}$
	2017 Jan 12.4	57,765.4	150.4	VLA	36.4	15.5	<0.029	$<2.7 \times 10^{24}$
	2017 Jan 12.4	57,765.4	150.4	VLA	36.4	6.0	<0.029	$<2.7 \times 10^{24}$
	2018 Jan 23.6	58,141.6	526.6	VLA	11.1	15.5	<0.030	$<2.8 \times 10^{24}$
	2018 Jan 23.6	58,141.6	526.6	VLA	11.1	6.0	<0.030	$<2.8 \times 10^{24}$
SPIRITS 17lb	2017 Jun 10.8	57,914.8	13.1	VLA	3.4	6.0	<0.25	$<3.8 \times 10^{26}$
	2017 Sep 4	58,000	99	ATCA	4.5	9.0	<1.7	$<2.6 \times 10^{27}$
	2017 Sep 4	58,000	99	ATCA	4.5	5.5	<6.5	$<9.8 \times 10^{27}$
	2018 Jan 6.2	58,124.2	222.5	VLA	11.1	6.0	0.059 ± 0.006	8.9×10^{25}
	2018 May 9.0	58,247.0	345.3	VLA	36.4	6.0	0.039 ± 0.009	5.9×10^{25}
	2018 May 9.0	58,247.0	345.3	VLA	36.4	3.0	0.067 ± 0.013	1.0×10^{26}
SPIRITS 17pc	2017 Oct 30.5	58,056.5	177.7	VLA	11.1	6.0	<0.090	$>3.6 \times 10^{25}$
	2018 Jan 21.7	58,139.7	260.9	VLA	11.1	6.0	<0.13	$>5.2 \times 10^{25}$
	2018 Apr 14.2	58,222.1	343.3	VLA	36.4	6.0	<0.025	$>9.9 \times 10^{24}$
SPIRITS 17qm	2017 Nov 23.3	58,080.3	18.1	VLA	11.1	6.0	<0.05	$>2.0 \times 10^{25}$
	2018 Apr 16.8	58,224.8	162.6	VLA	36.4	6.0	<0.025	$>1.0 \times 10^{25}$

4.2.1. Comparison to Spitzer SNe

In the right panel for each object in Figure 2, we compare the SPIRITS transients to the entire sample of SNe so far detected by *Spitzer*/IRAC. A large compilation including every available *Spitzer*/IRAC detection of known SNe through 2014 was recently presented by Szalai et al. (2019), including the previously published compilations of Szalai & Vinkó (2013), Tinyanont et al. (2016), and Johansson et al. (2017); detections of individual SNe originally reported by several authors; and new, previously unpublished detections. To this, we add new detections since 2014 of the optically discovered SNe in our control sample.

We divide this large comparison sample by subtype into hydrogen-rich SNe II (and interacting SNe IIn), stripped-envelope SNe Iib and SNe Ib/c (and interacting SNe Ibcn), and thermonuclear SNe Ia (and interacting SNe Ia-CSM) to demonstrate the diagnostic utility of IR light curves.

In the IR, as found by Johansson et al. (2017), SNe Ia are clearly separated from CCSNe by their rapidly declining [4.5]

light curves and evolution to blue [3.6]–[4.5] colors for the first 200 days. The IR emission of SNe Ia is powered by the tail of the hot thermal component of the SN peaking in the optical, and Johansson et al. (2017) placed stringent limits on the presence of dust within $\lesssim 10^{17}$ cm of $M_{\text{dust}} \lesssim 10^{-5} M_{\odot}$ for the SNe Ia SN 2014J, SN 2006X, and SN 2007le. Characterized by strong interaction with a dense circumstellar medium (CSM), SNe Ia-CSM may display redder colors from $0.0 \lesssim [3.6] - [4.5] \lesssim 1.0$ and show a clear IR excess over a normal SN Ia in their [4.5] light curves. Similarly, the unusual, dusty Type Iax SN 2014dt showed redder colors and developed a clear dust excess at [4.5] peaking at ≈ 500 days. With the exception of the ongoing outburst SPIRITS 17pc that shows an initial rise, all of the SPIRITS transients are characterized by declining [4.5] light curves and red IR colors throughout their evolution, inconsistent with the characteristic evolution of SNe Ia and largely dissimilar to the thermonuclear SN subtypes of SNe Ia-CSM and SNe Iax that have now been characterized by *Spitzer*.

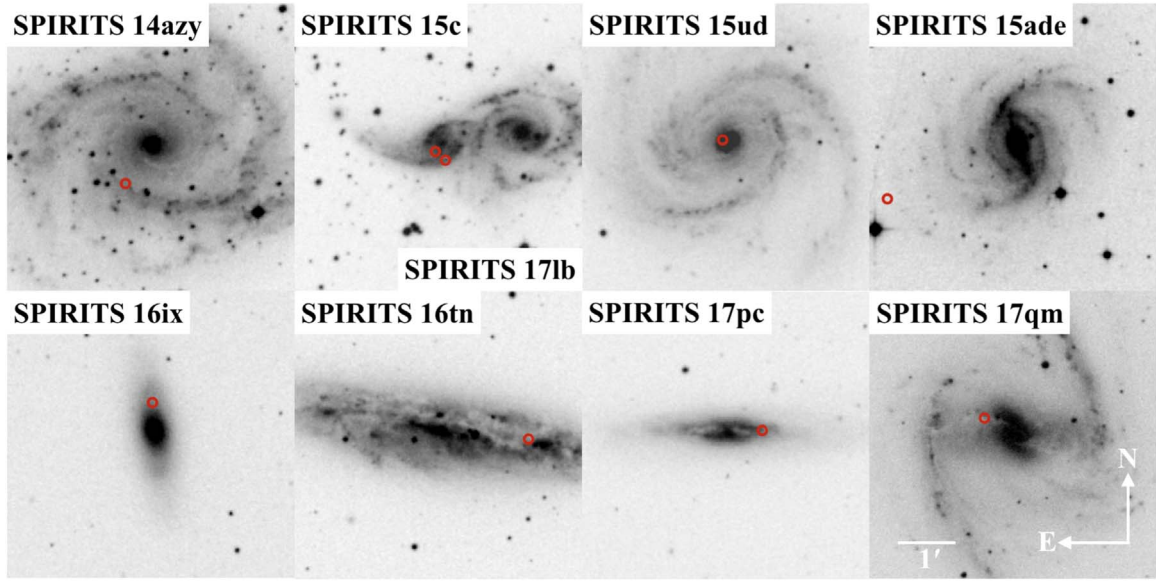


Figure 5. DSS2-red images of the host galaxies of the IR-selected sample of SPIRITS transients. The location of the transient(s) in each panel is indicated by the red circle. The orientation and scale are the same in each panel as indicated in the bottom right panel.

Table 7
Archival Imaging Progenitor Constraints

Name	UT Date	Tel./Inst.	Program/PI	Band	Vega Mag.	Abs. Mag. ^a
SPIRITS 14azy	2004 Dec 16.7	<i>Spitzer</i> /IRAC	PID 3333/M. Barlow	[3.6]	>16.7	>−13.8
	2004 Dec 16.7	<i>Spitzer</i> /IRAC	PID 3333/M. Barlow	[4.5]	>16.5	>−14.0
	2010 Oct 28.8	<i>HST</i> /WFC3 UVIS	SNAP-12229/L. Smith	F336W	>25.5	>−5.4
SPIRITS 15c	2005 Feb 22.7	<i>Spitzer</i> /IRAC	Super Mosaic	[3.6]	>15.5	>−17.3
	2005 Feb 22.7	<i>Spitzer</i> /IRAC	Super Mosaic	[4.5]	>15.5	>−17.3
	1998 Nov 11.7	<i>HST</i> /WFPC2 WFC	GO-6483/D. Elmegreen	F555W	>25.1	>−7.9
	1998 Nov 11.7	<i>HST</i> /WFPC2 WFC	GO-6483/D. Elmegreen	F814W	>24.0	>−8.9
SPIRITS 15ud	2004 May 27.5–2008 Jul 15.7	<i>Spitzer</i> /IRAC	Super Mosaic	[3.6]	>12.8	>−17.9
	2004 May 27.5–2008 Jul 15.7	<i>Spitzer</i> /IRAC	Super Mosaic	[4.5]	>12.7	>−18.0
	2001 Nov 12.1	<i>HST</i> /WFC3 UVIS	GO-11646/A. Crofts	F775W	>24.5	>−6.3
	2005 May 31.0	<i>HST</i> /ACS HRC	GO-9776/D. Richstone	F814W	>24.4	>−6.4
SPIRITS 15ade	2009 Aug 29.4	<i>Spitzer</i> /IRAC	S4G/K. Sheth	[3.6]	>19.7	>−12.2
	2009 Aug 29.4	<i>Spitzer</i> /IRAC	S4G/K. Sheth	[4.5]	>19.1	>−12.8
SPIRITS 16ix	2010 Aug 3.5	<i>Spitzer</i> /IRAC	S4G/K. Sheth	[3.6]	>16.3	>−15.2
	2010 Aug 3.5	<i>Spitzer</i> /IRAC	S4G/K. Sheth	[4.5]	>16.3	>−15.2
SPIRITS 16tn	2011 Feb 7.6	<i>Spitzer</i> /IRAC	S4G/K. Sheth	[3.6]	>15.0	>−14.7
	2011 Feb 7.6	<i>Spitzer</i> /IRAC	S4G/K. Sheth	[4.5]	>14.8	>−14.9
	1994 Jul 4.8	<i>HST</i> /WFPC2 WFC	SNAP-5446/G. Illingworth	F606W	>24.5	>−5.2
SPIRITS 17lb	2005 Feb 22.7	<i>Spitzer</i> /IRAC	Super Mosaic	[3.6]	>14.9	>−17.9
	2005 Feb 22.7	<i>Spitzer</i> /IRAC	Super Mosaic	[4.5]	>14.8	>−18.0
	2012 Dec 4.5	<i>HST</i> /WFC3 UVIS	SNAP-13029/A. Filippenko	F625W	>26.8	>−9.4
	2012 Dec 4.5	<i>HST</i> /WFC3 UVIS	SNAP-13029/A. Filippenko	F814W	>26.2	>−8.9
SPIRITS 17pc	2004 May 27.6–2008 Jul 17.7	<i>Spitzer</i> /IRAC	Super Mosaic	[3.6]	>14.6	>−16.7
	2004 May 27.6–2008 Jul 17.7	<i>Spitzer</i> /IRAC	Super Mosaic	[4.5]	>14.4	>−16.9
	2011 Jun 8.3	<i>HST</i> /WFC3 UVIS	GO-12185/J. Greene	F336W	>26.06	>−5.4
	2011 Jun 8.4	<i>HST</i> /WFC3 UVIS	GO-12185/J. Greene	F438W	>26.2	>−5.2
	2011 Jun 8.4	<i>HST</i> /WFC3 UVIS	GO-12185/J. Greene	F814W	24.21 ± 0.05	−7.1
	2011 Jun 8.2	<i>HST</i> /WFC3 IR	GO-12185/J. Greene	F110W	21.76 ± 0.04	−9.6
SPIRITS 17qm	2011 Jun 8.2	<i>HST</i> /WFC3 IR	GO-12185/J. Greene	F160W	20.60 ± 0.02	−10.7
	2004 Dec 16.4	<i>Spitzer</i> /IRAC	Super Mosaic	[3.6]	>15.3	>−16.0
	2004 Dec 16.4	<i>Spitzer</i> /IRAC	Super Mosaic	[4.5]	>14.9	>−16.5
	2001 Mar 8.3	<i>HST</i> /WFPC2 PC	SNAP-8597/M. Regan	F606W	22.45	−9.3
	2001 Jun 9.1	<i>HST</i> /WFPC2 WFC	SNAP-8597/M. Regan	F606W	20.77	−11.0

Note.

^a Corrected for Galactic extinction only.

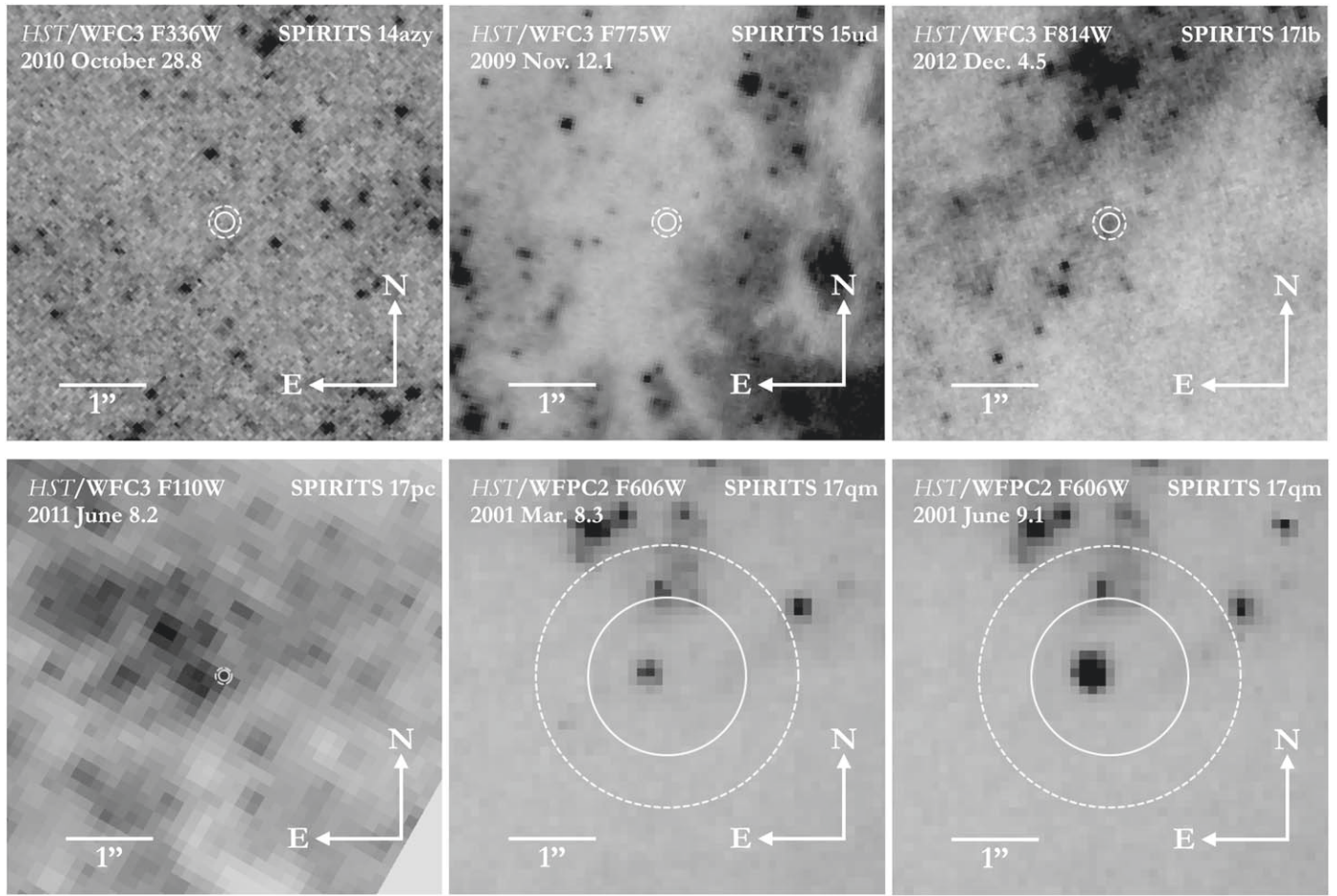


Figure 6. Archival *HST* images of the locations, from left to right, of SPIRITS 14azy, SPIRITS 15ud, and SPIRITS 17lb (top row), and SPIRITS 17pc and the two epochs covering SPIRITS 17qm (bottom row). The portion of each image shown is a $5'' \times 5''$ box, oriented with north up and east to the left. The 3σ (5σ) error circles on the locations of the transients in each image are shown as the solid (dashed) white circles. Each image is labeled with the instrument/filter combination used and the date of the observation.

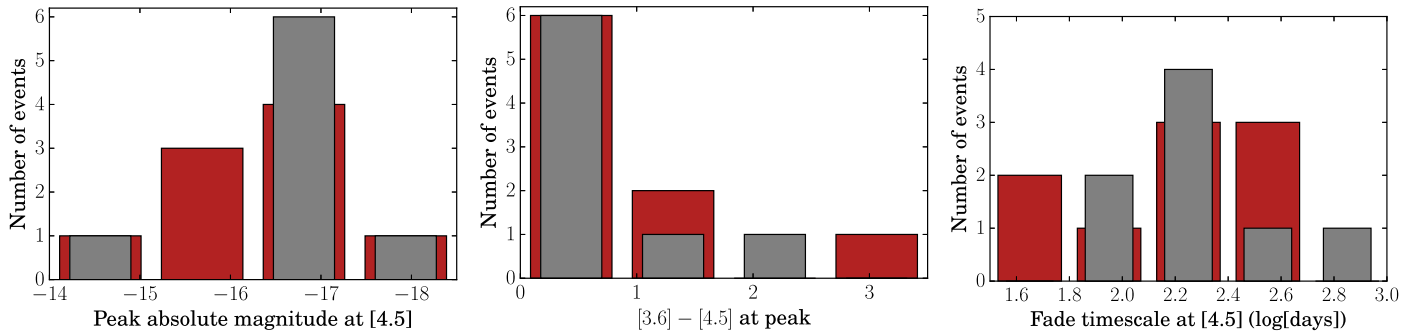


Figure 7. Observed distributions of peak absolute magnitude at [4.5] (left), [3.6]–[4.5] color at time of peak (middle), and fade timescale at [4.5] (right) for the IR-discovered sample (red) and the optically discovered control sample (gray).

CCSNe, on the other hand, are characterized by more slowly declining IR light curves and redder IR colors with $0 \lesssim [3.6] - [4.5] \lesssim 3$. The IR emission of CCSNe may be powered by thermal emission from the SN itself, or warm circumstellar dust that may be newly formed in the ejecta or preexisting dust heated by the light from the explosion. Additionally, if CO has formed in the ejecta as in the case of Banerjee et al. (2018), the emission at [4.5] may be additionally powered by the fundamental CO vibrational transition in this band, producing a significant [4.5] excess over the other IR bands. This likely

contributes to the extreme observed [3.6]–[4.5] colors in several cases. Among the sample of CCSNe, stripped-envelope events (including the interacting subtype Ibn) are relatively more homogeneous in their IR properties, characterized by monotonically declining [4.5] light curves with $M_{[4.5]}$ peaking between -17.5 and -19 , and fading at a typical rate of ≈ 0.01 mag day $^{-1}$. SNe II show a larger spread in both peak luminosity, spanning $M_{[4.5]}$ between -16 and -19 , and decay rates, with some objects having nearly constant [4.5] flux for the first ≈ 500 days. Strongly interacting SNe II may exhibit

Table 8
Properties Derived from Light Curves and Suggested Classifications

Name	t_0 (MJD)	Max Age days	t_{peak} (MJD)	$M_{[4.5],\text{peak}}$ (mag)	$[3.6]-[4.5]^a$ (mag)	$t_{\text{fade},[4.5]}$ (days)	A_V (mag)	Classification
SPIRITS 14azy	56,772.0	27.9	57,245.1	-14.4	0.55 ± 0.04	270	3.2	LRN ^b
SPIRITS 15c	56,890.4	27.0	57,057.4	-17.1	3.0 ± 0.2	85	2.2	SN Ib/Ilb
SPIRITS 15ud	57,271.7	381.4	57,271.7	-16.4	0.5 ± 0.1	170	$\gtrsim 3.7$	SN II ^b
SPIRITS 15ade	57,276.5	34.0	57,337.9	-15.7	0.67 ± 0.03	220	2.7	ILRT
SPIRITS 16ix	57,477.9	195.2	57,477.9	-15.8	1.61 ± 0.05	55	$\gtrsim 5.5$	SN II ^b
SPIRITS 16tn	57,615.0	82.0	57,615.1	-16.7	0.68 ± 0.03	55	7.8	SN II ^c
SPIRITS 17lb	57,901.7	149.8	57,901.7	-18.2	1.09 ± 0.03	160	$\gtrsim 2.5$	SN II ^{b,c}
SPIRITS 17pc	57,878.8	249.9	58,250.4	-16.3	0.39 ± 0.04	...	12.5	MSE
SPIRITS 17qm	58,062.2	234.0	58,062.2	-15.9	0.21 ± 0.04	480	12.1	MSE/LBV

Notes.

^a Measured at time t_{peak} .

^b Suggested classification for these sources is not spectroscopically confirmed.

^c SPIRITS 17lb was confirmed as a CCSN via the detection of its radio counterpart.

extreme [4.5] luminosities of $M_{[4.5]}$ brighter than -22 , though some SNe IIn have IR light curves similar to more typical SNe II.

Now, for each IR-selected SPIRITS transient, we discuss inferences on possible classifications by comparing their IR light curves directly to the *Spitzer*-observed SNe. Where appropriate, we also provide context for our final, suggested classifications based on all available observational data provided in the rightmost column of Table 8 and discussed in more detail in Section 5.

SPIRITS 14azy, peaking at only $M_{[4.5]} = -14.4 \pm 0.2$, is fainter than any previously observed CCSN. While consistent with the luminosity of an SN Ia at a phase of ≈ 120 days, the [4.5] fade rate is much slower, and the source is overluminous compared to an SN Ia by 400 days post-discovery. Furthermore, its color evolution is inconsistent with an SN Ia. Based only on the IR light curves and considering only SN subtypes, SPIRITS 14azy would be most consistent with a faint SN II; however, as discussed below in Sections 4.4 and 5, optical light curves bear strong similarity to the LRN M101 OT2015-1, arguing against SPIRITS 14azy as a true CCSN.

SPIRITS 15c, spectroscopically confirmed as an SN Ib/Ilb in Jencson et al. (2017), is fully consistent with the sample of stripped-envelope SNe in its [4.5] light curve. At $[3.6]-[4.5] = 3.0$ at peak light, it is the reddest stripped-envelope SN yet observed by *Spitzer*. The extreme IR color is likely attributable to CO emission at [4.5], corroborated by the detection of emission from the CO $\Delta v = 2$ vibrational overtone transitions in the *K* band also reported in Jencson et al. (2017).

The [4.5] light curve of SPIRITS 15ud appears most similar to the sample of SNe II. With an observed peak at $M_{[4.5]} = -16.4$, however, it may also be consistent with the class of SN 2008S-like transients (also including NGC 300 OT2008-1; Adams et al. 2016b). Given the large uncertainty in the phase of SPIRITS 15ud of $\gtrsim 400$ days, however, it is likely that the transient was significantly more luminous than SN 2008S, but the IR peak was missed by our observations.

SPIRITS 15ade again appears consistent with either a low-luminosity SN II or an SN 2008S-like event in both its [4.5] light curve and $[3.6]-[4.5]$ color evolution. We examine the classification of this object as an SN 2008S-like event also considering its near-IR spectrum and limits on the presence of an IR progenitor star in Section 5.

SPIRITS 16ix and SPIRITS 16tn, with largely similar IR properties, are unique among the SPIRITS IR transients presented here, and among all SNe previously observed by *Spitzer*. Their light curves at [4.5] decline more rapidly than any CCSN yet observed and appear consistent with the decline of an SN Ia. However, their red colors at $[3.6]-[4.5] \gtrsim 0.7$ rule out an SN Ia scenario. In Jencson et al. (2018d), we argued that the properties of SPIRITS 16tn were most consistent with a weak SN II, where the early bright IR emission was powered by a luminous dust echo, and the redder $[3.6]-[4.5]$ color at later times was likely attributable to a [4.5] excess from CO emission. This interpretation may also apply to SPIRITS 16ix given the similarity of these objects in the *Spitzer* bands.

SPIRITS 17lb is our most luminous transient at $M_{[4.5]} = -18.2 \pm 0.4$, and its light curve and color evolution are consistent with either a luminous SN II or stripped-envelope SN IIb or Ib/c. While we are unable to distinguish between CCSN subtypes based on the *Spitzer* data alone, we discuss the likely classification of SPIRITS 17lb as an SN II based on the rest of our follow-up data at optical, near-IR, and radio wavelengths in Section 5.

SPIRITS 17pc and SPIRITS 17qm are remarkable among the SPIRITS sample owing to the presence of multiple IR outbursts in the *Spitzer* light curves over the last ≈ 1000 –1500 days. As reported in Jencson et al. (2018a), SPIRITS 17pc shows three distinct IR peaks at [3.6] and [4.5], growing progressively more luminous and longer in duration. During the current, ongoing outburst, SPIRITS 17pc brightened to $M_{[4.5]} = -16.3 \pm 0.4$ over a period of at least 400 days, with a fairly constant color between $[3.6]-[4.5] = 0.2$ and 0.4. The increasing IR emission may indicate ongoing interaction of an SN blast wave with the surrounding CSM, or alternatively, active dust formation during a less extreme, nonterminal outburst.

SPIRITS 17qm, as reported in Jencson et al. (2018b), underwent a previous IR outburst ≈ 1300 days before the discovery by SPIRITS at $M_{[4.5]} = -15.2 \pm 0.1$. The observed peak at discovery of $M_{[4.5]} = -15.9 \pm 0.1$ and subsequent slow decline are consistent with an SN II, or even some previously observed interacting SN IIn. Given its eruptive history, however, the discovery outburst of SPIRITS 17qm may be due to a more intense nonterminal outburst, rather than a true SN explosion.

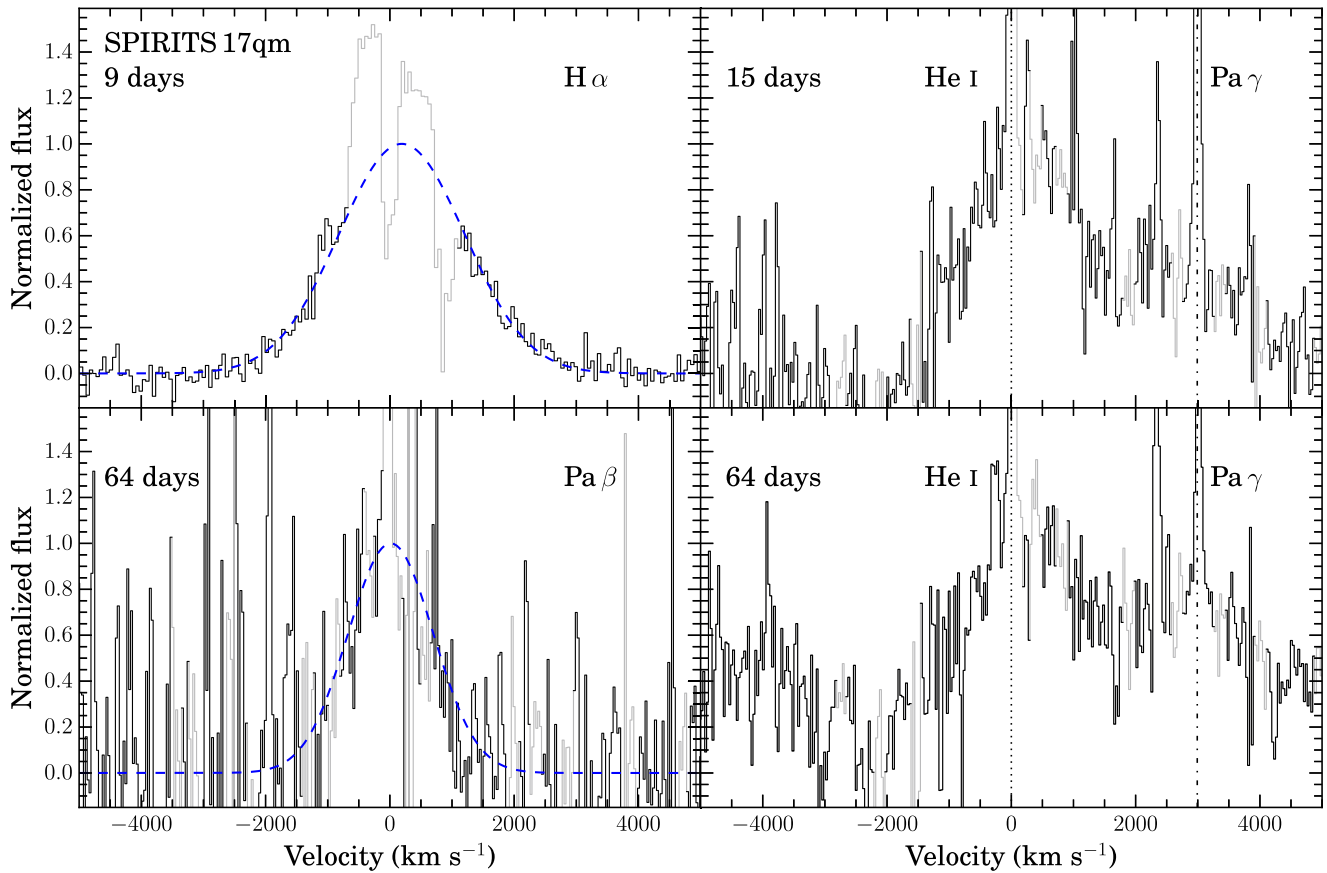


Figure 8. In the left panels we show the $H\alpha$ (top; 9 days) and $Pa\beta$ (bottom; 64 days) velocity profiles of SPIRITS 17qm in black. Gaussian fits to the data with FWHM velocities of 2400 and 1600 km s^{-1} , respectively, are plotted as blue dashed curves, where spectral bins contaminated by emission features of the underlying star-forming region or bright OH airglow emission lines are shown in light gray and excluded from the fits. In the right panels, we show the velocity profiles of He I ($\lambda 10830$; dotted vertical lines) at 15 days (top) and 64 days (bottom), with FWHM velocities of $\approx 2000 \text{ km s}^{-1}$. The red wing of the line is blended with emission from $Pa\gamma$ (dashed-dotted vertical lines).

4.3. Optical/Near-IR Spectroscopic Properties

Our optical spectroscopy of SPIRITS 16tn (79.5 days), SPIRITS 17pc (192.8 days), and SPIRITS 17qm (9.3 days) is shown in Figure 3. The spectrum of SPIRITS 16tn, previously presented in Jencson et al. (2018d), shows only a featureless red continuum beyond $\approx 8000 \text{ \AA}$. The spectrum of SPIRITS 17qm is dominated by strong $H\alpha$ emission with an FWHM velocity of 2400 km s^{-1} (top left panel of Figure 8), consistent with ejecta velocities of giant LBV eruptions. We do not detect any broader components that would indicate higher, explosive velocities of an interacting SN II. Additionally, in SPIRITS 17qm we detect weaker emission features of O I ($\lambda\lambda 8446, 9266$), but with no clear detection of the O I $\lambda 7771$ line, as well as detections of the Ca II IR triplet ($\lambda\lambda 8498, 8542, 8662$). In contrast, for SPIRITS 17pc, we detect narrow, unresolved emission features of the underlying star-forming region (including $H\alpha$), along with the Ca II triplet in emission, but no significant O I emission or broader components of $H\alpha$ associated with the transient. We confirmed the veracity of the weaker features reported here by close inspection of the reduced 2D spectra.

A zoom-in to the region around O I ($\lambda 8446$) and the Ca II triplet in the spectra of SPIRITS 17pc and SPIRITS 17qm is shown in Figure 9. The Ca II lines in SPIRITS 17pc are each double peaked, with a blueshifted component at $\approx -240 \text{ km s}^{-1}$ and a redshifted component at $\approx 100 \text{ km s}^{-1}$. For SPIRITS 17qm,

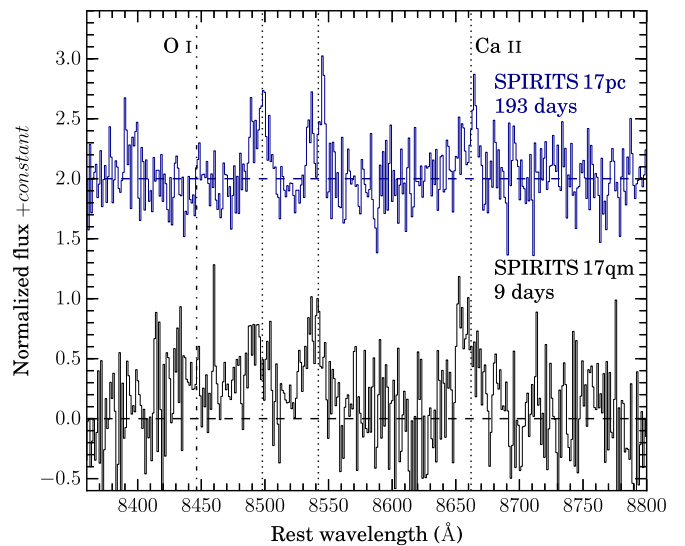


Figure 9. Comparison of the spectral region around O I ($\lambda 8446$; dashed-dotted vertical line) and the Ca II IR triplet (dotted vertical lines) in the optical spectra of SPIRITS 17pc (193 days) and SPIRITS 17qm (9 days). A linear approximation to the continuum emission has been subtracted from the spectra. The spectra were then normalized in flux, and the SPIRITS 17pc spectrum has been shifted vertically for clarity. The dashed blue and black horizontal lines show the zero-levels for SPIRITS 17pc and SPIRITS 17qm, respectively.

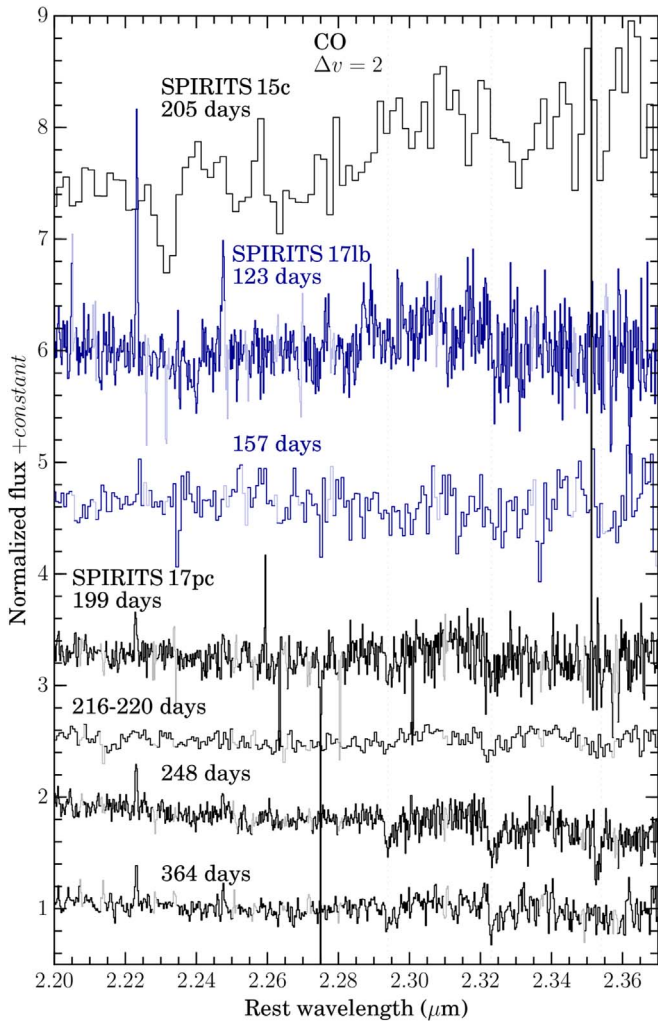


Figure 10. Comparison of the region of the K band between 2.2 and 2.37 μm in the near-IR spectra of SPIRITS 15c, SPIRITS 17lb, and SPIRITS 17pc. The spectra, shown in alternating colors for each object, are labeled on the figure along with their respective phases. Spectral bins of low S/N due to coincidence with bright OH airglow emission lines are plotted in lighter colors. The band heads of the $\Delta v = 2$ vibrational transitions of CO are indicated by the dotted vertical lines.

the lines show a single component centered at a velocity consistent with the host and with an FWHM velocity of $\approx 230 \text{ km s}^{-1}$. We also note that the O I line at 8446 \AA present in SPIRITS 17qm is absent or much weaker in SPIRITS 17pc.

The full set of our near-IR spectroscopy is shown in Figure 4, including spectra of six of the nine IR-discovered transients. In the near-IR, these objects are spectroscopically diverse, showing a range of properties and features. Our clearest example of a spectroscopically confirmed CCSN is SPIRITS 15c. In Jencson et al. (2017), we compared the near-IR spectra of SPIRITS 15c to those of the well-studied SN IIb SN 2011dh. We found strong similarities and identified several features in SPIRITS 15c based on the comparison, including He I (10830 \AA), emission features of neutral or singly ionized intermediate-mass elements and Fe, and emission from the $\Delta v = 2$ vibrational overtone transitions of CO (see Figure 10 in comparison to SPIRITS 17lb and SPIRITS 17pc). We do not detect any hydrogen in the spectrum but cannot rule out the

presence of hydrogen at earlier times. Thus, we find the spectrum to be consistent with a Type Ib or IIb classification.

Our near-IR spectroscopy of SPIRITS 16tn was first presented in Jencson et al. (2018d), where the spectrum was characterized as a largely featureless red continuum. The spectrum, however, displays broad bumps in each of the H and K bands that we originally believed may have been due to difficulty in properly flux-calibrating low-S/N data, especially in the regions of strong telluric H_2O absorption where little to no flux from the transient is received through the atmosphere. Here, after carefully checking our calibrations, we suggest a real, astrophysical origin for these broad features as absorption by water vapor at higher temperatures than the narrower telluric features. Such features have been observed in the atmospheres of cool giants with spectral types no earlier than M6 (Rayner et al. 2009), where models of pulsating Mira variables show the formation of water in the dense, cool ($< 1000 \text{ K}$) layers formed beyond periodic, outward-propagating shocks in their extended atmospheres (Bessell et al. 1989, 1996). To our knowledge, this would be the first detection of water vapor absorption associated with a luminous transient or SN, and we discuss possible interpretations in Section 5. As we detected no unambiguous SN features, however, we cannot definitively classify SPIRITS 16tn.

For SPIRITS 17lb, we detect a red continuum in the H and K regions, plausibly attributable to emission from warm dust. We note only possible excess emission beyond 23000 \AA from CO in the 123-day spectrum, but which appears to fade by 157 days. As with SPIRITS 16tn, there are no clear, broad features indicative of an SN. We find, however, that a lack of such features does not rule out an SN altogether for these objects. As discussed below in Section 4.5, nonthermal synchrotron emission from the interaction of high-velocity ejecta with CSM was detected in SPIRITS 17lb, confirming the core-collapse nature of this event. The strength of the radio emission suggests an SN II classification, possibly indicating that SNe II may be characterized by only weak or absent near-IR features at late phases. It is relevant to note here that we have not attempted to remove contamination from the host galaxy background from our spectra, and that the absence of strong, clear features may also be attributable to the inclusion of galaxy light as sources become faint at late times.

The spectra of SPIRITS 15ade show only the H I recombination lines $\text{Br}\gamma$ in the K band and $\text{Pa}\beta$ in the J band. As shown in Figure 11, the peak velocities are consistent with the recession velocity of the host, and the velocity profiles can be approximated by simple Gaussians with FWHM velocities of ≈ 360 and 390 km s^{-1} , respectively. These are similar to the low expansion velocities seen in the H I lines in optical spectra of the prototypical members of the class of ILRTs SN 2008S (e.g., Botticella et al. 2009) and NGC 300 OT2008-1 (Bond et al. 2009; Humphreys et al. 2011). The similarity of the [4.5] light curve of SPIRITS 15ade to that of SN 2008S (Section 4.2) strengthens its association with this class. There is also an apparent secondary peak in the $\text{Br}\gamma$ and $\text{Pa}\beta$ velocity profiles in SPIRITS 15ade at $\approx 300 \text{ km s}^{-1}$, possibly indicative of a bipolar or toroidal outflow geometry. Double-peaked profiles were also seen in the H I and Ca II emission features in NGC 300 OT2008-1 (Bond et al. 2009), but at lower velocities of $\approx 70\text{--}80 \text{ km s}^{-1}$.

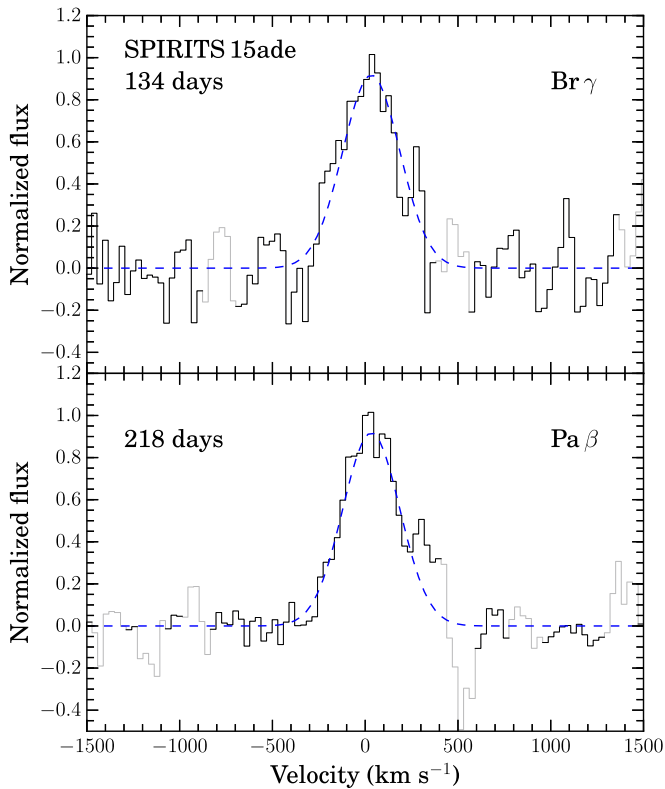


Figure 11. Velocity profiles of Br γ (134 days) and Pa β (218 days) in the spectra of SPIRITS 15ade are shown as the black solid lines in the top and bottom panels, respectively, in the rest frame of the host galaxy, NGC 5921. Gaussian fits to the profiles, excluding velocity bins of low S/N due to coincidence with bright OH airglow emission lines (plotted in light gray), are shown as the blue dashed curves.

The near-IR spectra of SPIRITS 17pc, taken between 199 and 364 days, show a relatively smooth continuum, with a few notable features. We identify an absorption band of molecular CN at $1.1 \mu\text{m}$ along with the CO $\Delta v = 2$ band heads beyond $2.3 \mu\text{m}$ (shown in more detail in Figure 10). These features are characteristic of mid-G to early K-type stellar spectra, and the spectra bear particular resemblance to G6 Ia–Ib supergiants (see the NASA Infrared Telescope Facility; IRTF spectral library of cool stars; Rayner et al. 2009). Despite good coverage of several near-IR H I recombination lines, we detect only narrow H lines from the underlying star-forming region and no broader features associated with the transient (also for He I $\lambda\lambda 10830, 20581$). As described above, the Ca II IR triplet emission (seen in absorption in mid-G to early K-type stellar spectra) suggests an outflow with velocities of $\approx 100\text{--}240 \text{ km s}^{-1}$. While we do not detect H recombination features from the transient, this is consistent with a temperature of $\approx 5400\text{--}5600 \text{ K}$ inferred by the presence of CN/CO absorption and the presence of Ca II in the spectrum, as such temperatures are too low for a significant fraction of the hydrogen to be ionized. The relatively low outflow velocities observed for SPIRITS 17pc and cooler, stellar-like spectrum suggest that this event is likely associated with nonterminal outbursts or eruptions of its progenitor, rather than a true SN.

In the near-IR, SPIRITS 17qm shows emission features of H I, as well as the He I $\lambda 10830$ line. As shown in Figure 8, these lines are relatively broad. The Pa γ line at 64 days, well approximated by a Gaussian with an FWHM velocity of 1600 km s^{-1} , is somewhat narrower than the H α emission line

observed at an earlier phase of 9 days. The spectra are consistent with a giant eruption from an LBV, and while a low-energy SN IIn may also be possible, the lack of higher-velocity features argues against the terminal explosion of the progenitor.

4.4. Multiband Light Curves and Extinction Estimates

Using available data, we compiled multiband light curves from the optical to near-IR for each luminous SPIRITS transient in our sample. These light curves are shown in Figure 12. We then estimate the visible extinction, A_V (after correcting for the Galactic contribution), which may come from the foreground interstellar medium (ISM) of the host galaxy, from the local circumstellar environment of the progenitor, or by dust formed in the event itself. We provide our estimates, based on the analysis below, in Table 8. In most cases, we are unable to make strong statements about the origin of the extinction, and throughout this section we assume a standard Milky Way ISM extinction law with $R_V = 3.1$ (Fitzpatrick 1999). To obtain A_V estimates where we have a reasonably secure classification of the transient, we attempt to make a direct comparison with template light curves from a well-studied object. Where the classification of a transient is less secure, or where good template light curves were not available, we adopt $m_X - m_{[4.5]}$ near the observed peak of the transient as an estimate of A_X , the extinction in broadband filter X (preferably optical), and convert to A_V with our assumed extinction law.

The light curves of SPIRITS 15c were discussed in detail in Jencson et al. (2017), where we estimated $A_V \approx 2.2$ based on comparison to the well-studied Type IIb SN 2011dh. Similarly, for SPIRITS 16tn we estimated $A_V \approx 7.8$ based on a comparison to the low-luminosity Type IIP SN 2005cs (Jencson et al. 2018d).

The light curves of SPIRITS 14azy are shown in Figure 12 in comparison to the 2015 LRN in M101 (M101 OT2015-1), a well-studied example of a common-envelope ejection in a merging stellar binary system (Blagorodnova et al. 2017, and 2019, in preparation). SPIRITS 14azy shows a short-lived, optical counterpart peaking at $g' = 20.0$ ($M_{g'} = -10.7$), which rises to peak and fades within $\lesssim 60$ days. The optical, broadband colors near peak are red, with $g' - r' = 0.9$ and $g' - i' = 1.1$. The transient displays a longer-lived, IR excess detected out to $\gtrsim 300$ days in the near-IR and to $\gtrsim 700$ days in the *Spitzer*/IRAC bands. Shifted in apparent magnitude to the distance of SPIRITS 14azy in NGC 2997, we see that the light curves of M101 OT2015-1 are similar to SPIRITS 14azy both in the absolute brightness of the transient in g' and the *Spitzer*/IRAC IR bands and in the timescale of the optical transient. While M101 OT2015-1 is characterized by somewhat redder optical colors and an even longer-lived IR excess, the overall similarity of the two events is readily apparent. We characterize the reddening for SPIRITS 14azy as $A_{g'} \approx g'_{\text{peak}} - [4.5]_{\text{peak}} = 3.7$, corresponding to $A_V = 3.2$. We caution that this estimate should not be directly interpreted as a measurement of the extinction from the host galaxy or local environment, and it may also be indicative of “intrinsic” reddening of the transient due to dust formation or the relatively cool effective temperatures associated with LRN-like events.

SPIRITS 15ud was inaccessible for ground-based observing owing to its proximity to the Sun from Earth at the time of the *Spitzer* discovery, and thus our constraints on any optical emission associated with the transient are only from phases before/after $\approx \pm 100$ days. As discussed below in Section 5, we

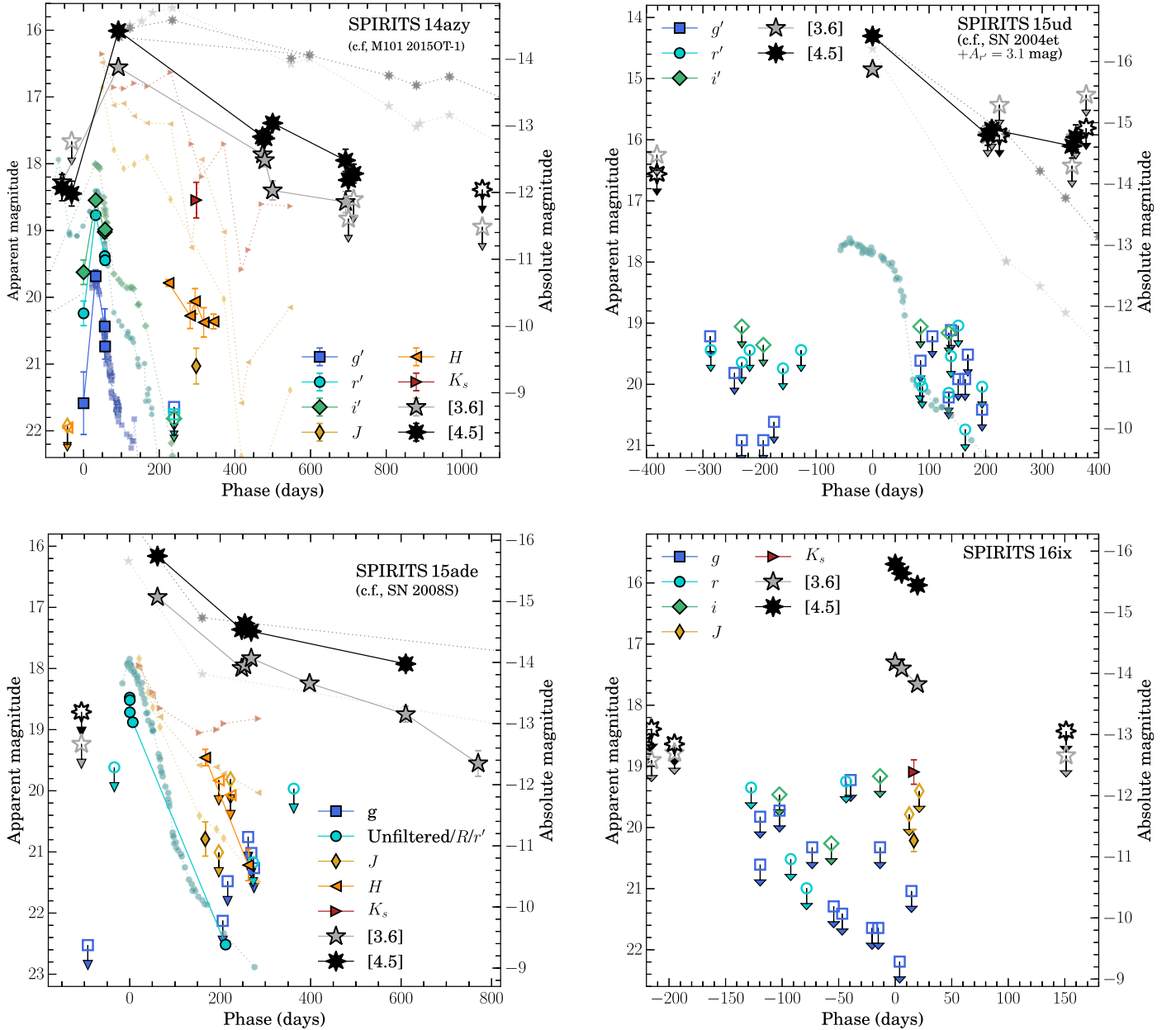


Figure 12. Multiband light curves of the SPIRITS sample of luminous, IR-discovered transients. The large, black-outlined, filled symbols are detections of the SPIRITS transient indicated in the upper right corner of each panel. Upper limits from nondetections are shown as the large, open symbols with downward-pointing arrows. The smaller, faint symbols show corresponding light curves of a well-studied comparison object, also listed in parentheses in the upper right corner of each panel. All light curves have been corrected for Galactic extinction, and comparison light curves are also corrected for additional host/intrinsic reddening as described in the text. Comparison light curves are then shifted in apparent magnitude to the distance of their corresponding SPIRITS event. The SN 2004et light curves, in comparison to SPIRITS 15ud, have additionally been shifted in apparent magnitude to match in [4.5] peak luminosity and then reddened by $A_V = 3.7$ to be consistent with our r' -band limits. Similarly, in comparison to SPIRITS 171b, the SN 2004et light curves have been reddened by $A_V = 2.5$ to be consistent with our V -band limit.

find the most likely interpretation of the IR light curves of this event to be an SN II. Our deepest limits on the post-peak optical flux of SPIRITS 15ud are in the r' band, and we compare to the light curve in this band of the Type IIP SN 2004et from Maguire et al. (2010) to obtain a constraint on the extinction. We shift the light curves in phase to match the time of the observed [4.5] peak of SPIRITS 15ud and in apparent magnitude to match the observed [4.5] brightness, and we find that our optical limits then require $A_V \gtrsim 3.1$ to be consistent with the declining light curve of SN 2004et. This corresponds to $A_V \gtrsim 3.7$, which we adopt as a lower limit on the extinction to SPIRITS 15ud.

The *Spitzer* light curves of SPIRITS 15ade, as discussed above in Section 4.2, show a distinct similarity to those of SN 2008S, a prototype of the class of ILRTs, in both IR luminosity at $M_{[4.5],\text{peak}} \approx -16$ and the subsequent IR light-curve decline. The first detection of the source was in an unfiltered optical CCD image taken on 2015 September 11.5, where the transient was identified as PSN J15220552 +0503160 by M. Aoki. Calibrated to the SDSS r band, our photometry yields an observed optical peak at $r = 18.6 \pm 0.2$ ($M_r = -13.4$) 61.3 days before the first detection by SPIRITS. The optical luminosity is similar to the R -band peak of SN 2008S (from Botticella et al. 2009, assuming $A_V \approx 1$ in

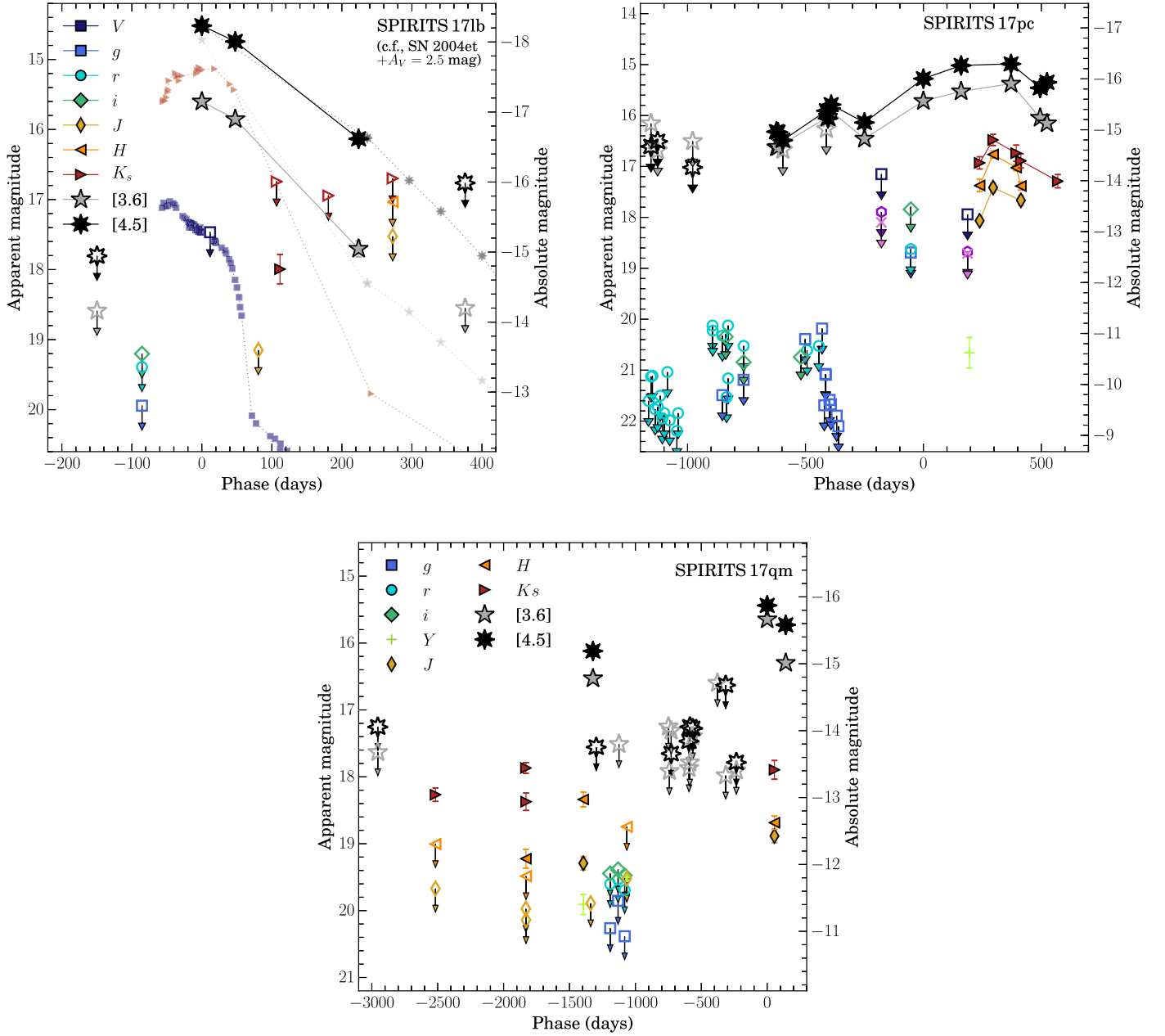


Figure 12. (Continued.)

excess of the Galactic contribution as in Botticella et al. 2009 and Szczygiel et al. 2012), and our late-time optical measurements are consistent with the optical fading of SN 2008S within ≈ 200 days. We detect a near-IR excess in the J , H , and K_s bands at a phase of ≈ 170 days, again similar to that observed in SN 2008S. We characterize the reddening to SPIRITS 15ade, though it may be intrinsic to the source, as $A_r = R_{\text{peak}} - [4.5]_{\text{peak}} = 2.3$, corresponding to $A_V = 2.7$.

SPIRITS 16ix is a near twin to SPIRITS 16tn in both their observed peak IR luminosities at $M_{[4.5],\text{peak}} \approx -16$ and their rapid IR decline rates (Section 4.2). Furthermore, both objects are remarkably red, as shown for SPIRITS 16ix in Figure 12. Our deepest optical limit during the IR observed peak of SPIRITS 16ix reached $g \gtrsim 22.2$ ($M_g \gtrsim -9.3$), indicating $A_g \gtrsim 6.3$. Corresponding to $A_V \gtrsim 5.5$, we adopt this as a lower limit on the extinction to SPIRITS 16ix.

Similar to our analysis for SPIRITS 15ud, we compare our photometric data for SPIRITS 17lb to those of SN 2004et. Shifting SN 2004et in phase to match the time of the observed [4.5] peak and in apparent magnitude to the distance of SPIRITS 17lb, we find that their [4.5] light curves track each other remarkably well, though SPIRITS 17lb is significantly redder than SN 2004et in [3.6]–[4.5] until $\gtrsim 150$ days. Applying reddening with $A_V \gtrsim 2.5$ is then required for the SN 2004et light curves to be consistent with our V -band limit at 11.7 days, which we adopt as a lower limit on the extinction to SPIRITS 17lb.

As discussed in Section 4.2, the *Spitzer* light curves of SPIRITS 17pc are characterized by multiple outbursts over the past ≈ 4 yr that appear to be progressively increasing in both brightness and duration. Deep optical limits constrain the optical variability of the source between ≈ -1200 and

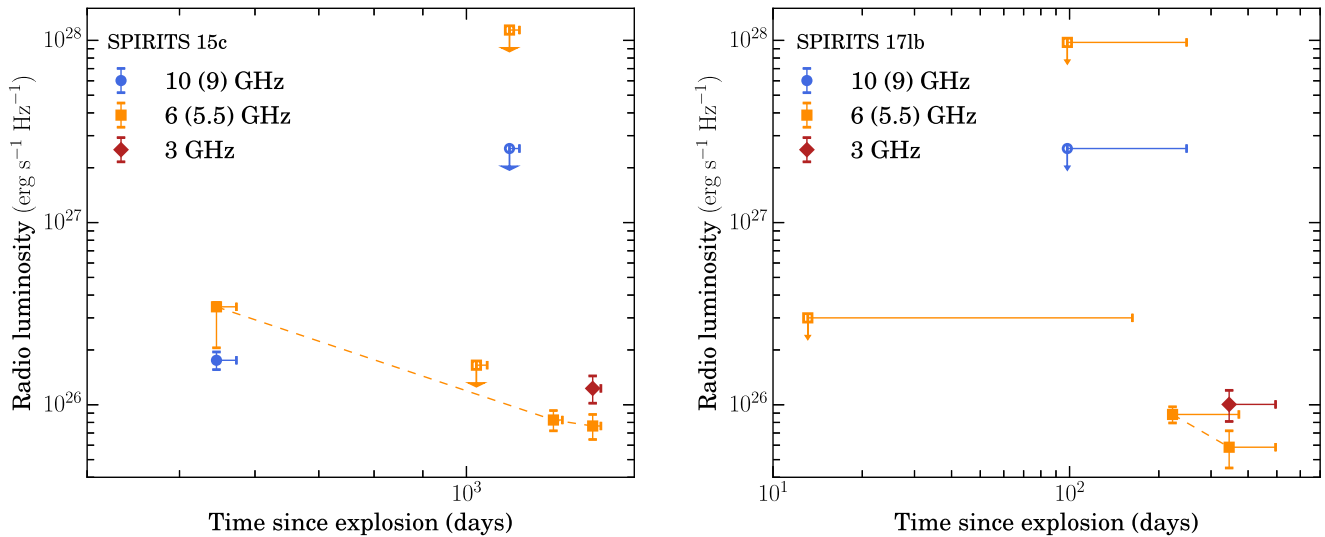


Figure 13. Radio light curves of SPIRITS 15c (left) and SPIRITS 17lb (right) in multiple frequency bands. Detections are indicated by filled symbols, while upper limits from nondetection are indicated by open symbols with downward-pointing arrows. Horizontal error bars indicate the uncertainty in the absolute phase since explosion for these events.

−300 days, and we note that the IR outburst peaking at $[4.5] = 15.8$ near −400 days was extremely red with $g' - [4.5] > 5.9$. During the brightest, longest-duration IR outburst seen in the *Spitzer*/IRAC bands lasting $\gtrsim 500$ days, we detected underlying near-IR variability peaking at $K_s = 16.5$ at 295.6 days with a red near-IR color of $J - K_s = 0.9$ with a comparatively shorter duration of $\lesssim 200$ days. We also obtained our only optical detection of SPIRITS 17pc at $Z = 20.7$ at 195.1 days, indicating $A_Z = Z - [4.5] = 5.7$. To estimate the extinction in Table 8, we convert this to $A_V = 12.5$ but again caution that the extreme optical–IR color may be intrinsic to the source and is not necessarily indicative of extinction by the host ISM or local environment of the progenitor.

The light curves of SPIRITS 17qm also indicate multiple epochs of significant variability across the near-IR and *Spitzer*/IRAC bands extending back to at least a phase of −2500 days before the discovery detection and observed IR peak at $[4.5] = 15.4$ ($M_{[4.5]} = -15.9$). During the pre-discovery outburst detected by *Spitzer*, our photometry indicates a notably red SED with $Y - [4.5] = 3.8$. Similarly, our near-IR follow-up observations during the post-peak decline at $t = 55.1$ days indicate $A_J = J - [4.5] = 3.3$, corresponding to $A_V = 12.1$. As with SPIRITS 17pc, rather than indicating host or environmental extinction, the extreme colors we observe may be intrinsic to the SED of the source or caused by dust formation.

4.5. Radio Constraints

Radio observations of CCSNe probe the nonthermal emission generated when the fastest ejecta interact with the CSM produced by the pre-explosion stellar wind of the progenitor. The spectrum is dominated by synchrotron emission as the blast wave propagates through the CSM, where turbulent instabilities may accelerate electrons to relativistic energies and amplify magnetic fields (Chevalier 1982). At early times, the synchrotron spectrum is self-absorbed at high frequencies, with possible additional contributions from internal free–free absorption, and free–free

absorption by the external, pre-shocked, ionized CSM (e.g., Chevalier 1982, 1998). As the shock propagates out into the CSM, the peak in the spectrum, below which the source is opaque, shifts to lower frequencies. As no SN Ia has been detected in the radio to deep limits in radio luminosity of $L_\nu \lesssim 10^{24}$ erg s $^{-1}$ Hz $^{-1}$, detection of this characteristic signature could provide strong confirmation our sources as CCSNe.

In Figure 13, we show the radio light curves of SPIRITS 15c and SPIRITS 17lb. For both sources, we detect a declining radio source consistent with optically thin synchrotron emission. At $t = 546.7$ days for SPIRITS 15c, the transient is detected at both 10 and 6 GHz, with a spectral index $\alpha = 1.32^{+0.05}_{-1.01}$, where the flux density is given by $S_\nu \propto \nu^{-\alpha}$. The source is observed to fade at 6 GHz, with a spectral index of $\alpha = 0.7 \pm 0.1$ between 3 and 6 GHz at $t = 1356.6$ days. We infer from these observations that SPIRITS 15c peaked at a 6 GHz radio luminosity of $L_\nu \gtrsim 3.5 \times 10^{26}$ erg s $^{-1}$ Hz $^{-1}$ at time $t \lesssim 546.7$ days (maximum age $\lesssim 573.7$ days). For SPIRITS 17lb, the source fades at 6 GHz between $t = 222.5$ and 345.3 days, with a spectral index of $\alpha = 0.78 \pm 0.13$ between 3 and 6 GHz at the later epoch. SPIRITS 17lb thus peaked at 6 GHz at $L_\nu \gtrsim 8.8 \times 10^{25}$ erg s $^{-1}$ Hz $^{-1}$ at time $t \lesssim 222.5$ days (maximum age $\lesssim 372.3$ days). The remaining SPIRITS events were undetected in our radio follow-up observations.

In Figure 14, we show the peak luminosities of radio CCSNe of various subtypes and the time to peak times the frequency of observation compared to our constraints for SPIRITS 15c and SPIRITS 17lb, as well as our limits on the radio luminosity of the rest of the sample. Following our discussion in Section 4.2.1 of Jencson et al. (2018d), we use the self-similar solution for the propagation of the SN blast wave into the CSM described in Chevalier (1998) and Chevalier & Fransson (2006). If synchrotron self-absorption (SSA) is the dominant absorption mechanism, and assuming that the emitting electron population is described by a power law with an energy spectral index $p = 3$, then, as calculated by Chevalier (1998), the size

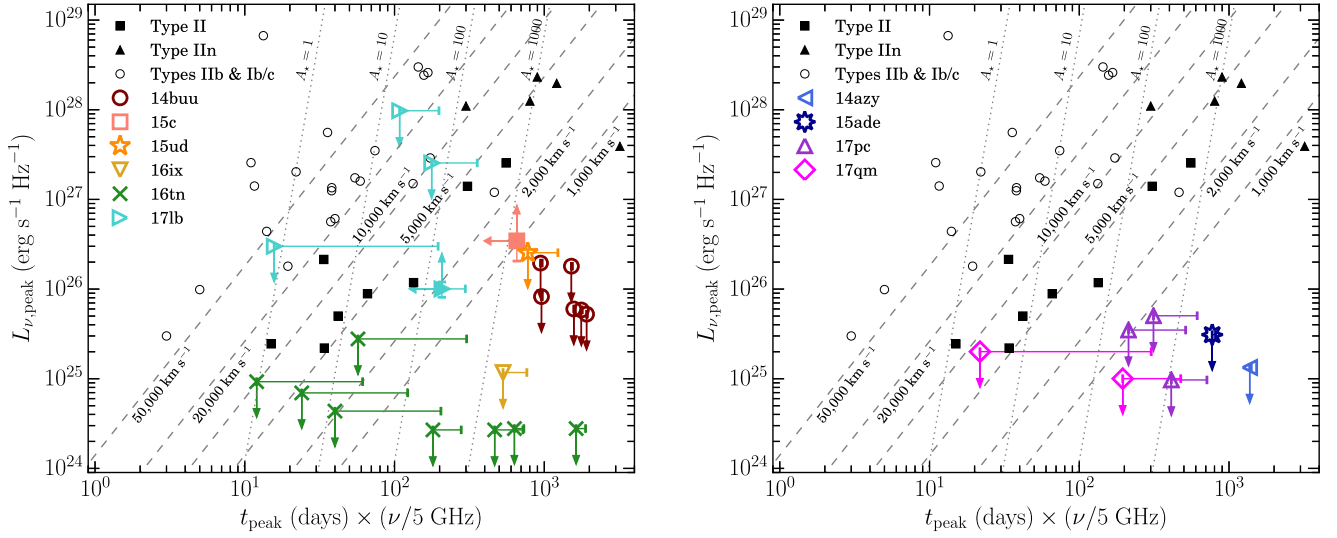


Figure 14. In each panel, we show the peak radio luminosity vs. time of peak times the frequency of observation for radio CCSNe adapted from, e.g., Chevalier et al. (2006) and Romero-Cañizales et al. (2014). This is an updated version of Figure 10 from Jencson et al. (2018d). SNe II are shown as black squares, and strongly interacting SNe IIn are shown as black triangles. Open circles represent stripped-envelope SNe Ib and Ib/c. Upper limits on the radio luminosity of SPIRITS transients at a given phase are shown as multicolor open symbols with downward-pointing arrows, where the horizontal error bars represent our uncertainty in the absolute phase since explosion. The possible CCSNe are shown in the left panel, while the non-SN events are shown in the right panel. Filled symbols for SPIRITS 15c and SPIRITS 17lb represent constraints on t_{peak} and $L_{\nu, \text{peak}}$ from detections of the transients. Symbols corresponding to each object are labeled in the legend on the left side of the figure. Assuming an SSA model with an electron distribution with $p = 3$ for the shock wave propagating through the CSM, one can infer the shock velocity (dashed lines) and CSM density parameter (A_* ; dotted lines) from the position on this diagram.

of the radio-emitting region is given by

$$R_s = 4.0 \times 10^{14} q^{-1/19} \left(\frac{f}{0.5} \right)^{-1/19} \left(\frac{F_p}{\text{mJy}} \right)^{9/19} \times \left(\frac{D}{\text{Mpc}} \right)^{18/19} \left(\frac{\nu}{5 \text{ GHz}} \right)^{-1} \text{ cm}, \quad (1)$$

where $q \equiv \epsilon_e/\epsilon_B$ is the ratio of the energy density in relativistic electrons to that in the magnetic field, f is the filling factor of the radio-emitting region, F_p is the peak flux at frequency ν , and D is the distance to the source. We show the inferred shock velocities assuming energy equipartition ($q = 1$) and $f = 0.5$ (as estimated by Chevalier & Fransson 2006) as the dashed lines in Figure 14.

Assuming that the CSM was produced by a steady pre-SN stellar wind, its density profile as a function of radius, r , will be given by $\rho_w = A/r^2 \equiv \dot{M}/(4\pi r^2 v_w)$, where \dot{M} is the mass-loss rate and v_w is the wind velocity. We define $A \equiv \dot{M}/(4\pi v_w)$ as the normalization of the CSM density profile, and $A_* \equiv A/(5 \times 10^{11} \text{ g cm}^{-1})$ is a dimensionless proxy for A as in Chevalier (1982). The radio emission at time t since explosion is then sensitive to the density profile of the CSM as

$$A_* \epsilon_{B-1} q^{8/19} = 1.0 \left(\frac{f}{0.5} \right)^{-8/19} \left(\frac{F_p}{\text{mJy}} \right)^{-4/19} \times \left(\frac{D}{\text{Mpc}} \right)^{-8/19} \left(\frac{\nu}{5 \text{ GHz}} \right)^2 \left(\frac{t}{10 \text{ days}} \right)^2, \quad (2)$$

where $\epsilon_{B-1} \equiv \epsilon_B/0.1$ (Chevalier & Fransson 2006). The inferred value of A_* depends very sensitively on t_{peak} , shown in Figure 14 as the nearly vertical dotted lines.

Our constraint on the peak radio luminosity for SPIRITS 15c is consistent with its spectroscopic classification as an SN Ib

or SN Ib, which tend to be more luminous radio sources ($10^{26} \lesssim L_{\nu, \text{peak}} \lesssim 10^{28} \text{ erg s}^{-1} \text{ Hz}^{-1}$) peaking on timescales between 10 and 100 days. Because our radio observations were post-peak, we are only able to place limits on the relevant parameters. Our observations require $v_s \gtrsim 1000 \text{ km s}^{-1}$ and $A_* \lesssim 1400$. This translates to a limit on the pre-SN mass-loss rate of $\dot{M} \lesssim 1.4 \times 10^{-3} \left(\frac{\epsilon_B}{0.1} \right) \left(\frac{v_w}{100 \text{ km s}^{-1}} \right) M_\odot \text{ yr}^{-1}$.

SPIRITS 17lb, despite its younger phase at the time of first observation with the VLA, is notably less luminous, more consistent with the population of radio SNe II. We find $v_s \gtrsim 800 \text{ km s}^{-1}$ and $A_* \lesssim 800$, corresponding to a limit on the pre-SN mass-loss rate of $\dot{M} \lesssim 8.0 \times 10^{-4} \left(\frac{\epsilon_B}{0.1} \right) \left(\frac{v_w}{100 \text{ km s}^{-1}} \right) M_\odot \text{ yr}^{-1}$.

As discussed in Jencson et al. (2018d), our deep radio nondetections for SPIRITS 16tn rule out a stripped-envelope classification, except possibly the most rapidly evolving, high-velocity events that may have fast-peaking radio light curves. The new late-time limits beyond $t \gtrsim 500$ days presented here also argue against a strongly interacting SN IIn, unless the radio emission is still strongly self-absorbed at this phase. A weak SN II is the most consistent with our observations for SPIRITS 16tn, and specifically, our inferred constraint on the pre-SN mass-loss rate of $\dot{M} \lesssim 2.4 \times 10^{-5} \left(\frac{\epsilon_B}{0.1} \right) \left(\frac{v_w}{100 \text{ km s}^{-1}} \right) M_\odot \text{ yr}^{-1}$ may suggest an RSG progenitor of lower initial mass (10–15 M_\odot). Similarly, the late-time limit for SPIRITS 16ix is significantly deeper than observed radio-luminous SNe IIn and stripped-envelope SNe and is most consistent with an SN II. Our weaker constraint for SPIRITS 15ud may be consistent with either an SN II or stripped-envelope classification.

As discussed below in Section 5, based on the sum of all available observational data, we do not believe that SPIRITS 14azy, SPIRITS 15ade, SPIRITS 17pc, and SPIRITS 17qm were terminal CCSN explosions. Thus, we do not expect strong radio counterparts for these events, but we show our radio limits in the right panel of Figure 14 for completeness. Specifically for SPIRITS 17qm, while the most likely interpretation is a giant LBV eruption, an SN IIn is

consistent with the optical/IR data but may be disfavored by the lack of radio emission detected thus far.

5. Putting it All Together: Suggested Transient Classifications

Here we discuss suggested classifications for each SPIRITS event in our sample based on the combined observational constraints across radio, IR, and optical wavelengths. We find that five of our nine IR events are confirmed or plausible CCSNe, while the remaining four are more likely non-SN massive-star outbursts of various origins. Our suggested classification for each event is given in Table 8.

5.1. The Confirmed and Plausible CCSNe

As discussed in detail in Jencson et al. (2017), SPIRITS 15c is a clear example of a confirmed, moderately obscured CCSN. Our assessment is based primarily on near-IR spectroscopy showing distinct similarity to the Type IIb SN 2011dh, and in particular the presence of a broad ($\approx 8400 \text{ km s}^{-1}$) double-peaked emission line of He I at $1.0830 \mu\text{m}$. The optical/near-IR light curves were well matched to those of SN 2011dh assuming $A_V = 2.2$ and a standard Milky Way ISM extinction law with $R_V = 3.1$. In this work we present new radio observations of SPIRITS 15c, which are characterized by the detection of a declining, optically thin synchrotron source consistent with the radio counterparts of other, previously observed stripped-envelope CCSNe.

SPIRITS 17lb, our most luminous IR transient at $M_{[4.5]} = -18.2$, clearly falls in the IR luminosity range of CCSNe (see Figure 2) and is more luminous than any other class of known IR transient. The IR light curves and color evolution are consistent with either a hydrogen-rich Type II or stripped-envelope Type Ib/c or IIb. The near-IR spectra, taken at phases of 123 and 157 days, show no strong features indicative of a CCSN or specific SN subtype. There is a possible weak detection of the CO $\Delta v = 2$ features in the 123 day K -band spectrum, which is not present at 157 days. We note that some SNe II, including the recent SN 2017eaw, have shown strong CO K -band features that may fade on timescales of months (e.g., Tinyanont et al. 2019), but this does not provide a definitive classification for SPIRITS 17lb. As discussed in Section 4.5, we detected a declining, optically thin synchrotron source at the location of SPIRITS 17lb, confirming this source as a CCSN. Our constraints on the peak radio luminosity and time of the synchrotron peak are most consistent with previously observed radio SNe of Type IIP. This rules out a strongly interacting SN IIn, as the observed emission is optically thin and thus not strongly self-absorbed by a dense wind, and disfavors a typically more luminous stripped-envelope event. Assuming a steady pre-SN wind, we derive constraints on the mass-loss rate of $\dot{M} \lesssim 8.0 \times 10^{-4} \left(\frac{\epsilon_B}{0.1} \right) \left(\frac{v_w}{100 \text{ km s}^{-1}} \right) M_\odot \text{ yr}^{-1}$, consistent with an RSG progenitor. We infer a lower limit on the extinction to SPIRITS 17lb of $A_V \gtrsim 2.5$ in Section 12 comparing to the Type IIP SN 2004et.

The evidence for SPIRITS 15ud, SPIRITS 16ix, and SPIRITS 16tn is more circumstantial, but we find a reddened CCSN to be a plausible interpretation for each of these events. For SPIRITS 15ud, at $M_{[4.5],\text{peak}} = -16.4$ the IR light curves are broadly consistent with an SN II, stripped-envelope Type Ib/c or IIb, or alternatively, an SN 2008S-like ILRT. Given the

large uncertainty in the age of SPIRITS 15ud at discovery (< 381.4 days), it is likely that our *Spitzer* observations missed the peak of this event and that its true peak luminosity was substantially higher. This would place SPIRITS 15ud firmly in the IR luminosity range characteristic of CCSNe and disfavors the ILRT interpretation. Despite the large uncertainty in its age in Section 12 and under the assumption that SPIRITS 15ud was an SN II, we placed a lower limit on the extinction of $A_V \gtrsim 3.7$. This interpretation is further supported by the location of SPIRITS 15ud in a prominent, nearly opaque dust lane in archival *HST* imaging.

We examined the observational constraints for SPIRITS 16tn in Jencson et al. (2018d) and again found an SN II, possibly a low-luminosity event similar to SN 2005cs, heavily obscured by $A_V = 7-9$ to be the most likely interpretation of this event. A new piece of the puzzle is the possible identification of water vapor absorption in the near-IR spectrum of SPIRITS 16tn (Section 4.3). In the CCSN scenario, a possibility is that the progenitor was encased in a dense molecular cloud, and water in the vicinity was heated by the explosion to produce the observed, broad absorption. The high extinction for SPIRITS 16tn is consistent with this interpretation. This would constitute the first direct identification of a CCSN associated with a molecular cloud, though Galactic candidates for SN remnants interacting with molecular gas have been previously noted (e.g., W44 and IC 443; Chevalier 1999). Interestingly, Chevalier (1999) argued that the progenitors of such events must be relatively low mass, i.e., early B-type stars on the main sequence ($8-12 M_\odot$), as the ionizing flux from a more massive O-type progenitor will clear a region $\approx 15 \text{ pc}$ in radius of molecular material. Our inferred limit on the pre-SN mass-loss rate from radio observations of SPIRITS 16tn was also consistent with a lower-mass RSG progenitor, which may add further support to this hypothesis.

Alternatively, given the apparent similarity of the water absorption features to those of late-type Mira variables, SPIRITS 16tn may represent a previously unknown class of transient associated with such stars. It is unclear, however, that water in the atmosphere would survive a luminous outburst or mass-loss event. Finally, an additional, though unlikely, possibility is chance positional coincidence between SPIRITS 16tn and an unrelated Mira variable. Continued monitoring for ongoing Mira-like variability in the near-IR is required to confirm or rule out this possibility.

SPIRITS 16ix is a near twin of SPIRITS 16tn in their IR properties, and thus we also consider a CCSN, possibly another weak or low-luminosity SN II, as a plausible interpretation. SPIRITS 16tn was clearly associated with active star formation, indicating a likely massive-star origin further suggestive of a CCSN. We note that for SPIRITS 16ix, however, there is no clear evidence of star formation at the site, and given the classification of the host as a lenticular S0 galaxy, the association is more ambiguous. We noted in Jencson et al. (2018d) that given the low explosion energy inferred for SPIRITS 16tn and lack of spectroscopic features distinctive of a CCSN, a nonterminal “impostor” explosion or eruption remains a viable scenario. Neither SPIRITS 16ix nor SPIRITS 16tn has shown any evidence of prior or subsequent IR variability other than the singular events described in this work. This further supports our interpretation that they were isolated, and possibly terminal, events in the lives of their progenitors. It is particularly notable that SPIRITS 16ix and

SPIRITS 16tn, while distinctly similar to each other in their IR light curves, are also unique compared to the rest of the IR- and optically discovered transients. Furthermore, they are the two most severely reddened possible CCSNe ($A_V \gtrsim 5.5$) presented in this work. We thus speculate that they may represent a new class of IR-dominated transients, possibly associated with low-energy CCSNe arising preferentially in particularly extinguished environments and/or from progenitors that are directly associated with or encased in dense molecular clouds.

5.2. ILRT: SPIRITS 15ade

As a distinct class of IR-dominated events, the nature of ILRTs remains unclear. The prototypical objects are the “impostor” SN 2008S and NGC 300 2008OT-1 (Bond et al. 2009). ILRTs are observed to have dust-obscured, IR-luminous ($M_{[4.5]} < -10$; $\nu L_\nu > 3.7 \times 10^3$) pre-explosion counterparts, suggested to be extreme AGB stars of intermediate mass (≈ 10 – $15 M_\odot$) self-obscured by a dusty wind (Prieto et al. 2008; Bond et al. 2009; Thompson et al. 2009). The recently discovered transient in M51 (M51 OT2019-1) was also proposed as a new member of this class. Its likely progenitor was a similar dust-obscured star, with significant IR variability detected in archival *Spitzer*/IRAC imaging over the past ≈ 12 yr (Jencson et al. 2019). Less luminous than typical CCSNe at peak, emission lines in their spectra (including H recombination and strong [Ca II] and Ca II features) also indicate lower velocities up to $\text{few} \times 100 \text{ km s}^{-1}$ (e.g., Bond et al. 2009; Botticella et al. 2009; Humphreys et al. 2011). A suggested physical scenario involves weak explosion, possibly an electron-capture SN (disfavored for the slow rise and extended phase of early dust destruction observed in M51 OT2019-1; Jencson et al. 2019), or massive stellar eruption that initially destroys the obscuring, circumstellar dust and produces a short-lived optical transient. In the aftermath, the development of a significant IR excess indicates the recondensation of dust and consequent reobscuration of the transient (Thompson et al. 2009; Kochanek 2011; Szczygiel et al. 2012). There is currently no evidence that the progenitor stars survive such events, as both prototypes have now faded below their pre-explosion luminosities in the IR (Adams et al. 2016b).

SPIRITS 15ade shares several properties with this class. While we do not directly detect a progenitor star, our limit from archival *Spitzer*/IRAC imaging at $M_{[4.5]}$ fainter than -12.8 is consistent with the IR progenitors of SN 2008S and NGC 300 OT2008-1. As we found in Section 12, the IR light curves (peaking at $M_{[4.5]} = -15.7$) and the observed peak and duration of the associated optical transient are also very similar to known ILRTs. Finally, we detect H recombination emission in our near-IR spectra, suggestive of an outflow at 300 – 400 km s^{-1} , similar to the low expansion velocities of known ILRTs (e.g., Bond et al. 2009; Botticella et al. 2009; Humphreys et al. 2011).

5.3. Possible LRN: SPIRITS 14azy

The class of extragalactic transients referred to as luminous red novae (LRNe) are believed to be more massive analogs of the population of stellar mergers observed in the Galaxy, including the striking example of the ≈ 1 – $3 M_\odot$ contact binary merger V1309 Sco (Tyndal et al. 2011; McCollum et al. 2014) and the B-type stellar merger V838 Mon (Bond et al. 2003; Sparks et al. 2008). While sharing several properties with

ILRTs, LRNe are distinctly characterized by multi-peaked, irregular light curves. At early times, their spectra show H emission features, but they develop red optical colors, atomic and molecular absorption features, and significant IR excesses as they evolve. Recent examples include the 2011 transient in NGC 4490 (NGC 4490 OT2011-1; Smith et al. 2016) and the 2015 event in M101 (M101 OT2015-1; Blagorodnova et al. 2017). Specifically in the case of NGC 4490 OT2011-1, the late-time IR excess was too luminous to be explained as an IR echo, indicating the presence of a surviving, merged remnant. With unobscured, directly detected progenitor systems in archival imaging estimated at 20 – $30 M_\odot$ for NGC 4490 OT2011-1 and $\approx 18 M_\odot$ for M101 OT2015-1, these events extend a correlation noted by Kochanek et al. (2014) for LRNe between progenitor masses and the transient peak luminosity. Specifically, the progenitor of M101 OT2015-1 was identified in archival imaging as having properties of an F-type supergiant with $L \approx 8.7 \times 10^4 L_\odot$ and $T_{\text{eff}} \approx 7000 \text{ K}$, likely having recently evolved off the main sequence and crossing the Hertzsprung gap as it expands.

Based primarily on our analysis of its multiband light curves, we find that SPIRITS 14azy is most consistent with the LRN class of IR transients, and in particular bears strong similarity to M101 OT2015-1 in its peak luminosity at both $[4.5]$ and g' . Thus, we suggest that it may have a similar mass progenitor system. In Section 4.1, we placed a limit on the flux of the progenitor in the *HST*/WFC3 UVIS F336W filter corresponding to M_U fainter than -5.4 . As the transient is located in a prominent dust lane of the host, the foreground extinction in U band may be significant. Even in the absence of host extinction, and assuming bolometric corrections from Flower (1996), with corrections by Torres (2010) using a consistent choice of $M_{\text{bol},\odot} = 4.73$ and Crowther (1997) filter transformations, this limit is approximately consistent with a zero-age main-sequence O9 star ($T_{\text{eff}} \approx 30,000 \text{ K}$, $L \approx 40,000 L_\odot$) of similar mass to the progenitor of M101 OT2015-1.

5.4. MSEs: SPIRITS 17pc and SPIRITS 17qm

SPIRITS 17pc has undergone multiple, IR-dominated outbursts over a time period spanning at least 1100 days. These outbursts are extremely red (we infer $A_V \approx 12.5$), possibly indicative of copious dust formation. Near-IR spectra taken during the most recent, longest-duration, and most luminous outburst show features similar to a mid- to late G-type supergiant spectrum, including CN and CO absorption. An optical spectrum shows double-peaked Ca II emission, but no H or He features, indicative of a cool, $\text{few} \times 100 \text{ km s}^{-1}$ outflow. We identified a luminous ($L \approx 2 \times 10^5 L_\odot$) star detected in 2011 archival, multiband *HST* imaging at the precise location of SPIRITS 17qm as a likely progenitor. The luminosity is lower than that of a classical LBV but still likely indicates a very massive progenitor. The progenitor photometry is consistent with a blackbody temperature of $T = 1900 \pm 100 \text{ K}$, likely indicating that active dust formation was occurring around the underlying star. Given the previous history of strong IR variability, cool spectral features, low outflow velocities, and lack of strong radio emission, we argue that the most recent outburst of SPIRITS 17pc represents a more intense mass-loss event or eruption, rather than a terminal SN explosion.

Similar to SPIRITS 17pc, SPIRITS 17qm has also undergone multiple IR outbursts in SPIRITS, and furthermore was also

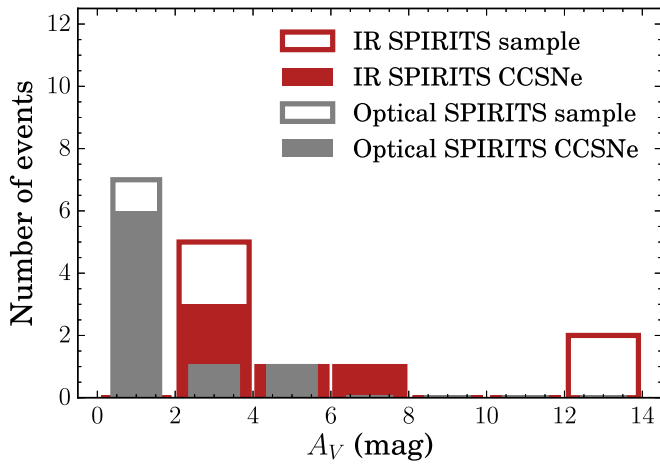


Figure 15. Distribution of A_V inferred for the IR-selected sample of luminous SPIRITS transients (red) and the optically selected control sample (gray). The filled regions of the histograms represent confirmed or possible CCSNe. The unfilled regions include the Type Ia SN 2014dt from the control sample and the non-SN stellar outbursts from the IR sample.

extremely red (estimated $A_V = 12.1$). However, we highlight several notable differences. The spectra of SPIRITS 17qm were dominated by broader ($v \approx 1500\text{--}2000 \text{ km s}^{-1}$) features of H and He and also showed prominent Ca II emission, consistent with a giant LBV eruption. Again, the lack of strong radio emission argues against the interpretation of SPIRITS 17qm as a terminal, Type IIc CCSN explosion. The presumed progenitor of SPIRITS 17qm detected in multipoint *HST* imaging was highly luminous and variable ($L \approx 2 \times 10^6 L_\odot$, $\Delta V = 1.7$), also consistent with the properties of an LBV. Assuming that the progenitor was undergoing S Doradus-like variability, the foreground extinction (host or circumstellar) was likely no larger than $A_V \approx 0.5$ at the time of the *HST* observations in 2001. Thus, we suggest that the extreme optical/IR color observed for SPIRITS 17qm may be due to the formation of copious dust in the intervening years and/or during the observed giant eruption. Incorporating ongoing monitoring, the physical details of SPIRITS 17qm and SPIRITS 17pc as self-obscuring MSEs will be explored more fully in a future publication.

6. The “Redness” Distribution of Luminous IR Transients

In Figure 15, we show the distribution of A_V (including lower limits) inferred for our sample of luminous SPIRITS transients. This includes confirmed and plausible CCSNe as the filled portions of the histograms, as well the Type Ia SN 2014dt from the optical control sample and the non-SN IR transients as the unfilled portions. For the non-SN transients, we emphasize that our A_V estimates are only a proxy for the observed optical–IR color and may be indicative of internal reddening (due to dust formation) or the intrinsically cool SEDs, rather than external extinction. We note that our IR-discovered events are overall much redder, all nine objects having $A_V \gtrsim 2$, compared to the optical control sample with seven of nine objects having $A_V \lesssim 2$. In particular, the MSEs SPIRITS 17pc and SPIRITS 17qm stand out as the reddest events in our sample with $A_V > 12$. For the five IR-discovered events interpreted as possible CCSNe, the estimates range from $2.2 \lesssim A_V \lesssim 7.8$. The optically discovered CCSNe in our

control sample are again notably less reddened, ranging from $A_V \sim 0$ to 4.3, with six of the eight events having $A_V \lesssim 2$. This suggests that the IR-selected sample of luminous SPIRITS transients may represent populations of much redder events that are largely inaccessible to optical searches, namely, heavily obscured CCSNe and exceptionally red or self-obscuring transients associated with massive-star outbursts of various origins.

The sample of all known CCSNe discovered between 2000 and the end of 2011 hosted by galaxies within 12 Mpc along with literature estimates of their host extinction compiled by Mattila et al. (2012, hereafter M12) provides another useful comparison for the SPIRITS sample. In Figure 16, we directly compare the distribution of host A_V for the SPIRITS sample of confirmed and plausible CCSNe (both optically and IR-selected events) to the M12 sample. We note that M12 excluded five SNe in galaxies with inclinations $>60^\circ$ from their primary analysis, as they believed that their volume-limited sample was incomplete for SNe in highly inclined hosts. We first include these events here for a more direct comparison to the SPIRITS sample, which includes some highly inclined galaxies. In the SPIRITS sample, 7 of the 13 CCSNe (58.3%) have $A_V \gtrsim 2$, and the median value is 2.2. For M12, only 6 of 18 events (33.3%) have $A_V \gtrsim 2$, and the median is significantly lower at $A_V = 0.25$. Shown as cumulative distributions in the right panel of Figure 16, we find that the M12 sample is bracketed between the optically known CCSNe in SPIRITS and the full SPIRITS sample including the IR-discovered events, where again a larger fraction of events were found with large host extinction. Here it is particularly important to reemphasize that for three of the five IR-discovered CCSNe in the SPIRITS sample, our A_V estimates are only lower limits, meaning that the true distribution may be even more skewed to large host extinctions.

If we now compare only those events in normal galaxies at inclinations $<60^\circ$, the M12 sample contained 2 of 13 SNe (15%) that appeared as outliers above the A_V distribution expected for dust smoothly distributed in disk galaxies with $A_V \gtrsim 3.5$ mag. The fraction in the SPIRITS sample (excluding events in highly inclined hosts and IC 2163, which is part of an interacting pair and a borderline LIRG; see our discussion of galaxy selection biases below in Section 7) is twice as high, with two of six events (33%) with $A_V > 3.5$ mag (SPIRITS 15ud and SN 2016bau). It is difficult to draw strong conclusions from this comparison given the small number of events included. It may hint, however, that the fraction of CCSNe suffering high host extinction, above that expected solely from inclination effects, and thus missing from optical searches, may be higher than previously estimated.

7. SPIRITS Constraints on the Optically Missed Fraction of Nearby CCSNe

We now consider constraints from our sample on the fraction of optically missed CCSNe in nearby galaxies, an important consideration for measurements of the local CCSN rate. $N_{\text{CCSNe}} = 13$ confirmed/plausible CCSNe were recovered by SPIRITS and pass our selection criteria, with $N_{\text{mCCSNe}} = 5$ events unreported by any optical search. If we assume that the completeness of our IR survey to optically discovered and optically missed SNe is the same (we examine this assumption in more detail below), then the fraction of missing CCSNe, f , is

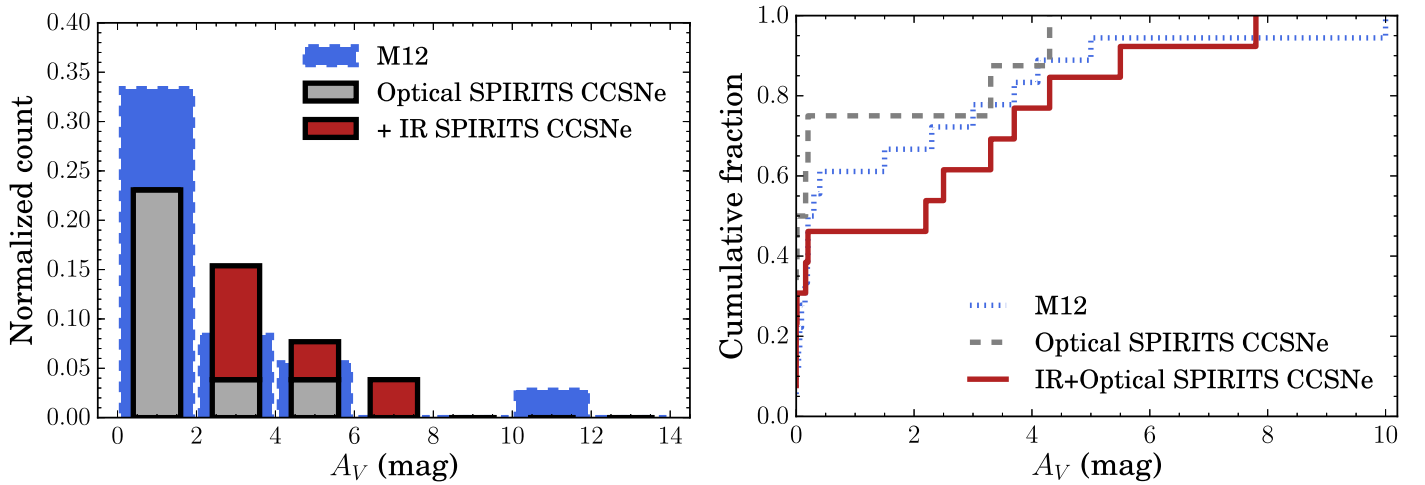


Figure 16. Left: normalized distribution of A_V for CCSNe from M12 sample, and the sample of confirmed/possible CCSNe in SPIRITS (filled histogram), including events from the optically discovered control sample (gray) and IR-discovered events (red). Right: cumulative distribution functions in host A_V estimates for M12 (blue short-dashed curve), optically known SPIRITS CCSNe from the control sample (gray dashed curve), and the full sample of likely SPIRITS CCSNe including both optically known and IR-discovered events (red solid curve).

given by the binomial distribution

$$P(f) \propto (1 - f)^{N_{\text{CCSNe}}} f^{N_{\text{mCCSNe}}}, \quad (3)$$

and the requirement that $\int_0^1 P(f) df = 1$ sets the normalization. The nominal, observed missed fraction is 0.385 with a 90% confidence interval of $0.166 < f < 0.645$.

Since 2 of 10 optically discovered and classified CCSNe, SN 2014bc and SN 2016adj, were not recovered in SPIRITS and selected as part of our sample with the criteria outlined in Sections 2.3 and 2.4, our selection efficiency for optically known CCSNe is 0.8. SN 2016adj in Cen A was itself flagged as a saturated source in our transient identification pipeline. An optically obscured CCSN in a galaxy as near as Cen A at a similar IR brightness would have been similarly flagged, and it is natural to assume that our survey incompleteness to optically bright and optically obscured CCSNe in the nearest galaxies ($D \lesssim 5$ Mpc) is the same. SN 2014bc was located in the saturated core of NGC 4285, and again we may expect our incompleteness to optically missed events located near the core of their host galaxies to be the same. Still, we may obtain a more conservative estimate of f if we assume that our sample was complete in optically missed events. With $N_{\text{CCSNe}} = 15$ total CCSNe in SPIRITS galaxies, and again with $N_{\text{mCCSNe}} = 5$, we obtain a missed fraction of 0.333 with a 90% confidence interval of $0.142 < f < 0.577$.

Next, we consider the effects of selection biases in our galaxy sample. For the first 3 yr (2014–2016), the full sample of 190 SPIRITS galaxies was more representative across galaxy types, though primarily composed of luminous and massive galaxies beyond 5 Mpc. IC 2163, producing both SPIRITS 15c and SPIRITS 17lb, also stands out from the sample in that with recent distance estimates it lies much farther than the rest of the sample at 35.5 Mpc, is currently undergoing strong tidal interactions with its companion galaxy, NGC 2207, and is a borderline LIRG at $L_{\text{IR}} \approx 10^{11} L_{\odot}$ (Sanders et al. 2003). Including only events discovered during the original 3 yr survey, and further excluding SPIRITS 15c in IC 2163, we have $N_{\text{CCSNe}} = 8$ and $N_{\text{mCCSNe}} = 3$, giving $f = 0.375$ with a 90% confidence interval of $0.111 < f < 0.711$. This is notably similar to our nominal estimate from the full sample, but with a

larger 90% confidence interval due to the smaller number of events.

Finally, we consider the possibility that some events interpreted here as CCSNe have been misclassified. SPIRITS 16tn and SPIRITS 16ix have uniquely fast-fading IR light curves compared to the full sample of CCSNe observed by *Spitzer*, and while SPIRITS 16tn is clearly associated with a region of active star formation, there is not such a clear association for SPIRITS 16ix. Excluding these two events, we have $N_{\text{CCSNe}} = 11$ and $N_{\text{mCCSNe}} = 3$, giving $f = 0.273$ with a 90% confidence interval of $0.079 < f < 0.564$.

Our data suggest an optically missed fraction of about 1/3 and cannot rule out a value twice as high. Such a large missing fraction could help explain the claimed factor of 2 discrepancy by Horiuchi et al. (2011) between the measured rate of CCSNe and rate of cosmic star formation at $z = 0$, but the precision of our measurement is limited by our small sample size and remaining ambiguous classifications. We also note that more recent volumetric CCSN rate estimates from the Supernova Diversity and Rate Evolution (SUDARE; Botticella et al. 2013) have challenged the claim by Horiuchi et al. (2011) and suggest better agreement between CCSN and star formation rates at medium redshift ($0.2 < z < 0.8$; Cappellaro et al. 2015). In the other direction, some local studies have even suggested that CCSNe may be overproduced compared to H α - and UV-inferred star formation rates (Botticella et al. 2012; Horiuchi et al. 2013; Xiao & Eldridge 2015), and interestingly, accounting for the population of heavily obscured nearby events uncovered by SPIRITS may further increase this tension.

We also now place our estimate in the context of other recent work to constrain the missing CCSN fraction and uncover events buried in densely obscured environments. M12 estimated that locally $18.9^{+19.2}_{-9.5}\%$ of CCSNe are missed by optical surveys, substantially higher than previous estimates by Mannucci et al. (2007) at 5%–10%. Our nominal estimate of $38.5^{+26.0}_{-21.9}\%$ of CCSNe missed in nearby galaxies is even higher, falling at the upper end of the allowed range by M12, but with substantial overlap with our 90% confidence interval. The estimates of Mannucci et al. (2007) and M12 rise steeply to $>30\%$ and $\sim 40\%$ by $z = 1$, respectively, and substantial work

has also been dedicated to uncovering missing supernovae at higher redshift, particularly in the densely obscured and highly star-forming nuclear regions of starburst galaxies and (U)LIRGs. With seeing-limited imaging (e.g., Mannucci et al. 2003; Miluzio et al. 2013) and high-resolution space- or ground-based adaptive optics imaging (Cresci et al. 2007; Mattila et al. 2007; Kankare et al. 2008, 2012; Kool et al. 2018), a total of 16 individual CCSNe have been uncovered in the IR in these galaxies. Radio very long baseline interferometry (VLBI) imaging of multiple (U)LIRGs (e.g., Lonsdale et al. 2006; Pérez-Torres et al. 2009; Romero-Cañizales et al. 2011, 2014; Bondi et al. 2012; Varenus et al. 2019, and references therein) has also revealed scores of radio sources interpreted as SN and SN remnants. Even with the resolution of the upcoming *James Webb Space Telescope*, probing the innermost nuclear regions of such systems will remain challenging, and recently Yan et al. (2018) undertook a successful pilot study examining the spatially integrated IR light curves of high-redshift (U)LIRGS for variability suggestive of ongoing SN explosions. Finally, deep, targeted optical searches of nearby galaxies may also achieve the sensitivity necessary to uncover heavily extinguished events, e.g., SN 2016ija uncovered by the $D < 40$ Mpc (DLT40) SN search in NGC 1532 with $A_V \approx 6$ (Tartaglia et al. 2018). In this context, we emphasize that our work represents the first attempt to uncover the obscured population and directly constrain the missing fraction of CCSNe in nearby galaxies in the IR.

8. Summary and Conclusions

We have presented a sample of nine luminous IR transients discovered in nearby ($D \lesssim 35$ Mpc) galaxies by the SPIRITS survey between 2014 and 2018. These events were selected as having M_{IR} brighter than -14 ($\nu L_\nu > 1.5 \times 10^5 L_\odot$ at [4.5]) in either the [3.6] or [4.5] channels of *Spitzer*/IRAC, and we required at least two SPIRITS detections and that these events were not present in the first epoch of SPIRITS imaging. Combining archival imaging constraints from *Spitzer* and *HST*, concomitant monitoring of SPIRITS galaxies with several ground-based telescopes, coverage in the iPTF survey from Palomar Observatory, and a dedicated ground- and space-based follow-up effort for our transients at optical, near-IR, and radio wavelengths, we construct detailed observational characterizations and attempt to determine their nature. Here we summarize our analysis of the sample and primary conclusions:

1. The IR-discovered sample of transients were predominantly found in the spiral arms of star-forming hosts, except for one event, SPIRITS 16ix, in a lenticular S0 galaxy. This strongly suggests an association with young stellar populations and massive stars. They span IR luminosities with $M_{[4.5],\text{peak}}$ between -14 and -18.2 , show IR colors between $0.2 < [3.6]-[4.5] < 3.0$, and fade on timescales between 55 days $< t_{\text{fade}} < 480$ days.
2. We define a control sample of optically discovered and classified transients recovered in SPIRITS using the same selection criteria (as outlined in Section 2.3). The control sample also consists of nine events, including eight known CCSNe and one SN Iax. Overall, the control sample and the IR-selected sample are similar in their IR properties, with similar distributions in $M_{[4.5],\text{peak}}$, their [3.6]–[4.5] colors at peak, and t_{fade} .

3. Of the nine IR-discovered events, we suggest that five may be significantly dust-obscured CCSNe. SPIRITS 15c was confirmed via a near-IR spectrum similar to the Type IIb SN 2011dh and detection of a radio counterpart consistent with an SN Ib/IIb (Jencson et al. 2017). SPIRITS 17lb, as the most luminous IR transient in our sample, and despite a lack of unambiguous SN features in its near-IR spectrum, was confirmed via its radio counterpart most consistent with an SN II. Our radio data constrain the pre-SN mass-loss rates of the progenitors of SPIRITS 15c and SPIRITS 17lb to $\dot{M} \lesssim 1.4 \times 10^{-3} \left(\frac{\epsilon_B}{0.1} \right) \left(\frac{v_w}{100 \text{ km s}^{-1}} \right) M_\odot \text{ yr}^{-1}$ and $\dot{M} \lesssim 8.0 \times 10^{-4} \left(\frac{\epsilon_B}{0.1} \right) \left(\frac{v_w}{100 \text{ km s}^{-1}} \right) M_\odot \text{ yr}^{-1}$, respectively. The IR light curve of SPIRITS 15ud is also most consistent with a CCSN classification. SPIRITS 16ix and SPIRITS 16tn may constitute a previously unknown class of rapidly fading, luminous IR transients occurring in the most densely obscured environments. We suggest that these two events are also CCSNe, possibly directly associated with or occurring within dense molecular clouds.
4. The four remaining luminous IR SPIRITS transients represent a diverse array of IR-dominated events arising from massive-star progenitor systems. The multiband optical and IR light curves of SPIRITS 14azy and SPIRITS 15ade are most similar to an LRN (possible massive stellar merger similar to M101 OT2015-1) and ILRT (possible weak or electron-capture SN similar to SN 2008S), respectively. SPIRITS 17pc underwent multiple, extremely red outbursts over several years, now showing G-type spectral features in the near-IR and double-peaked Ca II emission indicative of a few $\times 100 \text{ km s}^{-1}$ outflow. We identified a luminous ($L \approx 2 \times 10^5 L_\odot$) star detected in multiband archival *HST* imaging as a likely progenitor. SPIRITS 17qm, also undergoing multiple IR-dominated outbursts, showed high-velocity ($\sim 1500\text{--}2000 \text{ km s}^{-1}$) H and He features consistent with a giant LBV eruption. We identified a visually luminous ($L \approx 10^6 L_\odot$), highly variable progenitor in archival *HST* imaging. Future observations and continued monitoring of SPIRITS 17pc and SPIRITS 17qm may determine the physical origin of their IR outbursts and constrain the ultimate fate of their progenitors.
5. We estimated the visual extinction, A_V —either as a direct estimate of the host extinction (in the case of a CCSN) or as a proxy for the optical–IR color for non-SN transients that may be self-obscured or intrinsically red—for each event in our sample based on their multiband optical and IR light curves. All nine IR-discovered events, including the five confirmed/plausible CCSNe, have $A_V \gtrsim 2$, while only two of the nine objects in the optically discovered control sample have extinction estimates so high. Compared to a volume- and time-limited sample of CCSNe within 12 Mpc compiled by Mattila et al. (2012), we find that the SPIRITS sample of optically known and newly IR-discovered CCSNe contains a larger fraction of significantly obscured events ($A_V \gtrsim 2$). Furthermore, 7 out of the 13 plausible CCSNe detected by SPIRITS were significantly obscured. This makes it likely that optical transient/SN searches at larger distances are very incomplete because they miss highly obscured events.
6. A total of 13 confirmed/plausible CCSNe recovered in SPIRITS passed our selection criteria, including 8 optically discovered events in the control sample and 5 IR-discovered events presented here. For our galaxy

sample, this implies that a large fraction, as high as $38.5^{+26.0}_{-21.9}\%$ (90% confidence), of CCSNe are being missed by optical surveys in nearby galaxies.

We thank the anonymous referee for their thorough read of the paper and helpful comments. We thank C. Contreras and the staff of Las Campanas Observatory for help with conducting observations and data reduction. We thank E. Hsiao for helpful commentary and advice in the analysis and discussion of the spectra. We thank K. Mooley, D. Dong, M. Anderson, M. Eastwood, and A. Horeh for helpful advice and assistance with VLA data reduction. We thank S. Mattila and T. Reynolds for valuable discussions in revising this work.

This material is based on work supported by the National Science Foundation Graduate Research Fellowship under grant No. DGE-1144469. H.E.B. acknowledges that support for *HST* program Nos. GO-13935, GO-14258, and AR-15005 was provided by NASA through grants from the Space Telescope Science Institute, which is operated by the Association of Universities for Research in Astronomy, Incorporated, under NASA contract NAS5-26555. R.D.G. was supported by NASA and the United States Air Force. This work is part of the research program VENI, with project No. 016.192.277, which is (partly) financed by the Netherlands Organisation for Scientific Research (NWO).

This work is based in part on observations made with the *Spitzer Space Telescope*, which is operated by the Jet Propulsion Laboratory, California Institute of Technology, under a contract with NASA. This work is based in part on observations with the NASA/ESA *Hubble Space Telescope* obtained at the Space Telescope Science Institute and from the Mikulski Archive for Space Telescopes at STScI, which are operated by the Association of Universities for Research in Astronomy, Inc., under NASA contract NAS5-26555. We acknowledge the use of public data from the *Swift* data archive.

Some of the data presented herein were obtained at the W. M. Keck Observatory, which is operated as a scientific partnership among the California Institute of Technology, the University of California, and the National Aeronautics and Space Administration. The Observatory was made possible by the generous financial support of the W. M. Keck Foundation. The authors wish to recognize and acknowledge the very significant cultural role and reverence that the summit of Maunakea has always had within the indigenous Hawaiian community. We are most fortunate to have the opportunity to conduct observations from this mountain.

Part of the optical and near-infrared photometric data included in this paper were obtained by the Carnegie Supernova Project through the support of NSF grant AST-1008343.

Based on observations obtained at the Gemini Observatory acquired through the Gemini Observatory Archive and processed using the Gemini IRAF package, which is operated by the Association of Universities for Research in Astronomy, Inc., under a cooperative agreement with the NSF on behalf of the Gemini partnership: the National Science Foundation (United States), National Research Council (Canada), CONICYT (Chile), Ministerio de Ciencia, Tecnología e Innovación Productiva (Argentina), Ministério da Ciência, Tecnologia e Inovação (Brazil), and Korea Astronomy and Space Science Institute (Republic of Korea).

UKIRT is owned by the University of Hawaii (UH) and operated by the UH Institute for Astronomy; operations are enabled through the cooperation of the East Asian Observatory. When the data reported here were acquired, UKIRT was supported by NASA and operated under an agreement among the University of Hawaii, the University of Arizona, and Lockheed Martin Advanced Technology Center; operations were enabled through the cooperation of the East Asian Observatory.

Some of the data used in this paper were acquired with the RATIR instrument, funded by the University of California and NASA Goddard Space Flight Center, and the 1.5 m Harold L. Johnson telescope at the Observatorio Astronómico Nacional on the Sierra de San Pedro Mártir, operated and maintained by the Observatorio Astronómico Nacional and the Instituto de Astronomía of the Universidad Nacional Autónoma de México. We acknowledge the contribution of Leonid Georgiev and Neil Gehrels to the development of RATIR.

The National Radio Astronomy Observatory is a facility of the National Science Foundation operated under cooperative agreement by Associated Universities, Inc.

The Australia Telescope Compact Array is part of the Australia Telescope National Facility, which is funded by the Australian Government for operation as a National Facility managed by CSIRO. This paper includes archived data obtained through the Australia Telescope Online Archive (<http://atoa.atnf.csiro.au>).

The Digitized Sky Surveys were produced at the Space Telescope Science Institute under U.S. Government grant NAG W-2166. The images of these surveys are based on photographic data obtained using the Oschin Schmidt Telescope on Palomar Mountain and the UK Schmidt Telescope. The plates were processed into the present compressed digital form with the permission of these institutions. The Second Palomar Observatory Sky Survey (POSS-II) was made by the California Institute of Technology with funds from the National Science Foundation, the National Geographic Society, the Sloan Foundation, the Samuel Oschin Foundation, and the Eastman Kodak Corporation. The Oschin Schmidt Telescope is operated by the California Institute of Technology and Palomar Observatory. The UK Schmidt Telescope was operated by the Royal Observatory Edinburgh, with funding from the UK Science and Engineering Research Council (later the UK Particle Physics and Astronomy Research Council), until 1988 June, and thereafter by the Anglo-Australian Observatory. The blue plates of the southern Sky Atlas and its Equatorial Extension (together known as the SERC-J), as well as the Equatorial Red (ER) and the Second Epoch [red] Survey (SES), were all taken with the UK Schmidt. Supplemental funding for sky-survey work at the STScI is provided by the European Southern Observatory.

Funding for SDSS-III has been provided by the Alfred P. Sloan Foundation, the Participating Institutions, the National Science Foundation, and the U.S. Department of Energy Office of Science. The SDSS-III website is <http://www.sdss3.org/>. SDSS-III is managed by the Astrophysical Research Consortium for the Participating Institutions of the SDSS-III Collaboration, including the University of Arizona, the Brazilian Participation Group, Brookhaven National Laboratory, Carnegie Mellon University, University of Florida, the French Participation Group, the German Participation Group,

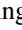
Harvard University, the Instituto de Astrofísica de Canarias, the Michigan State/Notre Dame/JINA Participation Group, Johns Hopkins University, Lawrence Berkeley National Laboratory, Max Planck Institute for Astrophysics, Max Planck Institute for Extraterrestrial Physics, New Mexico State University, New York University, Ohio State University, Pennsylvania State University, University of Portsmouth, Princeton University, the Spanish Participation Group, University of Tokyo, University of Utah, Vanderbilt University, University of Virginia, University of Washington, and Yale University.

This publication makes use of data products from the Two Micron All Sky Survey, which is a joint project of the University of Massachusetts and the Infrared Processing and Analysis Center/California Institute of Technology, funded by the National Aeronautics and Space Administration and the National Science Foundation.

Facilities: *Spitzer* (IRAC), *HST* (WFPC2, WFC3), *Swift* (UVOT), PO:1.5 m (CCD), PO:1.2 m, Swope (CCD), Du Pont (RetroCam), Magellan:Baade (FourStar, FIRE), Keck:I (LRIS, MOSFIRE), Keck:II (DEIMOS, NIRES), Hale (WIRC), Gemini:Gillett (GNIRS), Gemini:South (FLAMINGOS-2), UKIRT (WFCAM), OANSPM:HJT (RATIR), EVLA, ATCA, AMI.

Software: DOLPHOT (Dolphin 2000, 2016), DAOPHOT/ALLSTAR package (Stetson 1987), IRAF (Tody 1986, 1993), Gemini IRAF package (<http://www.gemini.edu/sciops/data-and-results/processing-software>), LPipe (Perley 2019, <http://www.astro.caltech.edu/~dperley/programs/lpipe.html>), MOSFIRE Data Reduction Pipeline (<https://keck-datareductionpipelines.github.io/MosfireDRP/>), Spextool (Cushing et al. 2004), CASA (McMullin et al. 2007).

ORCID iDs

Jacob E. Jencson  <https://orcid.org/0000-0001-5754-4007>
 Mansi M. Kasliwal  <https://orcid.org/0000-0002-5619-4938>
 Howard E. Bond  <https://orcid.org/0000-0003-1377-7145>
 Samaporn Tinnant  <https://orcid.org/0000-0002-1481-4676>
 Stuart D. Ryder  <https://orcid.org/0000-0003-4501-8100>
 Ann Marie Cody  <https://orcid.org/0000-0002-3656-6706>
 Frank J. Masci  <https://orcid.org/0000-0002-8532-9395>
 John Bally  <https://orcid.org/0000-0001-8135-6612>
 Nadejda Blagorodnova  <https://orcid.org/0000-0003-0901-1606>
 Christoffer Fremling  <https://orcid.org/0000-0002-4223-103X>
 Robert D. Gehrz  <https://orcid.org/0000-0003-1319-4089>
 Charles D. Kilpatrick  <https://orcid.org/0000-0002-5740-7747>
 Peter A. Milne  <https://orcid.org/0000-0002-0370-157X>
 Nidia Morrell  <https://orcid.org/0000-0003-2535-3091>
 Daniel A. Perley  <https://orcid.org/0000-0001-8472-1996>
 M. M. Phillips  <https://orcid.org/0000-0003-2734-0796>
 Schuyler D. van Dyk  <https://orcid.org/0000-0001-9038-9950>
 Robert E. Williams  <https://orcid.org/0000-0002-3742-8460>

References

Adams, S. M., Jencson, J. E., & Kasliwal, M. M. 2016a, *ATel*, **9441**, 1
 Adams, S. M., Kochanek, C. S., Prieto, J. L., et al. 2016b, *MNRAS*, **460**, 1645
 Amanullah, R., Goobar, A., Johansson, J., et al. 2014, *ApJL*, **788**, L21
 Aoki, M. 2016, *TNSTR*, **4**

Arbour, R. 2016, *TNSTR*, **215**
 Arcavi, I., Valenti, S., Hosseinzadeh, G., et al. 2014, *ATel*, **6466**, 1
 Bally, J., & Zinnecker, H. 2005, *AJ*, **129**, 2281
 Banerjee, D. P. K., Joshi, V., Evans, A., et al. 2018, *MNRAS*, **481**, 806
 Berger, E., Soderberg, A. M., Chevalier, R. A., et al. 2009, *ApJ*, **699**, 1850
 Bessell, M. S., Brett, J. M., Scholz, M., & Wood, P. R. 1989, *A&A*, **213**, 209
 Bessell, M. S., Scholz, M., & Wood, P. R. 1996, *A&A*, **307**, 481
 Blagorodnova, N., Kotak, R., Polshaw, J., et al. 2017, *ApJ*, **834**, 107
 Bock, G., Dong, S., Kochanek, C. S., et al. 2016, *ATel*, **9091**, 1
 Bond, H. E., Bedin, L. R., Bonanos, A. Z., et al. 2009, *ApJL*, **695**, L154
 Bond, H. E., Henden, A., Levay, Z. G., et al. 2003, *Natur*, **422**, 405
 Bondi, M., Pérez-Torres, M. A., Herrero-Illana, R., & Alberdi, A. 2012, *A&A*, **539**, A134
 Botticella, M. T., Cappellaro, E., Pignata, G., et al. 2013, *Msngr*, **151**, 29
 Botticella, M. T., Pastorello, A., Smartt, S. J., et al. 2009, *MNRAS*, **398**, 1041
 Botticella, M. T., Smartt, S. J., Kennicutt, R. C., et al. 2012, *A&A*, **537**, A132
 Brogan, C. L., Hunter, T. R., Cyganowski, C. J., et al. 2018, *ApJ*, **866**, 87
 Butler, N., Klein, C., Fox, O., et al. 2012, *Proc. SPIE*, **8446**, 844610
 Cao, Y., Kasliwal, M. M., McKay, A., & Bradley, A. 2014, *ATel*, **5786**, 1
 Cao, Y., Nugent, P. E., & Kasliwal, M. M. 2016, *PASP*, **128**, 114502
 Cappellaro, E., Botticella, M. T., Pignata, G., et al. 2015, *A&A*, **584**, A62
 Caratti o Garatti, A., Stecklum, B., Garcia Lopez, R., et al. 2017, *NatPh*, **13**, 276
 Casali, M., Adamson, A., Alves de Oliveira, C., et al. 2007, *A&A*, **467**, 777
 Cenko, S. B., Fox, D. B., Moon, D.-S., et al. 2006, *PASP*, **118**, 1396
 Cheng, Y.-C., Chen, T.-W., & Prentice, S. 2017, *ATel*, **10374**, 1
 Chevalier, R. A. 1982, *ApJ*, **259**, 302
 Chevalier, R. A. 1998, *ApJ*, **499**, 810
 Chevalier, R. A. 1999, *ApJ*, **511**, 798
 Chevalier, R. A., & Fransson, C. 2006, *ApJ*, **651**, 381
 Chevalier, R. A., Fransson, C., & Nymark, T. K. 2006, *ApJ*, **641**, 1029
 Cortini, G., Masi, G., Nocentini, F., et al. 2014, *CBET*, **3876**, 1
 Cresci, G., Mannucci, F., Della Valle, M., & Maiolino, R. 2007, *A&A*, **462**, 927
 Crowther, P. A. 1997, in *IAU Symp. 189, The Effective Temperatures of Hot Stars*, ed. T. R. Bedding, A. J. Booth, & J. Davis (Cambridge: Cambridge Univ. Press), **137**
 Cushing, M. C., Vacca, W. D., & Rayner, J. T. 2004, *PASP*, **116**, 362
 Dolphin, A. 2016, DOLPHOT: Stellar Photometry, Astrophysics Source Code Library, ascl:1608.013
 Dolphin, A. E. 2000, *PASP*, **112**, 1383
 Eikenberry, S., Elston, R., Raines, S. N., et al. 2006, *Proc. SPIE*, **6269**, 626917
 Elias, J. H., Joyce, R. R., Liang, M., et al. 2006, *Proc. SPIE*, **6269**, 62694C
 Faber, S. M., Phillips, A. C., Kibrick, R. I., et al. 2003, *Proc. SPIE*, **4841**, 1657
 Fazio, G. G., Hora, J. L., Allen, L. E., et al. 2004, *ApJS*, **154**, 10
 Ferrarese, L., Mould, J. R., Kennicutt, R. C., Jr., et al. 2000, *ApJ*, **529**, 745
 Fitzpatrick, E. L. 1999, *PASP*, **111**, 63
 Flower, P. J. 1996, *ApJ*, **469**, 355
 Foley, R. J., Van Dyk, S. D., Jha, S. W., et al. 2015, *ApJL*, **798**, L37
 Fossey, S. J., Cooke, B., Pollack, G., Wilde, M., & Wright, T. 2014, *CBET*, **3792**
 Gehrels, N., Chincarini, G., Giommi, P., et al. 2004, *ApJ*, **611**, 1005
 Gehrz, R. D., Roellig, T. L., Werner, M. W., et al. 2007, *RScI*, **78**, 011302
 Goodrich, R., & Cohen, M. 2003, *Proc. SPIE*, **4843**, 146
 Granata, V., Benetti, S., Cappellaro, E., et al. 2016, *ATel*, **8818**, 1
 Grossan, B., Spillar, E., Tripp, R., et al. 1999, *AJ*, **118**, 705
 Hess, K. M., Pisano, D. J., Wilcots, E. M., & Chengalur, J. N. 2009, *ApJ*, **699**, 76
 Hodgkin, S. T., Irwin, M. J., Hewett, P. C., & Warren, S. J. 2009, *MNRAS*, **394**, 675
 Horiuchi, S., Beacom, J. F., Bothwell, M. S., & Thompson, T. A. 2013, *ApJ*, **769**, 113
 Horiuchi, S., Beacom, J. F., Kochanek, C. S., et al. 2011, *ApJ*, **738**, 154
 Hosseinzadeh, G., Howell, D. A., Arcavi, I., McCully, C., & Valenti, S. 2016, *ATel*, **8859**, 1
 Hosseinzadeh, G., Valenti, S., McCully, C., et al. 2018, *ApJ*, **861**, 63
 Humphreys, R. M., Bond, H. E., Bedin, L. R., et al. 2011, *ApJ*, **743**, 118
 Humphreys, R. M., Davidson, K., & Smith, N. 1999, *PASP*, **111**, 1124
 Hunter, T. R., Brogan, C. L., MacLeod, G., et al. 2017, *ApJL*, **837**, L29
 Itagaki, K. 2016, *TNSTR*, **234**
 Jencson, J. E., Adams, S. M., Bond, H. E., et al. 2019, *ApJL*, **880**, L20
 Jencson, J. E., Bond, H. E., Adams, S. M., & Kasliwal, M. M. 2018a, *ATel*, **11577**, 1
 Jencson, J. E., Bond, H. E., Adams, S. M., & Kasliwal, M. M. 2018b, *ATel*, **11579**, 1
 Jencson, J. E., Bond, H. E., Adams, S. M., & Kasliwal, M. M. 2018c, *ATel*, **11803**, 1

- Jencson, J. E., Kasliwal, M. M., Adams, S. M., et al. 2018d, *ApJ*, **863**, 20
- Jencson, J. E., Kasliwal, M. M., Johansson, J., et al. 2017, *ApJ*, **837**, 167
- Johansson, J., Goobar, A., Kasliwal, M. M., et al. 2017, *MNRAS*, **466**, 3442
- Jordi, K., Grebel, E. K., & Ammon, K. 2006, *A&A*, **460**, 339
- Kankare, E., Mattila, S., Ryder, S., et al. 2008, *ApJL*, **689**, L97
- Kankare, E., Mattila, S., Ryder, S., et al. 2012, *ApJL*, **744**, L19
- Karambelkar, V. R., Adams, S. M., Whitelock, P. A., et al. 2019, *ApJ*, **877**, 110
- Kashi, A., & Soker, N. 2016, *RAA*, **16**, 99
- Kashi, A., & Soker, N. 2017, *MNRAS*, **467**, 3299
- Kasliwal, M. M., Bally, J., Masci, F., et al. 2017, *ApJ*, **839**, 88
- Kawabata, K. S., Nagae, O., Chiyonobu, S., et al. 2008, *Proc. SPIE*, **7014**, 70144L
- Khan, R. 2017, *ApJS*, **228**, 5
- Kilpatrick, C. D., & Foley, R. J. 2018, *MNRAS*, **481**, 2536
- Kim, M., Zheng, W., Li, W., et al. 2014, CBET, **3777**
- Kiyota, S., Holoien, T. W.-S., Stanek, K. Z., et al. 2014, ATel, **6460**, 1
- Kochanek, C. S. 2011, *ApJ*, **741**, 37
- Kochanek, C. S., Adams, S. M., & Belczynski, K. 2014, *MNRAS*, **443**, 1319
- Kochanek, C. S., Fraser, M., Adams, S. M., et al. 2017, *MNRAS*, **467**, 3347
- Kool, E. C., Ryder, S., Kankare, E., et al. 2018, *MNRAS*, **473**, 5641
- Kulkarni, S. R., Ofek, E. O., Rau, A., et al. 2007, *Natur*, **447**, 458
- Kumar, S., Zheng, W., Filippenko, A. V., et al. 2014, CBET, **3892**
- Li, W., Mo, J., Wang, X., et al. 2014, CBET, **3788**
- Lonsdale, C. J., Diamond, P. J., Thrall, H., Smith, H. E., & Lonsdale, C. J. 2006, *ApJ*, **647**, 185
- Maguire, K., Di Carlo, E., Smartt, S. J., et al. 2010, *MNRAS*, **404**, 981
- Maiolino, R., Vanz, L., Mannucci, F., et al. 2002, *A&A*, **389**, 84
- Mannucci, F., Della Valle, M., & Panagia, N. 2007, *MNRAS*, **377**, 1229
- Mannucci, F., Maiolino, R., Cresci, G., et al. 2003, *A&A*, **401**, 519
- Marples, P., Bock, G., & Parker, S. 2016, ATel, **8651**, 1
- Masci, F. J., Laher, R. R., Rebbapragada, U. D., et al. 2017, *PASP*, **129**, 014002
- Mattila, S., Dahlen, T., Efstathiou, A., et al. 2012, *ApJ*, **756**, 111
- Mattila, S., Väisänen, P., Farrah, D., et al. 2007, *ApJL*, **659**, L9
- McCollum, B., Laine, S., Väisänen, P., et al. 2014, *AJ*, **147**, 11
- McLean, I. S., Steidel, C. C., Epps, H., et al. 2010, *Proc. SPIE*, **7735**, 77351E
- McLean, I. S., Steidel, C. C., Epps, H. W., et al. 2012, *Proc. SPIE*, **8446**, 84460J
- McMullin, J. P., Waters, B., Schiebel, D., Young, W., & Golap, K. 2007, in ASP Conf. Ser. 376, *Astronomical Data Analysis Software and Systems XVI*, ed. R. A. Shaw, F. Hill, & D. J. Bell (San Francisco, CA: ASP), **127**
- Metzger, B. D., & Pejcha, O. 2017, *MNRAS*, **471**, 3200
- Milisavljevic, D., Margutti, R., Kamble, A., et al. 2015, *ApJ*, **815**, 120
- Miluzio, M., Cappellaro, E., Botticella, M. T., et al. 2013, *A&A*, **554**, A127
- Monard, L. A. G., Kneip, R., Brimacombe, J., et al. 2014, CBET, **3977**
- Morgan, C. W., Byard, P. L., DePoy, D. L., et al. 2005, *AJ*, **129**, 2504
- Muñoz-Mateos, J. C., Sheth, K., Gil de Paz, A., et al. 2013, *ApJ*, **771**, 59
- Nakano, S., Itagaki, K., Guido, E., et al. 2014, CBET, **4011**
- Nasonova, O. G., de Freitas Pacheco, J. A., & Karachentsev, I. D. 2011, *A&A*, **532**, A104
- Nousek, J. A. 2004, *Proc. SPIE*, **5165**, 169
- Ohner, P., Tomasella, L., Benetti, S., et al. 2014, ATel, **6648**, 1
- Pastorello, A., Botticella, M. T., Trundle, C., et al. 2010, *MNRAS*, **408**, 181
- Pérez-Torres, M. A., Romero-Cañizales, C., Alberdi, A., & Polatidis, A. 2009, *A&A*, **507**, L17
- Perley, D. A. 2019, *PASP*, **131**, 084503
- Persson, S. E., Murphy, D. C., Smee, S., et al. 2013, *PASP*, **125**, 654
- Prieto, J. L., Kistler, M. D., Thompson, T. A., et al. 2008, *ApJL*, **681**, L9
- Querejeta, M., Meidt, S. E., Schinnerer, E., et al. 2015, *ApJS*, **219**, 5
- Rayner, J. T., Cushing, M. C., & Vacca, W. D. 2009, *ApJS*, **185**, 289
- Riess, A. G., Macri, L. M., Hoffmann, S. L., et al. 2016, *ApJ*, **826**, 56
- Rodríguez, Ó., Clocchiatti, A., & Hamuy, M. 2014, *AJ*, **148**, 107
- Romero-Cañizales, C., Herrero-Illana, R., Pérez-Torres, M. A., et al. 2014, *MNRAS*, **440**, 1067
- Romero-Cañizales, C., Mattila, S., Alberdi, A., et al. 2011, *MNRAS*, **415**, 2688
- Roming, P. W. A., Kennedy, T. E., Mason, K. O., et al. 2005, *SSRv*, **120**, 95
- Sahu, D. K., Anupama, G. C., Srivastav, S., & Chakradhari, N. K. 2016, ATel, **8514**, 1
- Sanders, D. B., Mazzarella, J. M., Kim, D. C., Surace, J. A., & Soifer, B. T. 2003, *AJ*, **126**, 1607
- Sault, R. J., Teuben, P. J., & Wright, M. C. H. 1995, in ASP Conf. Ser. 77, *Astronomical Data Analysis Software and Systems IV*, ed. R. A. Shaw, H. E. Payne, & J. J. E. Hayes (San Francisco, CA: ASP), **433**
- Schlafly, E. F., & Finkbeiner, D. P. 2011, *ApJ*, **737**, 103
- Schlegel, D. J., Finkbeiner, D. P., & Davis, M. 1998, *ApJ*, **500**, 525
- Sheth, K., Regan, M., Hinz, J. L., et al. 2010, *PASP*, **122**, 1397
- Simcoe, R. A., Burgasser, A. J., Bernstein, R. A., et al. 2008, *Proc. SPIE*, **7014**, 70140U
- Simcoe, R. A., Burgasser, A. J., Schechter, P. L., et al. 2013, *PASP*, **125**, 270
- Smartt, S. J., Smith, K. W., Wright, D., et al. 2014, CBET, **3877**
- Smith, N. 2014, *ARA&A*, **52**, 487
- Smith, N., Andrews, J. E., Van Dyk, S. D., et al. 2016, *MNRAS*, **458**, 950
- Smith, N., Miller, A., Li, W., et al. 2010, *AJ*, **139**, 1451
- Sorce, J. G., Tully, R. B., Courtois, H. M., et al. 2014, *MNRAS*, **444**, 527
- Sparks, W. B., Bond, H. E., Cracraft, M., et al. 2008, *AJ*, **135**, 605
- Stetson, P. B. 1987, *PASP*, **99**, 191
- Stritzinger, M., Hsiao, E. Y., Morrell, N., et al. 2016, ATel, **8657**, 1
- Szalai, T., & Vinkó, J. 2013, *A&A*, **549**, A79
- Szalai, T., Zsíros, S., Fox, O. D., Pejcha, O., & Müller, T. 2019, *ApJS*, **241**, 38
- Szczygieł, D. M., Prieto, J. L., Kochanek, C. S., et al. 2012, *ApJ*, **750**, 77
- Tartaglia, L., Sand, D. J., Valenti, S., et al. 2018, *ApJ*, **853**, 62
- Theureau, G., Hanski, M. O., Coudreau, N., Hallet, N., & Martin, J.-M. 2007, *A&A*, **465**, 71
- Thompson, T. A., Prieto, J. L., Stanek, K. Z., et al. 2009, *ApJ*, **705**, 1364
- Tinyanont, S., Kasliwal, M. M., Fox, O. D., et al. 2016, *ApJ*, **833**, 231
- Tinyanont, S., Kasliwal, M. M., Krafton, K., et al. 2019, *ApJ*, **873**, 127
- Tody, D. 1986, *Proc. SPIE*, **627**, 733
- Tody, D. 1993, in ASP Conf. Ser. 52, *Astronomical Data Analysis Software and Systems II*, ed. R. J. Hanisch, R. J. V. Brissenden, & J. Barnes (San Francisco, CA: ASP), **173**
- Torres, G. 2010, *AJ*, **140**, 1158
- Tully, R. B. 1988, *Nearby Galaxies Catalog* (Cambridge: Cambridge Univ. Press)
- Tully, R. B., Courtois, H. M., Dolphin, A. E., et al. 2013, *AJ*, **146**, 86
- Tylenda, R., Hajduk, M., Kamiński, T., et al. 2011, *A&A*, **528**, A114
- Vacca, W. D., Cushing, M. C., & Rayner, J. T. 2003, *PASP*, **115**, 389
- Van Dyk, S. D., Peng, C. Y., King, J. Y., et al. 2000, *PASP*, **112**, 1532
- Varenius, E., Conway, J. E., Batejat, F., et al. 2019, *A&A*, **623**, A173
- Watson, A. M., Richer, M. G., Bloom, J. S., et al. 2012, *Proc. SPIE*, **8444**, 84445L
- Werner, M. W., Roellig, T. L., Low, F. J., et al. 2004, *ApJS*, **154**, 1
- Wiggins, P. 2017, CBET, **4390**
- Wilson, J. C., Eikenberry, S. S., Henderson, C. P., et al. 2003, *Proc. SPIE*, **4841**, 451
- Xiao, L., & Eldridge, J. J. 2015, *MNRAS*, **452**, 2597
- Yan, H., Ma, Z., Beacom, J. F., & Runge, J. 2018, *ApJ*, **867**, 21
- Zhang, J., Zheng, X., Wang, X., & Rui, L. 2016, ATel, **9093**, 1
- Zhang, T., Wang, X., Mo, J., & Chen, J. 2014, CBET, **3795**, 1